The role of MHD instabilities in the magnetospheric propeller outflow and emission in the nova-like variable star AE Aquarii

Louis Albert Venter

This thesis is presented in fulfillment of the requirements
for the degree PhD
in the Faculty of Natural and Agricultural Sciences,
Department of Physics
of the
University of the Free State

Promoter: Prof. P.J. Meintjes

February 2007

Acknowledgements

I would like to thank Prof. Pieter J. Meintjes for his excellent leadership and guidance during this study.

I gratefully acknowledge the financial support of the NRF during the period 2004-2006.

Graag bedank ek Prof. Meintjes vir sy voortgesette leiding, motivering en strewe na uitnemendheid, asook Prof. H. Swart en die Departement Fisika vir onontbeerlike ondersteuning.

Ek bedank al my familielede vir aanmoediging, liefde en ondersteuning. Daarsonder kan of wil mens nie.

Lof en dank aan ons Vader in die hemel vir onverdiende en ontelbare seëninge.

Abstract

AE Aquarii is a close binary consisting of a white dwarf primary star and a K4-5 red dwarf, the secondary. Mass is transferred from the Roche lobe filling secondary to the Roche lobe of the white dwarf. The white dwarf has a spin period $P_{spin} \sim 33$ s and a fast corotating magnetosphere. The trajectory of the flow brings it to a closest approach $r_{cl} \sim 10^{10}$ cm which is outside the corotation radius. Observational studies of the emisssion lines, in conjuction with the observed spin-down of the white dwarf, suggests that the bulk of the mass transfer is propelled from the system. The ejection of the flow is proposed to result from the interaction of the mass flow with the fast rotating magnetosphere. The interaction transfers angular momentum from the magnetosphere to the mass flow.

The unique contribution of this study lies therein that this plasma-magnetosphere interaction is modelled as being driven by the Kelvin-Helmholtz (KH) instability, which is assumed to grow at the interface between the mass flow and the magnetosphere. The process can be quantified by evaluating the Poynting flux S, of the magnetospheric field at the radius of closest approach. The energy dissipation rate of the field across the surface of the stream A is $P_{MHD} = S \times A \sim 10^{34}$ erg s^{-1}. Furthermore, if the mass transfer is ejected by the propeller at the escape velocity $v_{esc} \sim 1550$ km s^{-1}, the energy carried by the outflow is $P_{out} = \frac{1}{2}\dot{M}v_{esc}^2 \sim 5 \times 10^{33}$ erg s^{-1}, where $\dot{M}$ is the mass transfer rate. It is therefore plausible that the magnetospheric propeller is responsible for the ejection of the mass transfer. The ultimate energy source for the propeller is the spin of the white dwarf which has been shown to be losing rotational kinetic energy at the rate $P_{spin} \sim 10^{34}$ erg s^{-1}.

The KH driven magnetospheric propeller also results in the formation of magnetized plasmoids of energized electrons that emit synchrotron emission between infra-red and 1GHz radio frequencies as they are ejected from the system and expand. A large diffuse remnant, which emits in the MHz frequency range, is expected to form as the ejected bubbles coalesce outside the system. Furthermore, the KH instability triggers turbulence in the outflow, which eventually heats the gas and results in optical flares outside the white dwarf 's Roche lobe. On its trajectory outwards, the outflow disrupts the magnetic field of the secondary and currents are induced that may heat plasma trapped in the field to X-ray emitting temperatures. This Joule heated plasma can account for the observed non-pulsed X-ray emission from AE Aqr.

Key terms: magnetic cataclysmic variable; AE Aquarii, magnetospheric propeller, KH instability, turbulence, non-thermal radio emission, thermal optical and X-ray emission

Opsomming

AE Aquarii is 'n kompakte dubbelster, bestaande uit 'n wit dwerg primêre ster en 'n K4-5 rooi dwerg sekondêre ster. Massa word vanaf die Roche lob vullende rooi dwerg na die wit dwerg oorgedra. Die gesloteveldlyngebied van die sekondêre ster se magneetveld omsluit die wit dwerg. Die wit dwerg het 'n spin periode $P_{spin} \sim 33$ s en die magnetosfeer koroteer met die ster. Die baan van die massa vloei bring dit tot 'n minimum radiale afstand $r_{cl} \sim 10^{10}$ cm vanaf die wit dwerg. Studies van die waargenome stralingslyne en die toenemende spin periode, dui daarop dat die grootste deel van die massa oordrag uit die sisteem gegooi word. Daar word veronderstel dat die interaksie tussen die massa vloei en die vinnig roterende magnetosfeer die proses dryf. Die interaksie dra draaimomentum vanaf die magnetosfeer na die massa-vloei oor.

Die unieke bydrae van hierdie ondersoek lê daarin dat dié interaksie deur middel van die Kelvin-Helmholtz (KH) onstabiliteit gemodelleer word. Die teenwoordigheid van die onstabiliteit word by die skeiding tussen die massavloei en die magnetosfeer verwag. Die proses kan gekwantifiseer word deur die Poynting vloed S, van die magneetveld by r_{cl} te beskou, oftewel $S = \frac{1}{4\pi} v_{rel} B^2$. Die energieoordragtempo van die veld oor die oppervlak van die stroom A, is $P_{MHD} = S \times A \sim 10^{34}$ erg s^{-1}. Indien die massaoordrag teen die ontsnapsnelhied $v_{esc} \sim 1550$ km s^{-1} uitgegooi word, is die energie wat die uitvloei weg dra, $P_{out} = \frac{1}{2}\dot{M} v_{esc}^2 \sim 5 \times 10^{33}$ erg s^{-1}, waar $\dot{M}$ die massa-oordragtempo is. Dit is dus moontlik dat die magnetosferiese propeller verantwoordelik is vir die uitgooi van die massa-oordrag. Die primêre energiebron vir die propeller is die rotasie van die wit dwerg. Dit is aangetoon dat die ster rotasie kinetiese energie verloor teen die tempo $P_{spin} \sim 10^{34}$ erg s^{-1}.

Die KH-gedrewe magnetosferiese propeller het ook tot gevolg dat gemagnetiseerde plasmaborrels wat sinkrotron straling van IR tot GHz radio frekwensies straal, gevorm word. 'n Groot diffuse gasnewel, wat in die honderde MHz frekwensies straal, kan ook uit die ontsnapte borrels vorm. Die KH onstabiliteit inisieer verder ook turbulensie in die uitvloei wat tot die verhitting van die gas en optiese uitbarstings buite die wit dwerg se Roche lob lei. Die uitvloei versteur ook die magneetveld van die rooi ster en induseer elektriese strome wat die plasma tot X-straal temperature verhit. Hierdie Joule verhitte plasma kan verantwoordelik wees vir die waargenome nie-gepulseerde X-strale van AE Aqr.

Sleutelterme: magnetiese kataklismiese veranderlike; AE Aquarii, magnetosferiese propeller, KH onstabiliteit, turbulensie, nie-termiese radio straling, termiese X-straal en optiese straling

Contents

Chapter 1

Introduction

In December 2002 a third conference was held focusing on Magnetic Cataclysmic Variables(mCVs)(ASPC, 315, 2004). In his summary of the conference J.-P. Lasota (2004) remarked, "What are mCVs and why do they warrant a conference of their own?"

Cataclysmic variables consist of a white dwarf (the primary) and usually a cool main-sequence red dwarf star (the secondary) of spectral type G, K or M, orbiting their common centre of mass. The orbital periods lie between 1 and 15 hours which is an indicator of the binary separation, which for this period range means these binaries can fit into the Sun. The red dwarf secondary usually fills its Roche lobe[1] and gas flows from its tenuous outer envelope to the primary star. In the absence of a strong magnetic field on the primary, the gas can form an accretion disc around the white dwarf. The disc may extend down to the surface where the gravitational potential energy of the accretion is released as radiation in a thin boundary layer (Frank, King & Raine 2002, p. 152). However, if a significant magnetic field is present, the magnetosphere will influence the gas flow before it reaches the surface and in extreme cases the formation of a disc may be prevented. The most fascinating aspect of cataclysmic variables is that the peculiar variability is accretion related, i.e. these are accretion driven systems.

Lasota then proceeds in defining a magnetic CV as a system where the "the magnetic field of the white dwarf determines (at least) one of the fundamental properties of the system."He continues in saying "that the wealth of effects related to the magnetic character of CVs and the fascinating physics they involve, certainly deserve specialized conferences. ... our understanding is still far from complete. "

The novalike variable AE Aquarii is one of these magnetic CVs displaying a wealth of effects that are ill-understood. AE Aquarii's main distinguishing feature is rapid variability of emission over several decades in energy, from radio to VHE γ-rays (Bastian, Dulk & Chanmugam 1988, Abada-Simon et al. 1993 , Patterson 1979, Patterson et al. 1980, Meintjes 1992, Meintjes et al. 1994, Eracleous & Horne 1996 to name a few). Recently it was shown that the rapid variability in AE Aqr can be understood in conjunction with magnetospheric propellering by the white dwarf. The propeller mechanism and its consequences will constitute the main focus of this thesis.

[1]The Roche lobes are equipotential surfaces of the combination of the gravitational potential of the binary and the centrifugal potential due to the orbital motion.

In this chapter the general properties of magnetic cataclysmic variables will be presented after which AE Aqr's wealth of observational features will be discussed.

1.1 Magnetic CVs and novalikes

Magnetic CVs are classified into two main classes (cf. Warner 1995, Lamb 1995), the AM Her stars or Polars and the Intermediate Polars (IPs). These classifications arose from the different observational characteristics of these subclasses. For instance, the polars exhibit strongly polarized optical light while the intermediates have little or no optical polarization. The difference in the amount of polarized light indicates a difference in the magnetic field strengths of these systems. Polars have white dwarfs with fields $B_* > 10^7$ G and in the IPs $B_* < 10^7$ G. Intermediate polars have weaker fields and wider binary separation, i.e. $P_{orb}(Ip) > P_{orb}(polar)$. The spin of the white dwarf in IPs is not synchronized with the orbital period, as is found in Polars. The IPs typically have $P_{orb} > 3.5$ hours and white dwarf spin periods $P_* \gg 100$ s.

The spin and orbital periods in most IPs seem to obey the relation $P_* \sim 0.1P_{orb}$. This relation was shown to result from the mass transfer between the secondary and the compact primary being fragmented into large diamagnetic blobs (diamagnetic : not easily penetrated by external magnetic fields) (e.g. King & Lasota 1991, Wynn & King 1995). Large blobs may stay intact without being disrupted or influenced by the white dwarf magnetosphere at distances further than the circularization radius, r_{circ}. This is where the mass transfer flow from the secondary star would settle into a ring conserving its angular momentum after crossing the L_1 region. If r_{circ} is smaller than the corotation radius r_{co}, i.e. where the Keplerian velocity of orbiting material matches the angular velocity of the star, the orbiting gas does not experience a huge centrifugal barrier when accreting along the corotating field lines onto the stellar surface. In this way the white dwarf accretes the specific angular momentum associated with r_{circ}. The accretion process then also results in a gradual spin-up of the primary to an equilibrium period of $P_{eq} \sim 0.1P_{orb}$. This relation is applicable to systems without an accretion disc, but IPs can also accrete via a disc if the condition (Warner & Wickramasinghe 1991)

$$\frac{\mu_{34}}{\sqrt{\dot{m}_{18}}} < 0.4 \left(\frac{P_{orb}}{4hr}\right)^{7/6} M_1^{5/6}$$

is satisfied. Here μ_{34} represents the magnetic moment of the white dwarf in units of 10^{34} G cm^3, $\dot{m}_{18}$ is the accretion rate in units of 10^{18} g s^{-1} and M_1 is the white dwarf mass in solar units. The presence of an accretion disc can result in a significant deviation from the $0.1P_{orb}$ relation due to star-disc torques that influence the spin of the primary.

The DQ Her systems are a subset of the intermediate polars and are characterized by their short primary spin periods ($P_* < 100$ s) and lack of hard X-ray emission. The relation $P_* \ll 0.1P_{orb}$ hints that the compact white dwarf has been spun up significantly by accretion induced torques presumably due to an accretion disc (Ghosh & Lamb 1979a,b; Wang 1987).

Pulsed emission is observed and attributed to the accretion of mass transfered from the Roche lobe filling secondary star onto, among other areas, the magnetic poles of the primary (Figure 1.1 shows the typical structure of the critical surface in a close binary star where the secondary star fills its Roche lobe.). A brief discussion of the mass transfer/accretion process will be presented in Section 2.

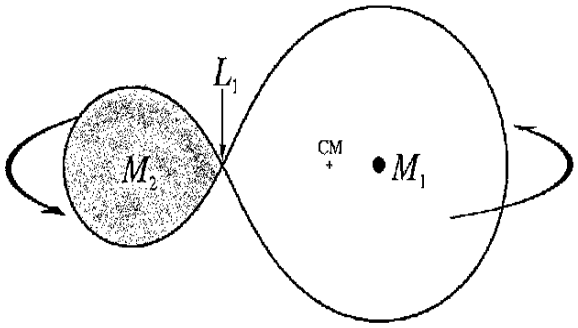

Figure 1.1: Schematic of a close binary with the secondary star filling its Roche lobe and indicating the L_1 point where a mass flow can escape from the secondary.

As already mentioned, these systems are accretion driven. That is to say, mass transfer and accretion determine most of the observed emission properties. For example in some disc accreting systems (dwarf novae) the disc intercepts the flow from the secondary. The interplay between the transfer and accretion processes results in an example of 'cataclysmic'behaviour in the form of the *dwarf nova* (DN) outburst. These outbursts are thought to be the result of a pile up of material from the secondary in the disc. This pile-up increases the effective viscosity in the disc, the disc spreads out as a result (more effective transport of angular momentum) and the accretion rate increases noticeably. The result is a large increase in the system's luminosity until the disc is drained of material. These bursts occur periodically as the disc cycles between phases of higher and lower viscosity.

A viable mechanism to explain the increased viscosity has only recently been introduced. The trigger for the process is described by the disc (thermal) instability model (DIM). The main idea behind the DIM is that material is transferred from the secondary star at a constant rate to a low viscosity accretion disc orbiting the primary. Osaki (1974) postulated that material accumulates in the disc, increasing the disc surface density Σ to a critical value, which triggers an instability resulting in the disc brightening. It has been observed that during the DN event, approximately $\sim 10\%$ (e.g. Frank, King & Raine 2002, p. 125) of the disc may accrete onto the surface of the white dwarf.

Here we see the important role of the mass transfer rate. If the transfer rate is too low, the thermal instability will not switch on and no outburst will occur. On the other hand the rate can be so high that the disc is stuck in a hot state and is permanently in "outburst"(Hellier 2001, ch. 5). Such stars are called *novalike variables*. This term is applied to cataclysmic variables with a mass transfer rate sufficient to keep a disc in a hot active state.

1.2 A brief review of AE Aquarii

AE Aquarii has been and remains a very interesting and productive astrophysical laboratory. The system does not seem to fit easily into any of the sub-groups of the variable binary stars. This, combined with its relative proximity to Earth, has ensured it remaining a source of continuous observational and theoretical

interest since its discovery on photographic plates (Zinner 1938). The inferred distance to the system is D = 100 pc (Welsh, Horne & Oke 1993). The system displays frequent explosions of relatively small amplitude compared to, for instance, nova outbursts, and was thought to be a typical novalike variable (Mumford 1967). It was also classified as a cataclysmic variable of the DQ Herculis type. In the following paragraphs AE Aqr's general and emission properties will be discussed.

1.2.1 General properties

An orbital period of $P_{orb} = 9.88$ hrs and the primary white dwarf's spin period $P_s \sim 33$ s has been established (Patterson 1979). The K4-5 red dwarf secondary's rotation is assumed to be tidally synchronized with the orbital motion. The large difference between the spin and orbital periods already distinguishes AE Aqr from the other systems in its assigned class. Optical, UV and X-ray observations (e.g. Eracleous et al.1994) have confirmed the spin period of the primary, but have also indicated that the accretion luminosity is much lower than would be expected from a system of this nature. The relatively low X-ray luminosity of $L_X \sim 5 \times 10^{30}$ erg s^{-1} (Wynn, King and Horne 1997) implies a small accretion rate onto the poles of the white dwarf with $\dot{M}_a \leq 10^{14}$ g s^{-1}. Eracleous & Horne (1996) analyzed UV spectra from the *HST* and concluded that the mass transfer rate from the secondary must be $\dot{M}_s \geq 4 \times 10^{17}$ g s^{-1}, which if accreted onto the surface of the white dwarf, can drive an accretion luminosity of

$$L_{acc} \sim \frac{GM_1\dot{M}_s}{R_*} \sim 10^{34} \left(\frac{M_1}{M_\odot}\right) \left(\frac{\dot{M}_s}{4 \times 10^{17}\text{g s}^{-1}}\right) \left(\frac{R_1}{10^9\text{cm}}\right)^{-1} \text{erg s}^{-1}. \quad (1.1)$$

Furthermore, the *HST* data indicated that the signal at the spin period is not enhanced during observed flares. This suggests that enhanced accretion is not the origin of the flares in the system. There thus seems to be evidence for a high mass transfer rate but a low accretion rate, which naturally points to some sort of propeller mechanism preventing significant accretion or the formation of an accretion disc. Figure 1.2 shows a simulation of the outflow from the propeller (Frank, King & Raine 2002). Eracleous & Horne (1996), Wynn, King & Horne(1997)(WKH) and Meintjes (2002) indicated that the mass transfer from the secondary in AE Aqr is too low for an accretion disc to develop. Therefore the fast rotating white dwarf acts as a propeller flinging the gas from the system.

Evidence in favour of a propeller in AE Aqr came from a pulse timing analysis of the $P_s \sim 33$ s spin period of the white dwarf (De Jager et al. 1994). The analysis of the pulse arrival times in optical data from different observations over a 14+ year period revealed a spin down rate of $\dot{P}_s = 5.64 \times 10^{-14}$ s s^{-1}. The white dwarf is therefore losing rotational energy at an approximate rate of

$$\dot{E}_{rot} = \frac{I}{I_{50}}\Omega\dot{\Omega} \sim 10^{34}\text{erg s}^{-1} \quad (1.2)$$

where $\Omega = 2\pi/P_s$ and I_{50} is the moment of inertia in units of 10^{50} g cm^2. Recently Mauche(2006) investigated ASCA, XMM-Newton, and Chandra X-ray observations spread over 10 yrs, resulting in a cumulative 27 yr baseline of spin periods of AE Aqr, revealing a somewhat faster spin-down in the recent past. The spin-down rate is a modest 3.5±1.8 % greater than the rate derived previously (De Jager et al. 1994). This small increase may be accounted for by a slight increase in the mass transfer rate from the secondary, which leads to a larger spin-down torque on the white dwarf.

Figure 1.2: The outflow of the propeller according to G. Wynn (Frank, King & Raine 2002), indicating the Roche lobe filling secondary star and the white dwarf (WD).

Ikhsanov (1998) proposed a pulsar-like spin-down model for AE Aqr. Within this framework the spin-down of the white dwarf is due to energy losses through magneto-dipole radiation. In a vacuum, a rotating star with a misaligned magnetic dipole loses rotational kinetic energy via dipole radiation at a rate L_d = -I$\Omega\dot{\Omega}$ = $2\mu^2 \sin^2\theta\Omega^4/3c^3$, where $\mu = \mathrm{BR}^3$ is the magnetic moment, B is the surface magnetic field strength, R is the stellar radius and θ is the angle between the rotation and magnetic axes. If magnetic-dipole radiation losses is the only mechanism responsible for the spin-down of the white dwarf, it implies that the magnetic moment $\mu \approx 10^{34}$ G cm or B $\sim$ 50 MG (Ikhsanov 1998). Keeping the strong dependence of L_d on Ω in mind, Mauche(2006) found the observed change in P_s incompatible with the dipole radiation spin-down model. A field of the strength indicated would also be expected to be associated with higher levels of circular polarization than is observed (see below).

If 99.9% of the mass transfer, at the rate $\dot{M}$, is ejected by the propeller and escapes at the escape velocity $\mathrm{v}_{esc} \sim 1500$ km s^{-1} (WKH, Venter & Meintjes 2006), then the energy carried away by the outflow is

$$L_{esc} = \frac{1}{2}\frac{\dot{M}}{\dot{M}_s}\left(\frac{\mathrm{v}}{\mathrm{v}_{esc}}\right)^2 \sim 10^{34}\mathrm{erg\ s}^{-1}. \tag{1.3}$$

These estimates suggest that the spin down of the white dwarf may quite possibly be driven by the propeller. The challenge is to understand the detailed process of momentum transfer from the white dwarf to the mass flow approaching it. The most plausible lever arm for flinging the gas from the system is the corotating magnetic field of the white dwarf.

Cropper(1986) and later Beskrovnaya et al. (1995) reported circular polarization at the level of (0.05 ± 0.01) % and (0.06 ± 0.03) % respectively in the optical light, which, if produced by cyclotron emission, may indicate a surface magnetic field in excess of $\mathrm{B}_* \sim 10^6$ G (Chanmugam & Frank 1987). Meintjes (2002) and Schenker et al. (2002) showed that the short rotation period in conjunction with the long orbital period

seem to suggest that AE Aqr has evolved through a high mass transfer/accretion phase, possibly accreting from a well developed disc. By inverting the disc-less accretion condition in intermediate polars (Warner & Wickramasinghe 1991), an accretion disc could have developed if the magnetic field of the white dwarf is $B \leq 2.4 \times 10^6 \left(\frac{\mu_{32}}{3}\right) \left(\frac{R}{R_*}\right)^{-3}$ G, which is in agreement with the field strength inferred from the observed circular polarization of the optical light (Meintjes & De Jager 2000, Meintjes 2002).

The pulse timing analysis by de Jager et al. (1994) constrained the masses of the two stars (in solar units) to $M_1 = 0.9\left(\frac{\sin i}{\sin 55^\circ}\right)^{-3}$ and $M_2 = 0.6\left(\frac{\sin i}{\sin 55^\circ}\right)^{-3}$. The angle i is the inclination of the system or the angle between the normal to the plane of the binary and the observer. Welsh et al. (1995) constrained i to $55^\circ \pm 7^\circ$ and their best estimates for the masses are $M_1 = 0.89M_\odot$ and $M_2 = 0.57M_\odot$.

Simultaneous spectroscopic and photometric data of AE Aqr were acquired in 2001. The spectroscopic data were obtained using the William Herschel Telescope (WHT) and the photometry was carried out using the Jacobus Kapteyn Telescope (JKT), both situated on La Palma. Watson, Dhillon & Shahbaz (2006) analyzed the spectra in order to perform a Roche tomography reconstruction of the secondary star. They "unambiguously imaged, for the first time, large starspots on the secondary, the distribution of which is similar to other rapidly rotating low-mass stars". The analysis indicates a high degree of magnetic activity which must be due to an efficient dynamo, driven by the rapid (compared to solar) rotation. Also from their analysis estimates of the system parameters were made. The inclination angle and masses of the stars are $i = 66^\circ$, $M_1 = 0.74M_\odot$ and $M_2 = 0.5M_\odot$, respectively. These values are in reasonable agreement with previous estimates (e.g. Welsh et al. 1995), but the authors believe that the system parameters derived for AE Aqr are the most accurate to date.

1.2.2 Observational properties

AE Aqr has been observed in frequency range, from radio to infra-red, optical, UV, X-rays and TeV γ-rays. In the optical the red dwarf secondary dominates the emission, but flares in the V-band with magnitudes of $\Delta m_v \leq 2$ occur frequently. These large amplitude flares were previously described for example, as the result of magnetospheric gating onto the white dwarf from an accretion disc (Van Paradijs, Kraakman & Van Amerongen 1989); these flares are the origin of AE Aqr's novalike status.

AE Aqr and AM Her are the only CVs observed to be radio sources (Beasley et al. 1994). Figure 1.3 shows the characteristic variable optical (characterized as flaring) and radio emission in this system. Figure 1.4 indicates average flux values over a wide frequency range.

AE Aqr has been observed at radio frequencies from a few GHz to the mid Infra-red. The radio emission is highly variable and no periodicity was found (Bastian, Beasley & Bookbinder 1996). Bookbinder & Lamb(1987) found variation on time-scales ≤ 5 minutes and Abada-Simon et al. (1993) found variation over 1-2 hrs time-scale and occasional 5 min. variations. There may also be variation over a several month time-scale. The radio flares are not correlated with optical flares (Abada-Simon et al. 1995a,b). Bastian, Dulk & Chanmugam (1988) first explained the radio emission as non-thermal in origin. The authors determined the brightness temperature $T_B = \frac{S_\nu c^2 D^2}{2k\nu^2 \pi r_s^2}$, as $T_B \approx 10^8 - 10^{12}$ K. The value depends on the projected source size πr_s^2, the distance D and the flux density S_ν at frequency ν. The high value of T_B suggests that the emission is of non-thermal origin. The source is thought to be expanding clouds of relativistic electrons and

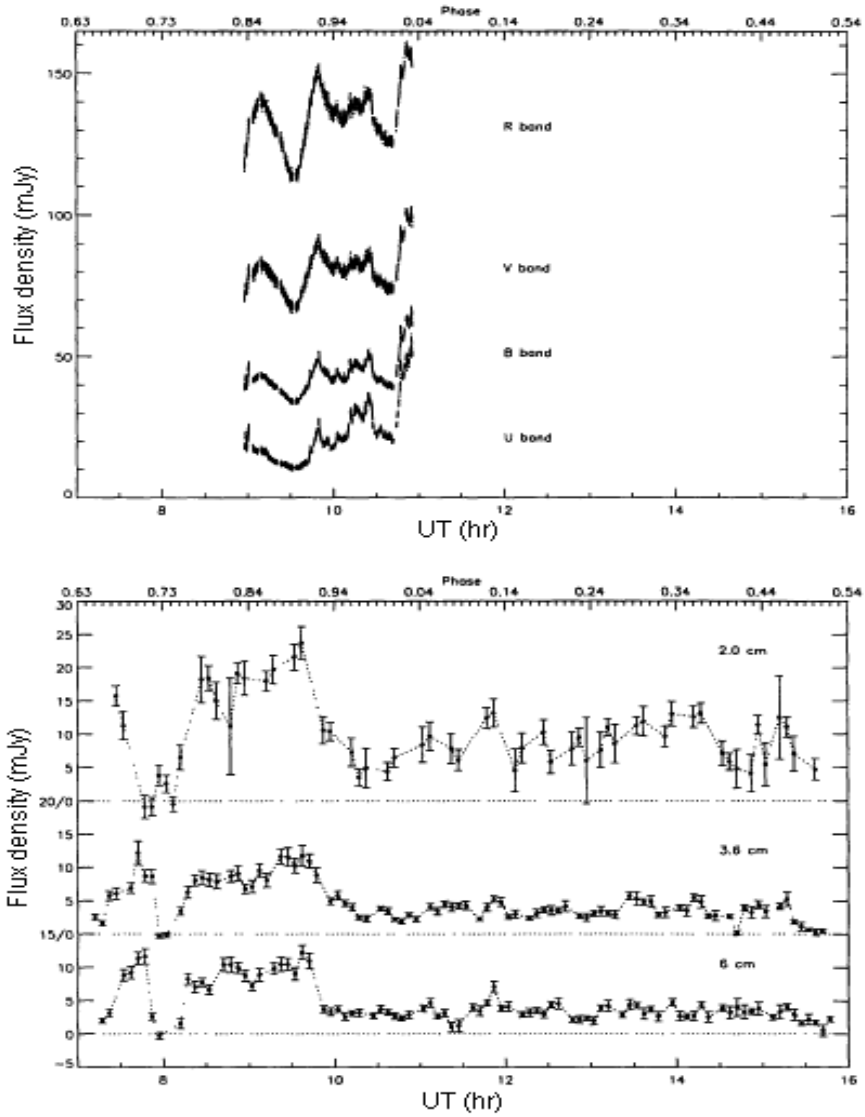

Figure 1.3: Simultaneous optical and radio lightcurves for AE Aqr (Abada-Simon et al. 1995)

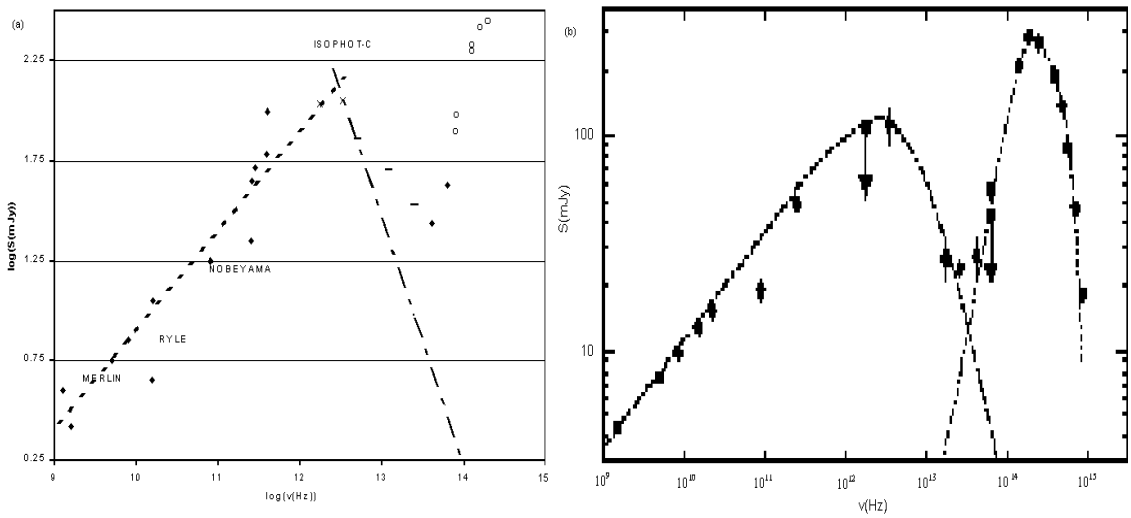

Figure 1.4: Average radio spectrum of AE Aqr ((a) Abada-Simon et al. 1999, (b) Dubus et al. 2004)

random frozen-in magnetic field emitting incoherent synchrotron emission. It has been shown (Abada-Simon et al. 1993, 1995, 1998, 2002) that the synchrotron spectrum shows a characteristic $S_\nu \propto \nu^{\alpha_1} (\alpha_1 \sim 0.5)$ self absorbed nature up to $\nu \sim$ few hundred GHz. This is reconcilable with a superposition of synchrotron flares (Bastian, Dulk & Chanmugam 1988). Recently it has been shown that the self-absorbed spectrum continues up to a few thousand GHz, after which it shows the optically thin synchrotron $\nu^{-\alpha_2}$ ($\alpha_2 \sim 1$) behaviour (Dubus et al. 2004). Figure 1.5 shows the variability of the mid-IR emission in AE Aqr (Dubus et al. 2004). Electrons, with mildly relativistic energies of 10-40 MeV, in blobs with fields of strength $B_{blob} = 300$ G, can radiate maximum synchrotron emission at frequencies of order $\nu_{max} \sim 10^{14}(\gamma/2)^2(B/B_{blob})$ Hz. This can account for the average spectrum (as seen in Fig. 1.4) with emission up to the mid-infrared range if a sufficient amount of electrons can be accelerated to the required energies.

In a series of papers (Meintjes & Venter 2003, Venter & Meintjes 2004, Meintjes & Venter 2005, Venter & Meintjes 2006) the transient radio synchrotron emission of AE Aqr was investigated. The radio flares were modelled in terms of expanding synchrotron emitting clouds, i.e. the so-called Van der Laan mechanism (Van der Laan 1963, 1966)(VDL). In a first attempt Meintjes & Venter (2003) proposed that blobs are magnetized as they leave the secondary at the L_1 funnel while advecting photospheric magnetic field. As the advected magnetized bubbles crash into the fast rotating magnetosphere, magnetic pumping in conjunction with magnetic reconnection and shocks can accelerate the trapped electrons in the clouds to relativistic energies (Meintjes & Venter 2003, Venter Meintjes 2004), resulting in expanding synchrotron clouds. However, in two follow-up papers (Meintjes & Venter 2005, Venter & Meintjes 2006) it was shown that the magnetized synchrotron bubbles are most probably the result of Kelvin-Helmholtz (KH) instabilities that develop at the interface between the fast rotating magnetosphere and the mass flow from the secondary star. This model combines the propeller ejection of gas from the system with the thermal and non-thermal emission. These mechanisms will form the backbone of this investigation and will be discussed in later chapters. In the Appendix a short discussion of synchrotron emission and the VDL model will be presented.

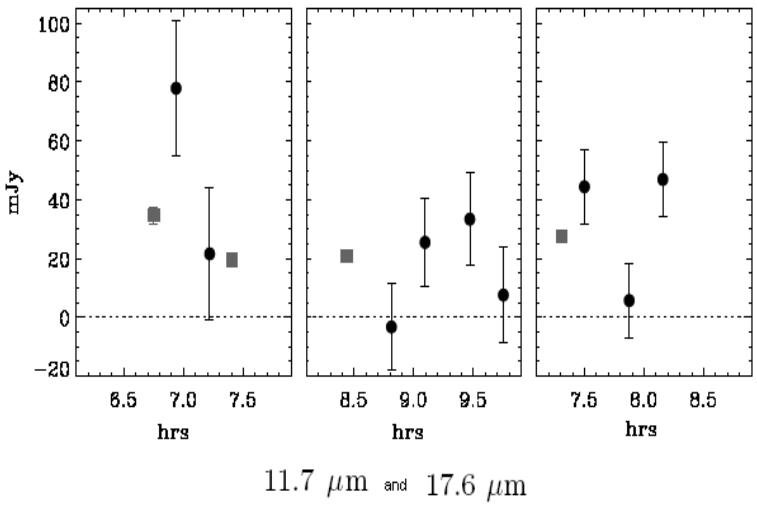

Figure 1.5: Infra-red detections of AE Aqr at two mid-IR frequencies showing high variability (Dubus et al. 2004).

Optical observations, both photometry and spectroscopy, provided the first information of AE Aqr's nature as a highly variable source showing continuous flares over a range of time-scales from minutes to hours. Faint $P_s = 33.08$ s pulsations in the optical are associated with the spin period of the white dwarf (Patterson 1979). This implies that AE Aquarii has the fastest rotating accreting white dwarf known. The rapid flaring in optical (e.g. Patterson 1979; van Paradijs et al. 1989) with the optical intensity varying between $m_v = 10$ - 12 on a regular basis, was initially believed to be the result of enhanced mass accretion onto the magnetic poles of the white dwarf. However, there is a weak correlation between the amplitude of the 33 s oscillation and increased intensity during optical outbursts (e.g. Patterson 1979; Meintjes 1992; Meintjes et al. 1994; O' Donoghue et al. 1995). This casts doubt on whether enhanced mass accretion is the source of the optical outbursts. Figure 1.6 shows lightcurves that are indicative of the highly variable optical emission from AE Aqr (Patterson 1979).

The system was intensively observed by the Hubble Space Telescope (*HST*) in the UV band (Eracleous et al. 1994). A very strong modulation at the 33 s rotation period was found, but no significant increase in the pulsed signal during strong outbursts was noted. The average luminosity was found to be $L_{UV} \sim 2 \times 10^{31}$ erg s^{-1}. This luminosity is assumed to be mainly the result of mass accretion onto the poles of the white dwarf. Jameson, King & Sherrington (1980) analyzed spectroscopic UV data and found strong emission lines of low and high ionization species. The emission lines originate at different sites in the system, possibly in the propeller ejected outflow. Figure 1.7 shows UV variation over a period of some 12 hours.

AE Aqr has been observed by a multitude of X-ray satellites, *EINSTEIN, EXOSAT, ROSAT* and *ASCA* and most recently by *XMM-Newton* and *Chandra* (2005 August, cf. Mauche 2006). Figure 1.8 shows the large variation that occur over timescales of a few hours in the X-ray luminosity. The *EINSTEIN* observation (Patterson et al. 1980) showed pulsations which had the same period and phase as that seen in optical data

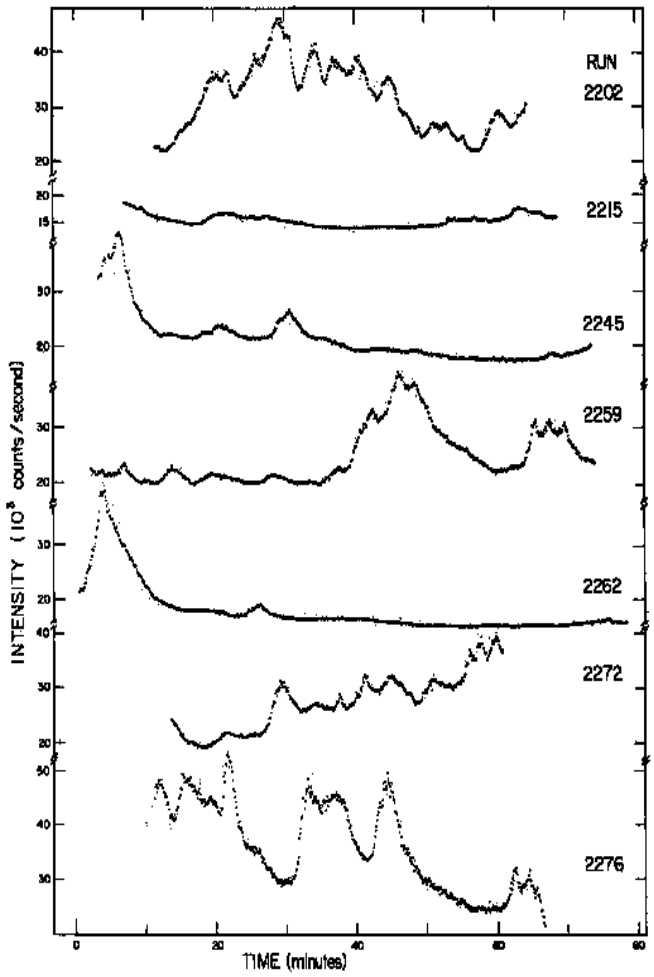

Figure 1.6: Optical lightcurves of AE Aqr (Patterson 1979). The highly variable emission is apparent.

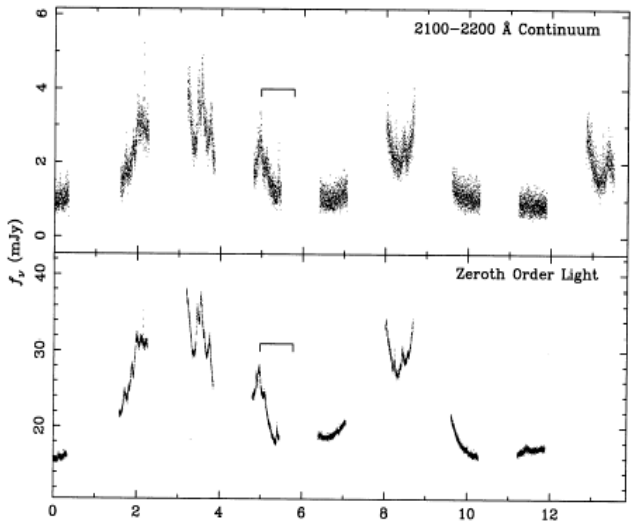

Figure 1.7: UV lightcurve from the HST over a total time of $\sim$ 12 hours (Eracleous et al. 1994)

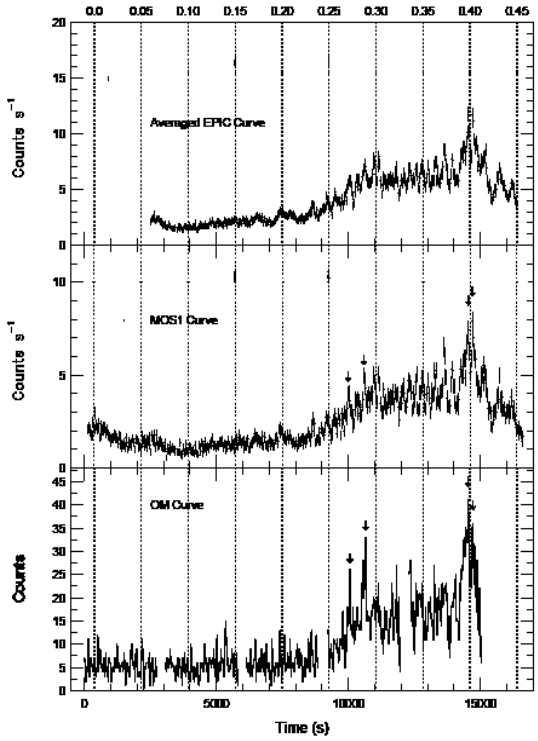

Figure 1.8: X-ray lightcurve from XMM-Newton(2001 data) over a total time of $\sim$ 4 hours (Choi & Dotani 2006)

(Patterson 1979). The pulsed emission was inferred as coming from an accretion hot spot on the surface of the rotating white dwarf. *ROSAT* observations (Reinsch et al. 1995, Clayton & Osborne 1995) showed that at low X-ray energies, the emission may be described by a single temperature thermal bremsstrahlung model (Eracleous 1999). Eracleous (1999) analyzed spectral X-ray data from *ASCA* and found that the average spectrum can be fit by a two temperature thermal plasma. The spectrum does not change when comparing flare and quiescent states. It has been proposed that the blob-like mass transfer from the secondary crashes into the magnetosphere of the white dwarf and gets shock heated to X-ray temperatures (e.g. Eracleous 1999).

Choi et al. (1999) reported results from X-ray observations of AE Aqr made with *Ginga* and *ASCA*. They find a clear sinusoidal pulse profile, but the pulse amplitude is relatively small, and the modulated flux remains nearly constant despite a factor of 3 change in the average flux during a flare. They also reproduce the time-averaged spectrum in the 0.4-10 keV energy band by a thermal emission model using two temperatures and using the same heating scenario as proposed by Eracleous(1999), i.e. interaction between the mass flow and the propeller.

The best spectral resolution thus far has been that obtained by *XMM-Newton* (Nov. 2001). Itoh et al. (2006) fit the spectra (see Figure 1.9) with a 4 temperature optically thin plasma model with temperatures T_x = 1-5 $\times$ 10^7 K and an average luminosity $L_X = 10^{31}$ erg s^{-1}. They measured the electron number density of the hot plasma to be $n_e \sim 10^{11}$ cm^{-3} by considering the intensity ratios in the He-like triplets of Nitrogen,

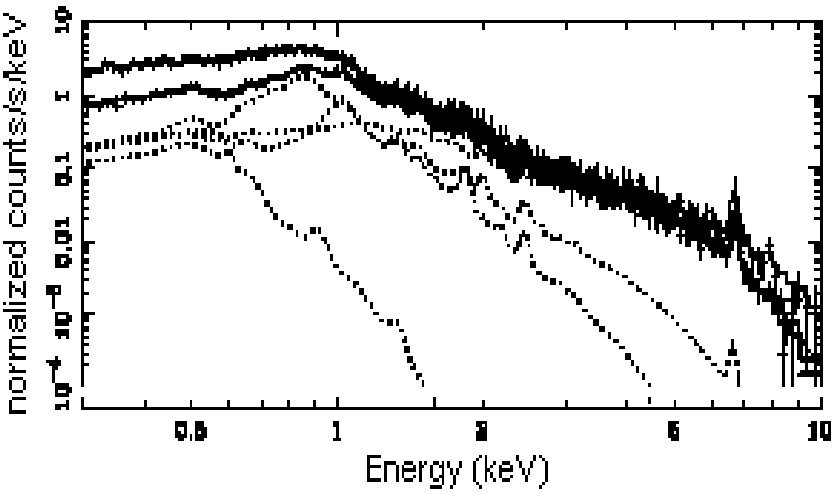

Figure 1.9: X-ray spectra from three XMM-Newton spectrometers fitted with a 4-temperature model (Itoh et al. 2006)

Oxygen and Neon. With this density and the total emission measure, EM = 1.29×10^{54} cm^{-3}, they found a linear scale of the plasma to be $l_x = (\mathrm{EM}/\mathrm{n}_e^2)^{1/3} \sim 5\times10^{10}$ cm. Considering the low density and large scale of the emitting plasma, Itoh et al.(2006) infers that the X-rays originate within the Roche lobe of the white dwarf due to expanding gas after being energized due to its interaction with the magnetospheric propeller.

TeV γ-ray observations (Meintjes et al. 1992, 1994; Bowden et al. 1992) showed occasional flare-like events with pulsations at or close to the spin period of the primary. The strongest flares had luminosity $\mathrm{L}_\gamma \sim 10^{34}$ erg s^{-1}. This would suggest that all of the spin-down power is occasionally directed into particle acceleration and TeV γ-ray emission. In the energy range $\mathrm{E}_\gamma > 1$ GeV the main source of γ-rays are the decay of π°-mesons from high energy collisions between ultra-relativistic protons with target gas. In Figure 1.10, arrows indicate the two strongest bursts in the TeV count rate as observed by Meintjes et al. (1994).

The transient non-thermal radio synchrotron and VHE γ-ray emission may indicate the presence of a very effective particle accelerator in the system. This has been the subject of intensive investigation (e.g. Meintjes et al. 1994, De Jager 1994, 1995, Meintjes & De Jager 1995, Kuijpers et al. 1997, Meintjes & De Jager 2000). For example, it has been suggested (Kuijpers et al. 1997) that magnetic pumping in the white dwarf magnetosphere can accelerate huge populations of electrons to mildly relativistic energies, which may be released through some instability, to form expanding synchrotron emitting clouds(VDL mechanism). However, this model fails to explain the acceleration of particles to TeV γ-ray energies or the kind of magnetospheric instability required to release such populations of electrons. The first attempt to explain the particle acceleration in context of the propeller mechanism was presented by Meintjes & De Jager (2000). These authors showed that the MHD power dissipated in the boundary layer between the magnetosphere and flow can result in magnetic reconnection and double layer formation (e.g. Priest & Forbes 2000, Priest 1981, Aly & Kuijpers 1990, Hamilton, Lamb & Miller 1994), which can result in the acceleration of electrons and protons(ions) to energies E > 1 TeV. These authors also showed that under certain conditions, exploding

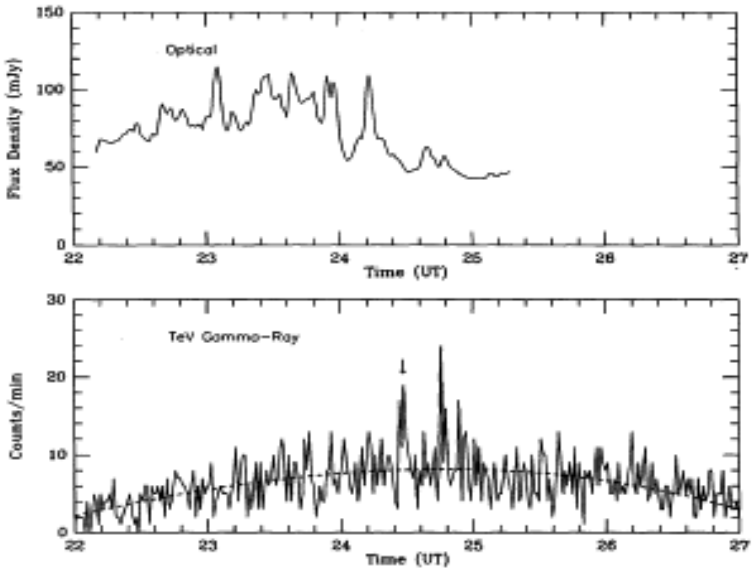

Figure 1.10: The optical lightcurve and the simultaneous TeV count rate profile showing at least two bursts (Meintjes et al. 1994)

double layers can result in an impulsive release of TeV particles with luminosity $L \sim P_{MHD} \sim 10^{34}$ erg s^{-1}, explaining the observed burst-like TeV emission (Meintjes et al. 1994).

Outline of thesis:

Chapter 1 presented a qualitative discussion as an introduction.
Chapter 2 contains a more quantitative discussion related to mass transfer and accretion modes in the magnetic cataclysmic variables, with special emphasis on possible magnetospheric propelling, is presented in the next chapter. A qualitative discussion of the magnetospheric drag model (Wynn, King & Horne 1997) is presented, with particular focus on the magnetohydrodynamics of magnetospheric drag and its observational consequences.

The lack of observational support for the magnetospheric drag of large diamagnetic blobs, especially surface heating, justifies the alternative model proposed by this study as presented in Chapter 3 (Section 3.4).

Chapter 2

Accretion in Magnetic Cataclysmic Variables (mCVs)

It has been mentioned in Chapter 1 that the current low ratio of accretion power to spindown power in AE Aqr, i.e. $\alpha = \frac{L_{acc}}{L_{sd}} \sim 0.1\%$, as well as the transient emission properties of the system, can be integrated into a single unified model, namely a magnetospheric propeller process (e.g. Meintjes and de Jager 2000). The underlying driving mechanism of the propeller process is the angular momentum exchange between a faster rotating magnetosphere and slower orbiting plasma. This process may be common to many astrophysical environments and may manifest itself in many different guises.

In this chapter the fundamental properties of magnetospheric accretion in close binaries (as applied to the magnetic cataclysmic variables), as well as the magnetospheric propeller process will be discussed. A magnetospheric propeller may operate in systems with or without discs and therefore the basic properties of disc and disc-less accretion will be reviewed. Different manifestations of propellering applicable to each mode of accretion will be discussed. A more detailed discussion of the propellering associated with disc-less accretors, of which AE Aqr is an example, will follow. The magnetospheric drag model (e.g. King 1993, Wynn & King 1995), which has been used to explain (quantify) the propeller in AE Aqr, will also be reviewed. The strengths and weaknesses of the drag process will be highlighted in order to put the fundamental contribution of this thesis, namely the proposed Kelvin-Helmholtz driven MHD propeller process, into perspective. The strength of the latter process lies in that it provides a theoretical framework within which the propeller as well as the total thermal and non-thermal emission of the system can be incorporated.

2.1 Mass transfer and accretion in magnetic CVs

Accretion in close binaries invariably is initiated by mass flow from one star to its companion. The principal mode of mass transfer in the mCVs is via the Roche lobe overflow of a somewhat evolved secondary star. The basic properties of this process is reviewed here.

The main driving mechanism behind the transient, eruptive nature of the emission in AE Aqr and mCVs

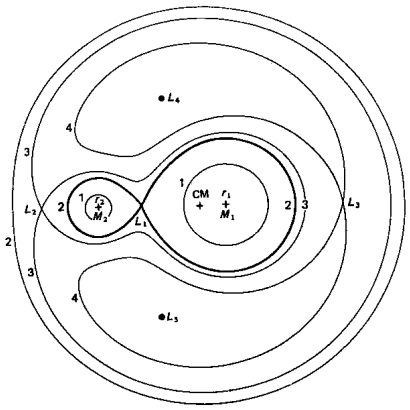

Figure 2.1: Diagram showing the Roche equipotentials in a close binary (Frank, King & Raine 2002)

in general is the gravitational interaction between the stellar components of these systems. The short orbital periods of these systems, i.e.$\mathrm{P}_{orb} \leq$ few $\times 10$ hours, implies that these systems are extremely compact. In fact, it can be shown, using Kepler's 3rd law, that these systems have typical binary separation (e.g. Frank, King & Raine 2002, p. 49)

$$a \approx 3.5 \times 10^{10} \left(\frac{\mathrm{P}_{orb}}{hr}\right)^{2/3} \left(\frac{M_1}{M_\odot}\right)^{1/3} (1+q)^{1/3}\mathrm{cm}, \tag{2.1}$$

where $q = M_2/M_1$ represents the mass ratio and M_1 represents the primary mass in solar units. It is clear that for $\mathrm{P}_{orb} \leq 10$ hrs and $q \sim 0.5$, $a/D_\odot \leq 1$, where $D_\odot \sim 1.4 \times 10^{10}$ cm is the diameter of the Sun. Therefore these systems can readily fit into the Sun.

The gravitational interaction between the stellar components in compact binaries is extremely complex, but a reasonably accurate approach is to consider the two stellar components as point masses, applying the so-called Roche gravitational potential, i.e.

$$\Phi_R = -\frac{GM_1}{|\mathbf{r}-\mathbf{r_1}|} - \frac{GM_2}{|\mathbf{r}-\mathbf{r_2}|} - \frac{1}{2}(\mathbf{\Omega_{orb}} \times \mathbf{r})^2 \tag{2.2}$$

where $\mathbf{r}_1$, $\mathbf{r}_2$ and $\mathbf{r}$ represent the coordinate vectors from the centre of mass (CM) of the system to the centre of the primary, secondary and arbitrary point P, respectively. A schematic representation of the Roche potential in a close binary is given in Figure 2.1. The effective gravity at an arbitrary point P in the system then is

$$\begin{aligned} \mathbf{g_{eff}} &= -\nabla\Phi_R \\ &= \frac{GM_1}{|\mathbf{r_1}-\mathbf{r}|^2}\hat{e}_1 + \frac{GM_2}{|\mathbf{r_2}-\mathbf{r}|^2}\hat{e}_2 + \Omega_{orb}^2\mathbf{R}, \end{aligned} \tag{2.3}$$

where $\mathbf{R}$ represents the horizontal component of $\mathbf{r}$ in the equatorial plane and $\hat{e}_1$ and $\hat{e}_2$ represent the unit vectors directed from P to the centres of the primary and secondary respectively. If the y-axis represents the axis through the centres of the two stars (x; z = 0), the effective gravity anywhere between the two stars can be estimated, i.e.

$$\mathbf{g}_{y,eff} = \frac{GM_1}{(y_1-y)^2}\hat{e}_{y_1} + \frac{GM_2}{(y_2-y)^2}\hat{e}_{y_2} + \Omega^2 y\hat{e}_y. \tag{2.4}$$

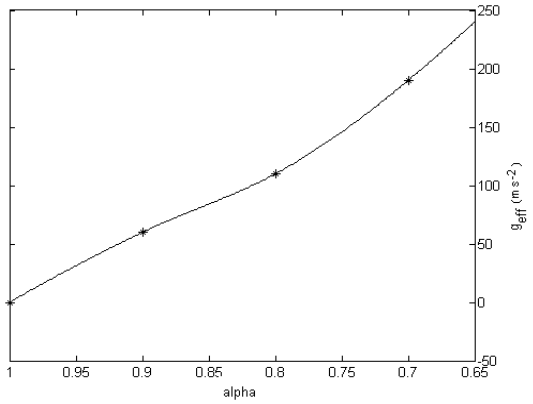

Figure 2.2: Effective gravity on the line of centres inside the Roche lobe of the primary star

The effective gravity between the two stars, in the Roche lobe of the primary, can be obtained with reasonable accuracy (Meintjes 2002) using the parameterization, i.e.

$$\mathbf{g}_{y,eff} = \frac{GM_1}{(\alpha b_1)}\hat{e}_{y_1} + \frac{GM_2}{(a-\alpha b_1)^2}\hat{e}_{y_2} + \Omega_{orb}^2 y\hat{e}_y \tag{2.5}$$

where α represents the fractional distance from the point P with respect to the distance of L_1 from the primary, i.e. $b_1 = (0.5 - 0.277\log_e q)a$ (Frank, King & Raine 2002, p. 54). For illustrative purposes the effective gravity on the line of centres (the L_1 point is represented by $\alpha = 1$), is plotted in Figure 2.2 (values listed in Table 1) for AE Aqr.

α	$\mathbf{g}_{eff}(ms^{-2})$	x $= g_{eff}/g_{earth}$
1	0	0
0.9	60	6
0.8	110	11
0.7	190	19

Table 1: Calculated values of the effective gravity at a few distances from the L_1 point in the primary's Roche lobe. The third column represents the ratio x of the effective gravity with respect to the gravitational acceleration on Earth, i.e. $g_{earth} \approx 10$ m s^{-2}.

This analysis illustrates that the photosphere of a lobe-filling secondary star will experience zero effective gravity in the immediate vicinity of the L_1 region. If the separation between the photosphere and the L_1 region is of the order of the pressure scale height of the secondary star, that is $\frac{R_{L_1}-R_{2,*}}{H_p} \sim 1$, thermal motions will carry gas particles across the L_1 region. This will result in a ballistic stream plunging into the Roche lobe of the primary. Considering the conservation of mass flux, it can be shown that the mass flow rate through the funnel around the L_1 point is

$$-\dot{M}_2 = \frac{1}{4\pi}\rho_{L_1} c_s^3 P_{orb}^2 \tag{2.6}$$

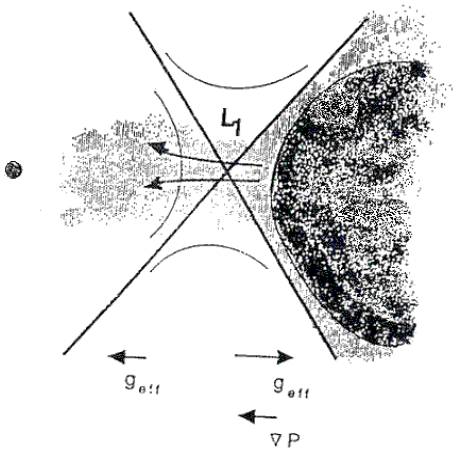

Figure 2.3: Diagram of the L_1 region (Shore 1992). A pressure gradient can push material across the L_1 point, at which point the gravitational potential of the primary star becomes significant.

where

$$\rho_{L_1} \approx \frac{1}{\sqrt{e}} \rho_{phot} \exp\left[-\left(\frac{R_{L_1} - R_{2,*}}{H_p}\right)\right] \tag{2.7}$$

and $\rho_{phot} \approx 10^{-6}$ g cm^{-3} (Frank, King & Raine 2002, p. 353) represents the typical photospheric density of lobe-filling secondaries. R_{L_1} and $R_{2,*}$ represent the distance of the L_1 point from the centre of the secondary and the photospheric radius of the secondary, respectively. The pressure scale height, H_p, is given by

$$H_p \approx c_s^2 R_{2,*}^2 / GM_2 \sim 10^7 \text{cm}$$

(that is $\frac{H_p}{R_{2,*}} \sim 10^{-4}$).

The gas flows across the zero gravity region with a velocity that is limited by the local sound speed. However, while falling into the Roche lobe of the primary, it accelerates continuously as it plunges deeper into the potential well. Figure 2.3 shows the L_1 region where material is pushed into the primary's Roche lobe by thermal motions.

Secondary stars in mCVs have photospheric temperatures T $\sim$ 3000-4000 K, with orbital periods $P_{orb} \leq$ 10 hours and $\frac{R_{L_1} - R_{2,*}}{H_p} \sim 3.5$ [for AE Aqr, Meintjes (2004)], resulting in typical mass transfer rates of the order of

$$\dot{M}_2 \leq 4 \times 10^{17} \left(\frac{c_s}{6 \times 10^5 \text{cm s}^{-1}}\right)^3 \left(\frac{P_{orb}}{10\text{hr}}\right)^2 \text{g s}^{-1}.$$

The fate of the mass flow, accelerating in the primary's Roche lobe, is either to be accreted directly or through an accretion disc or to be ejected/propelled from the Roche lobe. A brief discussion of the major constraints determining the mode of mass accretion will be presented.

2.2 Modes of mass accretion in mCVs

It has been mentioned that the mass transfer via Roche lobe overflow is driven by the thermal motions of the photospheric plasma across the L_1 point, which is constrained by the local sound speed (typically of the

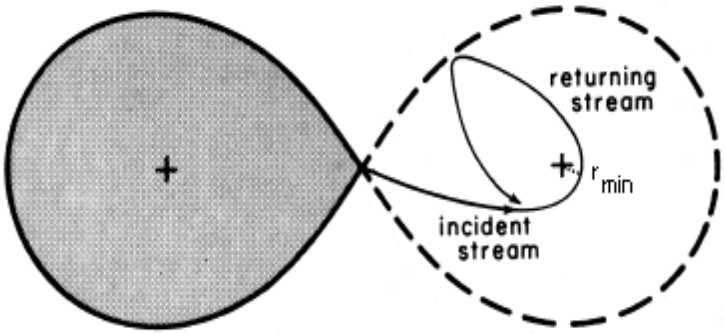

Figure 2.4: Trajectory of mass transfer flow inside a weakly magnetic primary star's Roche lobe (Lubow & Shu 1975)

order of $c_s \sim 10$ km s^{-1} for K-M type stars). However, the L_1 point is orbiting the centre-of-mass with a velocity of the order of $v_\phi \sim 100$ km s^{-1}. Therefore, the mass transfer stream crossing the L_1 point is injected into the Roche lobe of the primary with an enormous specific angular momentum, i.e.

$$j_\phi = v_\phi r_{L_1} \sim 10^{19}\mathrm{cm}^2\mathrm{s}^{-1},$$

where $r_{L_1} \sim 10^{11}$ cm (for AE Aqr) represents the distance of the L_1 point from the centre of the primary. The stream thus swings into orbit around the compact object due to the conservation of angular momentum, in conjunction with the Coriolis effect, rather than flowing directly towards it (Frank, King & Raine 1992, p. 81). The stream then follows a trajectory determined by the injection velocity and the gravity of the compact object (e.g. Lubow & Shu 1975), which is illustrated in Figure 2.4.

The mode of interaction of the stream along its trajectory, keeping in mind the large specific angular momentum, depends on the physical size of the primary star and/or its magnetosphere. For example, in the Algol systems the mass accreting star occupies a significant fraction of the volume of its Roche lobe. The mass flow therefore rams directly into it at supersonic velocities, which is the mechanism behind the peculiar transient emission these systems display and the reason for the name carried by these systems (Algol: The Devil's star). If the primary star is a magnetized compact object, as is the case in magnetic CVs, the interaction of the mass flow with the compact object will be controlled by the extent of the magnetosphere, which is determined by the magnetic dipole moment $\mu = B_s R_*^3$ of the primary star. In the absence of a magnetospheric field, the stream will settle in an orbit conserving its initial angular momentum, i.e. it will settle at the circularization radius, given by (Frank, King & Raine 2002 (FKR), p. 60),

$$\begin{aligned} \frac{R_{circ}}{a} &\approx (1+q)\left(\frac{b_1}{a}\right)^4 \\ &\approx (1+q)[0.5 - 0.277 \ln q]^4 \end{aligned} \tag{2.8}$$

where a represents the orbital separation, $q = M_2/M_1$ and (b_1/a) (Warner 1995, p. 33), the distance of the L_1 point from the white dwarf relative to a. It can be shown that for $q \leq 1$ (which usually does apply),

$$\frac{R_{circ}}{a} \sim 0.13 \quad [q = 1].$$

The approximate radial extent of the Roche lobe of the white dwarf is given by (FKR)

$$\begin{aligned} \frac{R_1}{a} &= \frac{0.49q^{-2/3}}{0.6q^{-2/3}+\ln(1+q^{-1/3})} \\ &\approx 0.4 \quad [q=1], \end{aligned} \tag{2.9}$$

showing that $R_{circ} < R_1$. In fact it can be shown that for all $q \leq 1$, $R_{circ}/R_1 \leq 1$. This shows that for all mass ratios ($q \leq 1$) applicable to mCVs, the stream can settle into an orbit around the compact object that fits into its Roche lobe.

However, if the primary has a significant magnetospheric field, the stream may be intercepted before it can settle at R_{circ}, and be dominated by the magnetic pressure. If the ram pressure of the flow significantly dominates the field at R_{circ}, the stream can settle in a ring which may spread into an accretion disc as a result of viscosity.

In mCVs the categories of disc-less and disc accretors are contained in

- Disc-less systems → Polars (or AM Her systems)
- Accretion disc systems → Intermediate polars and DQ Her systems

The basic constraints related to the mass accretion will briefly be reviewed.

2.2.1 Disc-less accretors: The Polars

The Polars or AM Herculis stars are a subclass of the mCVs where the white dwarfs possess magnetic fields $B_* \approx 15-56$ MG, confirmed by Zeeman splitting and polarization measurements (Schmidt 1999). The strong magnetic field of the white dwarf has two important consequences :
i) Polars are synchronously rotating systems ($P_{spin} = P_{orb}$), with orbital periods $P_{orb} \sim 18-222$ minutes (e.g. Chanmugam & Ray 1984). This phase locked interaction is the direct result of the strong magnetic interaction between the white dwarf and the secondary star.
ii) The short orbital periods ($P_{orb} \leq 3$ hrs) and the strong fields imply a small binary separation and an extended magnetosphere. This results in the interception of the mass flow from the secondary star by the significant magnetospheric field of the white dwarf. The stream then pushes through the magnetosphere until the magnetospheric pressure dominates the ram pressure of the flow which is now channeled onto one or both poles of the primary.

Evolutionary models (e.g. Warner & Wickramasinghe 1991) show that for disc-less accretion and magnetic locking to occur in mCVs, the magnetic moment $0.4 \leq \mu_{34} \leq 7$ [in units of 10^{34} Gauss cm^3], for mass transfer rates $\dot{M}_2 \leq 10^{18}$ g s^{-1}. This shows that disc-less accretion occurs in these compact binaries ($P_{orb} \leq 4$ hrs) if the white dwarf has a surface field

$$B_* \geq 10\frac{\mu_{34}}{R^3_{*,9}}\text{MG}$$

where $R_{*,9}$ represents the radius of the white dwarf in units of 10^9 cm.

It has been mentioned that the magnetosphere channels the flow to one or both poles of the white dwarf. Close to the surface of the white dwarf the highly supersonic flow is shock heated to temperatures $T_{ps} \sim 10^8$ K in the post shock region (above the surface) of the stand-off shock (see Figure 2.5). This

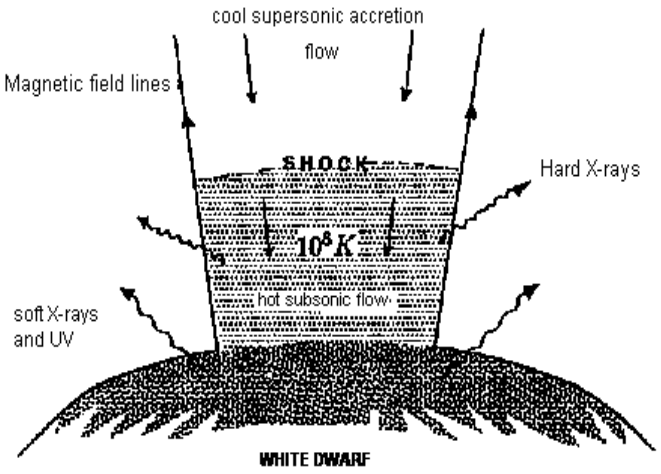

Figure 2.5: The accretion column and shock above the surface of an accreting primary star (FKR from Watson 1986)

facilitates the release of the enormous amount of gravitational potential energy in the form of heat and radiation (e.g. Kuijpers & Pringle 1982).

The radiation released in the accretion process is characterized by
i) highly polarized optical and IR emission (from this the name Polars),
ii) intense soft, and in some cases, hard X-ray emission,
iii) an emission line spectrum that reflects the large streaming motion of the accreted matter in the magnetosphere of the white dwarf (e.g. Beuermann 1988).

2.2.2 Disc accreting systems : The Intermediate Polars (IPs) and DQ Her stars

The IPs and DQ Her systems are both asynchronous rotators ($P_{spin} \neq P_{orb}$) with rotation periods $P_{spin} > 100$ sec (IPs) and $P_{spin} < 100$ sec (DQ Hers), and orbital periods $P_{orb} > 3$ hrs (Warner 1995). The white dwarfs in these systems have magnetic fields $B_* \leq 10$ MG ($\mu_{33} \sim 1$) in IPs and $B_* \sim 1$ MG ($\mu_{33} \sim 0.1$) in DQ Hers. The emission from IPs are characterized by the presence of hard X-rays, which is absent in the DQ Her systems. This is also why AE Aqr has been classified as a DQ Her system.

The weaker white dwarf field (compared to Polars) and the wider binary separation ($P_{orb} > 3$ hrs) imply a noticeably weaker magnetospheric influence on the mass transfer stream, depending ultimately on the mass transfer variations in these systems. For example, Warner & Wickramasinghe (1991) showed that cyclic variation between lower and higher mass transfer states in IPs, results in corresponding disc and disc-less accretion. The short spin periods in DQ Her stars implicitly indicates that these systems are predominantly disc accretors, where accretion disc torques (e.g. Wang 1987) have spun up the white dwarfs to periods $P_{spin} \ll P_{orb}$. For example, it can be shown (Wang 1987) that accretion disc torques can spin the white dwarf (in DQ Her stars) up to these short periods over time-scales

$$t_{s-u} \sim 2 \times 10^6 \mu_{32}^{-8/7} \dot{M}_{18}^{-3/7} \mathrm{yr},$$

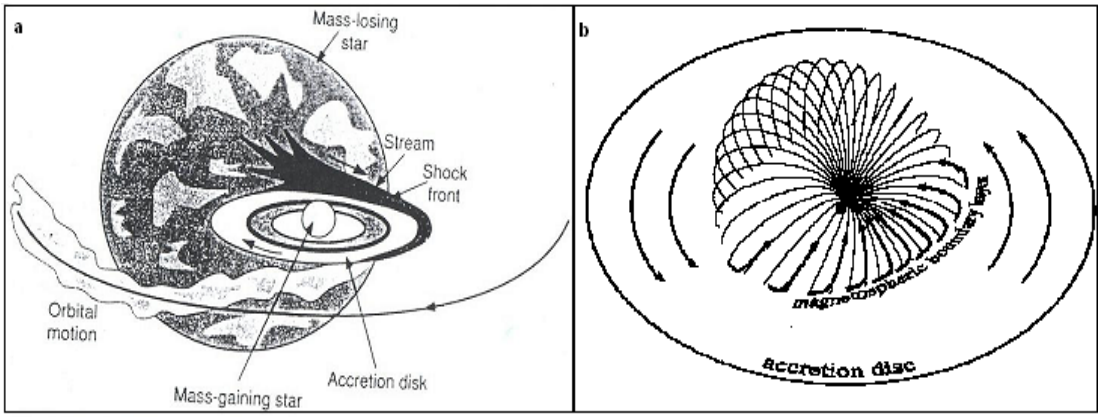

Figure 2.6: A schematic representation of accretion disc formation in the immediate vicinity of a) unmagnetized white dwarf (e.g. Shore 1992) and b) a magnetized white dwarf (e.g. FKR). It is apparent from (b) that the extent of the magnetosphere determines the inner boundary of the accretion disc.

where μ_{32} represents the magnetic moment of the white dwarf and $\dot{M}_{18}$ the accretion rate onto the star (in units of 10^{18} g s^{-1}).

It has been shown (Hameury, King & Lasota 1989) that variations in the mass transfer from the secondary star (i.e. $\dot{M}_2$) can vary by a factor $\alpha = \frac{\dot{M}_{max}}{\dot{M}_{min}} \sim 10^5$ over time scales similar to the spin-up time scale. These mass transfer variations drives the IPs to cycle between disc and disc-less accretion phases. For example, a noticeable decrease in the mass transfer rate from the secondary in a disc-accreting IP can allow the magnetosphere to gradually push the disc inner edge outward to distances exceeding the corotation radius, resulting in a gradual spin-down of the white dwarf. The system will also enter an "accretion inhibited" phase, since the disc material outside the corotation radius will experience a huge centrifugal expulsion as it attempts to follow the field lines to the surface of the star. This defines so-called magnetospheric propeller action by an accreting magnetized white dwarf. Magnetospheric propeller action plays a fundamental role in the spin evolution of the white dwarfs in mCVs, which also implicitly influences the binary evolution (e.g. Meintjes 2002). The process may also be driving the spin-down of the white dwarf and the peculiar transient emission in AE Aqr. Therefore, this propeller mechanism will be discussed in a more quantitative manner.

2.3 The magnetospheric propeller

Fundamentally a magnetospheric propeller is a process wherein angular momentum is transferred to orbiting gas (or micro gas parcels). The specific angular momentum associated with orbiting gas is

$$\begin{aligned} j_\phi &\approx v_\phi r \qquad [v_\phi = r\Omega_K] \\ &\approx \Omega_K r^2 \\ &\approx (\mathrm{GM}r)^{1/2} \end{aligned} \tag{2.10}$$

where $\Omega_K = (\mathrm{GM/r^3})^{1/2}$ represents the Keplerian velocity of gas orbiting the compact object. Since $j_\phi \propto r^{1/2}$, it can be seen that continuous transfer of angular momentum to the gas will result in it orbiting at

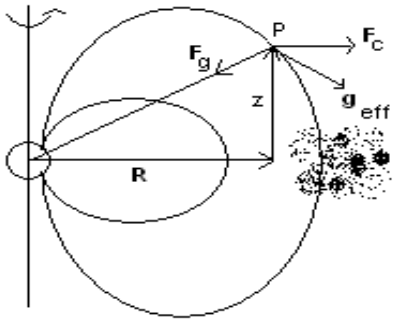

Figure 2.7: Simple sketch of the geometry of corotating field lines in a cylindrical coordinate frame

ever increasing radius, until it leaves the system completely. A very effective propeller mechanism therefore would imply the ejection of large quantities of gas from the binary system.

The magnetospheric transfer of angular momentum can also be explained in terms of the effective gravity of the gas (or plasma), trapped in the rotating magnetosphere, experiences. A quantitative discussion of the basic properties of this process now follows.

Consider a fast rotating compact object interacting with orbiting material in the equatorial plane (see Figure 2.7) As the field sweeps across the orbiting clumps of material (or disc), small parcels of plasma attache themselves to the field lines. The following analysis focuses on the centrifugal effect these parcels experience.

The effective potential for plasma trapped in the magnetosphere at point P can be determined by evaluating

$$\begin{aligned} \Phi_{eff} &= \Phi_{grav} - \frac{1}{2}|\mathbf{\Omega}_* \times \mathbf{R}|^2 \\ &= \Phi_{grav} - \frac{1}{2}\Omega^2 R^2 \sin\theta \\ &= \Phi_{grav} - \frac{1}{2}\Omega^2 R^2 \quad (\theta = 90^\circ) \end{aligned} \tag{2.11}$$

where Ω is the angular velocity the field lines. The effective gravity then is $\mathbf{g}_{eff} = -\nabla\Phi_{eff}$. In a cylindrical coordinate system we can write

$$\Phi_{grav} = -\frac{GM}{(R^2+z^2)^{1/2}} \tag{2.12}$$

$$\Phi_{centrif} = -\frac{1}{2}\Omega^2 R^2. \tag{2.13}$$

Hence

$$\Phi_{eff} = -\frac{GM}{(R^2+z^2)^{1/2}} - \frac{1}{2}\Omega^2 R^2 \tag{2.14}$$

resulting in an effective gravity given by

$$\begin{aligned} \mathbf{g}_{eff} &= -\nabla\Phi_{eff} \\ &= \left[\left(\frac{\partial}{\partial R}\Phi_{eff}\right)\hat{e}_R + \frac{1}{R}\left(\frac{\partial}{\partial\phi}\Phi_{eff}\right)\hat{e}_\phi + \left(\frac{\partial}{\partial z}\Phi_{eff}\right)\hat{e}_z\right] \end{aligned}$$

$$
\begin{aligned}
&= \frac{\partial}{\partial R}\Phi_{eff}\hat{e}_R + \frac{\partial}{\partial z}\Phi_{eff}\hat{e} \quad \text{[axial symmetry]} \\
&= -\frac{GM}{(R^2+z^2)^{3/2}}(R\hat{e}_R + z\hat{e}_z) + \Omega^2 R\hat{e}_R \\
&= -\frac{GM}{r^3}\mathbf{r} + \Omega^2 R\hat{e}_R \\
&= -\frac{GM}{r^2}\hat{e}_r + \Omega^2 R\hat{e}_R \qquad (2.15)
\end{aligned}
$$

where $\mathbf{r} = R\hat{e}_R + z\hat{e}_z$ and $\hat{e}_r = \frac{\mathbf{r}}{|\mathbf{r}|}$. It can be seen that plasma tied to the fields lines through the Lorentz force may, under certain circumstances, experience significant centrifugal expulsion. Two regimes can be distinguished

1) $z \gg R$ and $\Omega \to \Omega_*$ [field lines corotate with star]

2) $z \ll R$ and $\Omega \to \Omega_*$ [field lines corotate with star] .

In these two regimes the effective gravity can be written as

$$
\begin{aligned}
\mathbf{g}_{eff} &= -\frac{GM}{z^2}\hat{e}_z + \Omega_*^2 R\hat{e}_R \quad [z \gg R] \qquad (2.16) \\
&= -\frac{GM}{R^2}\hat{e}_R + \Omega_*^2 R\hat{e}_R \quad [z \ll R] \qquad (2.17)
\end{aligned}
$$

From both these equations it can be seen that a dominant centrifugal component above and in the equatorial plane may result in an outward directed effective gravity. This will result in material trapped in, or attached to a fast rotating field, being centrifugally driven from the system, which is the basis of magnetospheric propeller action.

The condition to satisfy $\mathbf{g}_{eff} > 0$ in the orbital plane ($z \ll R$) is

$$
\left[-\frac{GM}{R^2} + \Omega_*^2 R\right]\hat{e}_R \geq 0
$$

$$
\begin{aligned}
\Rightarrow \quad \Omega_*^2 R &\geq \frac{GM}{R^2} \\
\Omega_* = \frac{2\pi}{\mathrm{P}_*} &\geq \left(\frac{GM}{R^3}\right)^{1/2} \\
\mathrm{P}_* &\leq \frac{2\pi}{\sqrt{GM/R^3}} \qquad (2.18)
\end{aligned}
$$

Using this equation the rotation period of potential propeller systems can be constrained. Plasma or small parcels of gas attached to corotating field lines in regions corresponding to the circularization radii in the IPs ($\mathrm{R}_{circ} \sim 0.15a$ for q ~ 0.5 and $a \sim 10^{11}\left(\frac{\mathrm{P}_{orb}}{5hrs}\right)^{2/3}$ cm), will experience magnetospheric propeller action for white dwarf rotation periods

$$
\mathrm{P}_* \leq 1000\left(\frac{M}{M_\odot}\right)^{-1/2}\left(\frac{R}{R_{circ}}\right)^{3/2} \text{sec}, \qquad (2.19)
$$

which is reconcilable with the spin periods of white dwarfs in IPs and DQ Her stars.

The large (factor $\alpha \sim 10^5$) variations of the mass transfer rate from the secondary stars in mCVs combined with the magnetospheric propeller may produce a range of outcomes. One can imagine a scenario

of anomalously low mass transfer rates which allows the magnetosphere to bring plasma (or minute parcels of gas) into corotation (or close to) at larger radial distances R, from the compact object. Since $P_* \propto R^{3/2}$, the effective gravity $\mathbf{g}_{eff} > 0$, even for slower rotating magnetospheres. Therefore, the magnetospheric propeller may even eject plasma accelerated azimuthally to Keplerian periods satisfying the period relation above.

The centrifugal acceleration of material as discussed above, depends on material corotating with the magnetic field of the central rotating object. The effectivity of the magnetospheric propeller process is determined by the efficiency of angular momentum transfer to orbiting plasma or gas parcels via the magnetospheric field. Since $B(r) \propto r^{-3}$, this process is limited to the magnetospheric zone where the force-free condition holds, i.e. where the field lines are allowed to corotate with the compact white dwarf. Outside this zone, the plasma will dictate the dynamics and will not continue to corotate with the field.

An interesting consequence of the centrifugal magnetospheric propeller is that it also results in jet formation under *s*pecial conditions. According to the analysis above, the R-component [cylindrical coordinates] of the effective gravity of a bulk outflow with a finite z-velocity and residual angular velocity Ω_{out}, can be obtained as follows.

$$\begin{aligned} \mathbf{g}_{eff} &= -\frac{GM}{r^3}\mathbf{r} + \Omega_{out}^2 R\hat{e}_R \\ &= -\frac{GM}{(R^2+z^2)^{3/2}}(R\hat{e}_R + z\hat{e}_z) + \Omega_{out}^2 R\hat{e}_R \end{aligned} \tag{2.20}$$

or where

$$g_{grav}\hat{e}_R = -\frac{GMR}{(R^2+z^2)^{3/2}}\hat{e}_R$$

$$\text{and} \quad g_{cent}\hat{e}_R = \Omega_{out}^2 R\hat{e}_R = (v_\phi^2/R)\hat{e}_R$$

are the R-components.

Therefore if the gravity component (inwards) is to dominate we have

$$\begin{aligned} |g_{grav}| &> |g_{cent}| \\ \frac{GMR}{[R^2(1+(z/R)^2]^{3/2}} &> \Omega_{out}^2 R \\ \Rightarrow \quad \frac{GM}{R^2[1+(z/R)^2]^{3/2}} &> \Omega_{out}^2 R \end{aligned} \tag{2.21}$$

It can be seen that pairs of sufficiently small R and z values exist that satisfy this inequality, which would indicate that an outflow (with say a positive z-velocity) that originates anywhere from the magnetosphere (possibly also as a result of propeller action), will be collimated to the spin axis of the rotating propeller, i.e. a well collimated jet will be formed.

The effect discussed above, here simplified substantially, with the addition of magnetic pressure effects (not within the context of this discussion), may explain the jets from the subclass of protostars, the so-called Herbig Haro objects, as well as the microquasar phenomenon (e.g. Matsumoto et al. 1998). To illustrate this a brief discussion is presented.

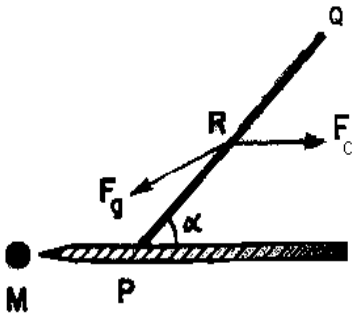

Figure 2.8: Diagram of a field line anchored in an accretion disc (Choudhuri 1998). M represents a central mass, PQ is a magnetic field line anchored in a disc around M. A particle on the field line is subject to a gravitational and a centrifugal acceleration.

2.4 Propeller driven mass outflow in disc-accreting systems

The micro-quasar and Herbig-Haro phenomenon

Elaborating on the principle discussed above, Blandford & Payne (1982), in a more refined analysis, presented the fundamental principles of magnetospheric propellering from well developed accretion discs. Their analysis of centrifugal propelling of material from accretion discs lay the foundation for the Herbig-Haro and microquasar phenomena (observed bipolar jets), which will briefly be reviewed.

Consider a magnetized star or compact object accreting from a well developed accretion disc (see Figures 2.8 and 2.7). Particles in the magnetic field find themselves in a rotating reference frame. A magnetic field line PQ is anchored in the accretion disc and makes an angle α with the disc, which is in the equatorial plane. Material at P moves at the Keplerian angular velocity

$$\Omega_\circ(R) = \left(\frac{GM}{R_\circ^3}\right)^{1/2} \tag{2.22}$$

where $R_\circ$ is the distance from P to the central mass M. Since Ferraro's law holds, the angular velocity along a field line is constant and in that case plasma on PQ moves with angular velocity $\Omega_\circ$. At an arbitrary point R on the line PQ, the forces are the centrifugal force $\mathrm{F}_c = \Omega_\circ^2 R$ away from the rotation axis and the gravitational force F_g due to the mass M. The magnetic force ($\mathbf{J} \times \mathbf{B}$) does not play a role in plasma motions along B and is therefore neglected. If the sum of the two forces F_c and F_g has a net outward component along RQ, plasma at R would be accelerated away from the disc.

The potential for the combination of the two forces is given by

$$\phi_{eff}(R,z) = \Phi_{grav} - \frac{1}{2}|\mathbf{\Omega} \times \mathbf{R}|^2.$$

The gravitational and centrifugal potentials at R are given respectively by

$$\Phi_{grav} = -\frac{\mathrm{GM}}{r} = -\frac{\mathrm{GM}}{(R^2+z^2)^{1/2}} \tag{2.23}$$

and

$$\begin{aligned}\Phi_{cen}(R,z) &= -\frac{1}{2}(|\mathbf{\Omega_K}\times\mathbf{R}|^2)\\ &= -\frac{1}{2}\left[\left(\frac{GM}{R_\circ^3}\right)^{1/2}\right]^2 R^2\\ &= -\frac{1}{2}\left(\frac{GM}{R_\circ^3}\right)R^2. \end{aligned} \tag{2.24}$$

The potential for the resultant force is given (in cylindrical coordinates) by

$$\phi(R,z) = -\frac{GM}{R_\circ}\left[\frac{1}{2}\left(\frac{R}{R_\circ}\right)^2 + \frac{R_\circ}{(R^2+z^2)^{1/2}}\right]. \tag{2.25}$$

Now write $R = R_\circ + R'$ and expand terms in the above equation, assuming $|R'|$, $|z| < |R_\circ|$. Then keeping terms to the order $1/R_\circ^2$ results in

$$\phi(R,z) = -\frac{GM}{R_\circ}\left[\frac{3}{2} + \frac{3}{2}\frac{R'^2}{R_\circ^2} - \frac{1}{2}\frac{z^2}{R_\circ^2}\right]. \tag{2.26}$$

Now measure the distance from P along the field line, s, so that $R' = s\cos\alpha$, $z = s\sin\alpha$. Substitution into the above equation and taking the negative derivative with respect to s gives the force along the field line as

$$-\frac{\partial\phi}{\partial s} = \frac{GMs}{R_\circ^3}(3\cos^2\alpha - \sin^2\alpha). \tag{2.27}$$

If $\alpha < 60°$, the force is in the outward direction and plasma on the field line would be centrifugally driven away along the field line. The material lost from the disc (corona) also removes angular momentum from the system. As the material moves outward, it is forced to rotate with the field at the angular speed $\Omega_\circ$. But where the field has weakened to the extent that the outflow kinetic energy dominates the field energy, the material is no longer kept in corotation. This results in the twisting of the field lines (see Figure 2.9). Following the analysis presented earlier, at $z \gg R$ the outflow will be collimated towards the rotation axis to form a magnetically collimated jet (e.g. Fig. 2.9).

In this section a qualitative discussion has been given illuminating some of the most fundamental aspects of magnetospheric propeller action in terms of centrifugal expulsion of material from a fast rotating magnetosphere. The validity of this treatment does however depend on the effective coupling between the magnetospheric field and ionized plasma or small parcels of gas that can be permeated by the field over sufficiently short time scales. On the other hand, it is believed that the mass transfer stream in IPs consists of large diamagnetic blobs, which are not readily permeated by magnetic field (e.g. King 1993). This will have dramatic consequences for the accretion process and potential propeller action. A discussion focusing on the fundamental properties of this process will be presented next.

2.5 The accretion of large diamagnetic blobs: Magnetospheric drag

Litwin, Rosner & Lamb (1999) investigated the penetration of plasma into astrophysical magnetospheres which may result in accretion in a wide variety of astrophysical systems, ranging from protostellar systems,

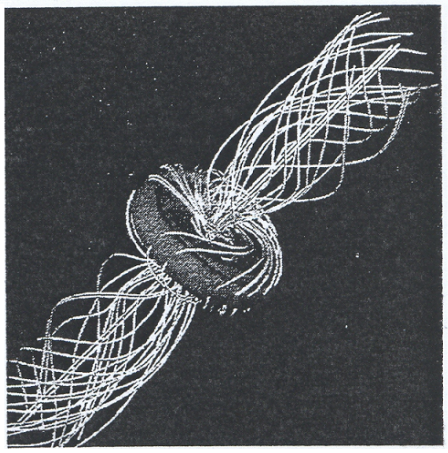

Figure 2.9: 3D simulation of a jet and twisted magnetic field lines formed from an initial torus (Matsumoto et al. 1998)

cataclysmic variables (CV) and neutron stars to active galactic nuclei. At large distances from the central object, surface plasma currents screen the external magnetic field B from the plasma interior and the plasma propagates ballistically (Chapman & Ferraro 1931). In this 'diamagnetic'mode of propagation, the ballistic plasma motion can take place as long as $\beta = 4\pi\rho v^2/B^2 \gg 1$ (ρ and v are the density and flow velocity of the in falling matter, respectively). Penetration is commonly believed to cease in the region where $\beta \leq 1$ (e.g. Davidson & Ostriker 1973; Lamb, Pethick & Pines 1973 in the context of accretion-powered pulsars; Hameury, King & Lasota 1986; Lamb 1988 in the context of CVs). It has been argued that turbulent mixing [driven by, for example, Rayleigh-Taylor (Elsner & Lamb 1976, 1977; Arons & Lea 1976) or Kelvin-Helmholtz (Burnard, Lea & Arons 1983) instabilities] can lead to deeper penetration into the stellar magnetosphere by allowing the ionized matter to attach to magnetospheric field lines.

2.5.1 Diamagnetic blob accretion in mCVs

Observational evidence exists for a clumpy mass transfer in the mCVs through a detailed study of the Ginga X-ray data of AM Her (Beardmore & Osborne 1997). These authors explained the variability of the hard X-ray emission from AM Her as shot noise caused by the accretion of an inhomogeneous blob-like mass flow with typical densities $n_{blob} \approx 10^{15} - 10^{17}$ cm^{-3} onto the highly magnetized white dwarf. Blobs with these densities and typical sizes $\ell_{blob} \sim 10^8 - 10^9$ cm, are probably diamagnetic and not easily penetrated by magnetic field. The concept of fragmented mass transfer and accretion flows in interacting binaries has been considered in earlier studies (e.g. Arons & Lea 1976, 1980; Hameury, King & Lasota 1986). These studies considered the fragmentation through Rayleigh-Taylor (interchange) instabilities. It has also been shown (Meintjes 2004, Meintjes & Jurua 2006) that the fragmentation may also be initiated by surface magnetic fields (prominences) that break up the stream in the L_1 funnel. King (1993) pointed out that the magnetospheric interaction with a tenuous stream or spray of plasma (as in the earlier discussion) differs radically from the interaction with a stream of large (dense) diamagnetic blobs.

As mentioned in (1.1) King & Lasota (1991) and King (1993) showed that the peculiar $P_{spin} \sim 0.1P_{orb}$

spin-up relation in IPs can readily be explained by the fact that the magnetic white dwarf accretes from a stream of large diamagnetic blobs. Some of the key aspects of this process will be discussed.

Earlier it was mentioned that a ballistic stream plunging into the Roche lobe of a magnetic white dwarf will, if not disrupted greatly by the magnetic field, settle in an orbit at r_{circ}. The specific angular momentum associated with an orbit at r_{circ} is

$$\begin{aligned} j_{r_{circ}} &= r_{circ}^2 \Omega_K(r_{circ}) \\ &= (\mathrm{G M_1} r_{circ})^{1/2} \end{aligned} \tag{2.28}$$

where $\mathrm{M_1}$ is the mass of the compact object. The specific angular momentum of an orbiting clumpy ring at r_{co}, i.e. where the angular velocity of orbiting material matches the stellar (and magnetospheric field) angular velocity, is

$$j_{r_{co}} = (\mathrm{G M_1} r_{co})^{1/2}.$$

The ratio of the specific angular momentum at the two radii is

$$\beta = \frac{j_{r_{circ}}}{j_{r_{co}}} = \left(\frac{r_{circ}}{r_{co}}\right)^{1/2}. \tag{2.29}$$

For IPs where the typical white dwarf spin period and binary orbital periods are $\mathrm{P_*} \sim 1000$ sec and $\mathrm{P}_{orb} \sim 4$ hrs respectively, it can be shown (King & Lasota 1991)

$$\frac{r_{co}}{R_\odot} = 0.22 \left(\frac{\mathrm{M_1}}{\mathrm{M_\odot}}\right)^{1/3} \left(\frac{\mathrm{P_*}}{1000\mathrm{s}}\right)^{2/3} \tag{2.30}$$

$$\frac{r_{circ}}{R_\odot} = 0.13 \left(\frac{\mathrm{P}_{orb}}{4\mathrm{hr}}\right)^{2/3}. \tag{2.31}$$

Therefore $\frac{r_{co}}{r_{circ}} \sim 2$ in IPs, implying that the white dwarf will accrete material with less angular momentum than is associated with orbiting gas at r_{co}. Put differently, the white dwarf will freely accrete angular momentum associated with material orbiting at r_{circ}, resulting in a gradual spin-up of the accreting white dwarf. An upper limit for the spin/orbital period ratio can be obtained by considering $r_{co} = r_{circ}$, which requires

$$\frac{\mathrm{P}}{2\pi}(\mathrm{G M_1})^{1/3} = \frac{b_1}{\mathrm{G M_1}} \left(\frac{b_1}{a}\right)^3 b_1 \tag{2.32}$$

$$\Rightarrow \quad \frac{\mathrm{P_*}}{\mathrm{P}_{orb}} = (1+q)^2 \left(\frac{b_1}{a}\right)^6 \tag{2.33}$$

where $\mathrm{q} = \mathrm{M_2/M_1}$ and $b_1/a = 0.5 - 0.277 \ln q$. This relation, for typical q-values associated with IPs (i.e. $q \sim 0.5$) results in $\frac{\mathrm{P_*}}{\mathrm{P}_{orb}} \sim 0.1$ (King & Lasota 1991).

This elementary analysis suggests that the accretion of material form large diamagnetic blobs that survive their ballistic path through the magnetosphere (with $\beta = 8\pi\rho v^2/\mathrm{B}^2 \gg 1$) and settle in an orbit at $r_{circ} < r_{co}$, can explain many of the observational properties of mCVs. Based upon the interaction of a blobby stream with a rotating magnetosphere, Wynn, King & Horne (1997) modelled the propeller process in AE Aqr in terms of a magnetospheric drag process (Drell, Foley & Ruderman 1965). The fundamental MHD aspects of

magnetospheric drag will be reviewed, focusing particularly on the influence of the drag on the dynamics of a ballistic blob-like stream. The discussion will be concluded by reviewing the magnetospheric drag propeller as applied to AE Aqr, focusing on the observational consequences.

2.5.2 Magnetospheric drag: The fundamental principles

The dynamics of a diamagnetic blob in a co-moving reference frame is determined by Newton's second law according to $\rho\frac{d\mathbf{v}}{dt} = \mathbf{F}_{em} + \mathbf{F}_{other}$.

$$\rho\frac{d\mathbf{v}}{dt} = \frac{1}{\mathrm{c}}(\mathbf{J}'_{\mathbf{i}} \times \mathbf{B}') + [-\nabla P + \rho\mathbf{g}_{eff} + \mathbf{f}_{\mathbf{v}}], \tag{2.34}$$

where the first term represents the electromagnetic force as a result of induced eddy currents (surface currents), and the term in square brackets represents the combined influence of pressure gradients, the effective gravity and viscosity. The induced currents, in the co-moving frame, is given by Ohm's law,

$$\mathbf{J}'_i = \sigma\mathbf{E}'_i$$

where σ is the electrical conductivity of the fluid. For a non-relativistic flow, the current density transforms invariably to the laboratory system, i.e. $\mathbf{J}_i = \mathbf{J'}_c$. The transformation of the electric and magnetic fields to the laboratory system (in the limit $\gamma \to 1$) (e.g. Jackson 1975, p. 552) is:

$$\mathbf{E}' = \mathbf{E} + \frac{1}{\mathrm{c}}(\mathbf{v} \times \mathbf{B}),$$

$$\mathbf{B}' = \mathbf{B} + \frac{1}{\mathrm{c}^2}\{\mathbf{v} \times (\mathbf{v} \times \mathbf{B})\}.$$

The Lorentz force (Hall effect) acting on the conduction electrons on the surface of the blobs propagating through the magnetosphere will induce eddy currents. Using the transformed fields

$$\mathbf{J}_i = \sigma\left(\mathbf{E}_i + \frac{\mathbf{v}}{\mathrm{c}} \times \mathbf{B}\right). \tag{2.35}$$

Therefore the equation of motion can be expressed as

$$\rho\frac{d\mathbf{v}}{dt} = \frac{\sigma}{\mathrm{c}}(\mathbf{E_i} \times \mathbf{B}) + \frac{\sigma}{\mathrm{c}^2}[(\mathbf{v} \times \mathbf{B}) \times \mathbf{B}] + \rho\mathbf{g}_{eff}. \tag{2.36}$$

This expression reduces to

$$\begin{aligned}
\rho\frac{d\mathbf{v}}{dt} &= \frac{\sigma}{\mathrm{c}}\left[(\mathbf{E}_\perp \times \mathbf{B}) + (\mathbf{E}_\parallel \times \mathbf{B})\right] + \frac{\sigma}{\mathrm{c}^2}\left\{[(\mathbf{v}_\perp \times \mathbf{B}) \times \mathbf{B})] + [(\mathbf{v}_\parallel \times \mathbf{B}) \times \mathbf{B})]\right\} + \rho\mathbf{g}_{eff} \\
&= \frac{\sigma}{\mathrm{c}}(\mathbf{E}_\perp \times \mathbf{B}) + \frac{\sigma}{\mathrm{c}^2}[(\mathbf{v}_\perp \times \mathbf{B}) \times \mathbf{B})] + \rho\mathbf{g}_{eff} \\
&= \frac{\sigma}{\mathrm{c}}\left[\frac{B^2}{\mathrm{c}}\mathbf{w}\right] + \frac{\sigma}{\mathrm{c}^2}[(\mathbf{v}_\perp \cdot \mathbf{B})\mathbf{B} - (\mathbf{B} \cdot \mathbf{B})\mathbf{v}_\perp] + \rho\mathbf{g}_{eff},
\end{aligned} \tag{2.37}$$

where $\mathbf{w} = \frac{\mathrm{c}}{B^2}(\mathbf{E}_\perp \times \mathbf{B})$ represents the guiding centre drift speed of the electrons in the plasma, effectively carrying the magnetic field with them. This results in

$$\begin{aligned}
\rho\frac{d\mathbf{v}}{dt} &= \frac{\sigma}{\mathrm{c}^2}B^2\mathbf{w} - \frac{\sigma}{\mathrm{c}^2}B^2\mathbf{v}_\perp + \rho\mathbf{g}_{eff} \\
&= \rho\mathbf{g}_{eff} - \frac{\sigma B^2}{\mathrm{c}^2}[\mathbf{v}_\perp - \mathbf{w}].
\end{aligned} \tag{2.38}$$

The components of the acceleration parallel and perpendicular to the field then is

$$\frac{d\mathbf{v}_{\parallel}}{dt} = \mathbf{g}_{eff\parallel},$$

$$\frac{d\mathbf{v}_{\perp}}{dt} = \mathbf{g}_{eff\perp} - \frac{\sigma B^2}{\rho c^2}(\mathbf{v}_{\perp} - \mathbf{w}).$$

It is clear from these equations that the effective gravity alone is responsible for acceleration of a blob parallel to the field, while a combination of effective gravity and magnetospheric drag propels the blob perpendicularly across field lines. These equations can be quantified as follows

The contribution of the magnetospheric drag term towards the propulsion of diamagnetic blobs across field lines can be summarized by the relations

$$\frac{d\mathbf{v}_{\perp}}{dt} < 0 \quad \text{if } (\mathbf{v}_{\perp} - \mathbf{w}) > 0 \tag{2.39}$$

$$\frac{d\mathbf{v}_{\perp}}{dt} > 0 \quad \text{if } (\mathbf{v}_{\perp} - \mathbf{w}) < 0. \tag{2.40}$$

Therfore, in the absence of other forces, magnetospheric drag manifests in a deceleration of the blobs across the field if the blob velocity exceeds the drift speed, i.e. the field velocity across the blob. In the alternative case, magnetospheric drag can propel the blob across the field if the guiding centre drift speed exceeds the translational blob velocity. The first case most probably explains the deceleration and associated altitude loss of low Earth orbiting satellites (Drell, Foley & Ruderman 1965), while the second case may lead to propeller action under specific conditions, i.e. when the magnetospheric drag dominates the effective gravity and/or pressure gradient. The magnitude of the propulsion depends on the so-called drag coefficient, k $\approx \frac{\sigma B^2}{\rho C^2}$. It can be seen that the conductivity of the plasma and magnetic field strength play fundamental roles.

2.6 Mass transfer and the diamagnetic blob propeller in AE Aqr

The application of the magnetospheric drag effect to AE Aqr is based upon the assumption of a fragmented mass transfer flow consisting of diamagnetic blobs and interaction with the white dwarf magnetosphere outside of the corotation radius. These assumptions will be discussed before presenting a summary of the results of WKH.

2.6.1 Fragmented flow

A detailed emission line analysis (Eracleous & Horne 1996) constrained the mass transfer from the secondary to a value $\dot{M}_2 \sim 4 \times 10^{17}$ g s^{-1}. A relation between the transfer rate, the density of the flow and the local sound speed (Meintjes 2004, Warner 1995 p. 34) is

$$-\dot{M}_2 = \frac{1}{4\pi}\rho_{L_1} c_s^3 P_{orb}^2,$$

with the sound speed $c_s \geq 6 \times 10^5 \left(\frac{T}{4000\mathrm{K}}\right)^{1/2}$ cm s^{-1} (Meintjes 2004). The average density of the fluid in the transfer nozzle at the L_1 point then is $\rho_{L_1} \sim 2 \times 10^{-8}$g cm^{-3}.

The magnetic nature and activity of the secondary is expected to play a significant role in controlling the stream's flow rate and density and therefore the magnetization and fragmentation of the stream close to the L_1 region was investigated by Meintjes(2004). The influence of starspots or prominences on the surface of the donor star could have on the stream was investigated by Livio & Pringle (1994) and Steeghs et al. (1996).

Magnetic pressure in the nozzle may dominate the ram pressure of the flow which, described as an effective magnetic viscosity, may play an important role in the flow dynamics of the transfer stream. Meintjes (2004) describes the stream as consisting of a weakly ionized[1] fluid with temperature T $\sim$ 4000 K. This fluid must move across magnetic field lines to escape from the secondary star through the L_1 funnel. An important parameter in this process is the electrical conductivity and the associated magnetic diffusivity of the fluid. For a weakly ionized gas the Coulomb conductivity is $\sigma \approx 10^9 T^{3/2}$ esu (e.g. Lang 1998, p. 210) and so for the stream, $\sigma \sim 2.5 \times 10^{14} (T/4000\,\mathrm{K})^{3/2}$ esu. The magnetic diffusivity is given by $\eta = \mathrm{c}^2/(4\pi\sigma)$ and so for a lower conductivity, the diffusivity increases. This is important when considering the flow in the presence of the magnetic field of the secondary. At the L_1 point the forces on the fluid are the pressure gradient, the ordinary viscosity and the magnetic forces.

In a magnetofluid the time-evolution of the field is determined by

$$\frac{\partial \mathbf{B}}{\partial t} = \nabla \times (\mathbf{v} \times \mathbf{B}) - \nabla \times \eta(\nabla \times \mathbf{B}),$$

where the second term on the RHS determines the diffusion of field into or out of a plasma, as determined by the diffusivity η, or equivalently the conductivity. The diffusion term is compared to the first term by considering the magnetic Reynolds number, $\mathrm{R}_m = \mathrm{Lv}/\eta = 4\pi\sigma L v/c^2$, where v is the flow speed and L the length scale of the field. Therefore if $\sigma \to \infty$, then $(1/\mathrm{R}_m) \to 0$ and the diffusion term vanishes. This means that the field is effectively frozen into the fluid and is dragged with it. For the funnel being considered here, $\mathrm{R}_m \sim 7 \times 10^9$, where it is assumed that v $\approx$ c_s and the length scale L is put equal to the funnel width H $\sim$ $\mathrm{c}_s/\Omega_{orb} \sim 3 \times 10^9$ cm (e.g. Frank et al. 2002, p. 352). Such a high value of the magnetic Reynolds number suggests that the field dominates the flow in the funnel.

On the other hand, if the fluid comes into contact with a magnetic field, magnetic viscosity may retard the motion. The ratio of the magnetic to the fluid viscosity(μ) is the square of the Hartmann number M (Jackson 1975, p. 477), which is given by

$$M = \left(\frac{\sigma B^2 L^2}{\mu c^2} \right)^{1/2}.$$

Here we see that the field strength becomes important in contrast to the frozen-in condition where the conductivity is the deciding parameter. If M $\gg$ 1, the magnetic viscosity dominates and if the field strength and/or the conductivity is large enough, the fluid may encounter a magnetic obstruction. This means that a magnetic field in the path of the mass transfer at the L_1 funnel, can determine the dynamics of the escape of plasma from the secondary. If the magnetic field is dominant, material can build up until the pressure is high enough and mass can escape through the magnetic obstruction. The mass flow is then fragmented into a blob-like or clumpy flow.

[1]The ionization temperature of hydrogen is $\mathrm{T}_H \sim 6500$ K (FKR p. 117)

The stream falling towards the white dwarf is therefore expected to consist of blobs of plasma and less dense interblob plasma. The stream follows a ballistic trajectory and according to Lubow & Shu (1975)(cf. Reinsch & Beuermann 1994), will pass the white dwarf at a closest approach (see Fig. 2.4) given by

$$r_{cl} = 1.4 \times 10^7 \mathrm{P}_{orb}^{2/3}(s) M_1^{1/3} \mathrm{cm} = 1.5 \times 10^{10} (\mathrm{P}_{orb}/9.88h)^{2/3} (M_1/M_\odot)^{1/3} \mathrm{cm}, \tag{2.41}$$

with M_1 the mass of the white dwarf in solar units. The speed of the gas at the closest approach, relative to the white dwarf, is of the order of ~ 1000 km s^{-1}, slightly below the escape velocity which is $\mathrm{v}_{esc} \sim 1550$ km s^{-1}. To effectively escape from the binary system, the gas has to be accelerated to velocities exceeding the escape velocity.

2.6.2 The propeller in AE Aqr: Wynn, King & Horne (1997)

Welsh, Horne & Gomer (1998) studied optical spectra of AE Aqr and specifically the variation of the Hα line in order to make Doppler tomograms of the gas flow in the system. No evidence for the presence of an accretion disc in AE Aqr was found in the tomograms, but emission from low velocity (< 500 km s^{-1}) gas was detected. They found that on different nights the tomogram has a different appearance, indicating that the emission is not a stable feature. The mean tomogram for the entire data set was used in WKH. However, the tomograms do have a common feature: most of the emission arises from a region with small negative v_x and v_y components. They did not however find any obvious signature of the mass transfer stream. The main conclusions were then that no evidence for an accretion disc was found and that the propeller model is favored as an explanation of the data.

The propeller model basically entails that the transferred mass is centrifugally ejected by the spinning white dwarf magnetosphere (Wynn & King 1995). This requires an interaction of the transfer stream and the magnetosphere. King (1993) and Wynn & King (1995) modelled the transfer flow in Intermediate Polars as consisting of large, diamagnetic gas blobs with density ρ_b and length l_b. The interaction between the blobs and the magnetosphere, as described by WKH, occurs via a surface drag force dependent on the local magnetic field (Drell, Foley & Ruderman 1965). The magnetic field cannot diffuse into the diamagnetic blobs on the dynamical time scale. Screening currents are induced on the surface, which interact with the external field (i.e. Lenz's law applies) and influences the blob dynamics. The time scale of energy loss or gain is

$$t_{mag} \approx \frac{c_A \rho_b l_b}{\mathrm{B}^2} \frac{|\mathbf{v}_\perp|}{|[\mathbf{v} - \mathbf{v}_f]_\perp|}. \tag{2.42}$$

Here c_A is the Alfvén speed in the plasma medium wherein the blobs are propelled and v and v_f represent the blob and field velocities respectively. The blobs gain energy or angular momentum if $\mathrm{v}_f > \mathrm{v}$, while the spinning white dwarf spins down as a result of the transfer of angular momentum. This mechanism is most effective when the relative velocity of the blobs is perpendicular to the field. In AE Aqr it is assumed that the white dwarf has a dipole field which, averaged over the spin period, is perpendicular to the plane and therefore also the mass transfer flow.

WKH parameterizes the effective acceleration due to the surface drag force as $\mathbf{g}_{mag} = -k[\mathbf{v} - \mathbf{v}_f]_\perp$, where the drag coefficient per unit mass $\mathrm{k} \sim 1/\mathrm{t}_{mag}$ in the slow rotator limit where $|v_f| \ll |v|$ and $\mathrm{t}_{mag} \sim c_A \rho_b l_b / \mathrm{B}^2$. In order to simulate the motion of a blob through the magnetosphere, the coefficient k is parameterized as k

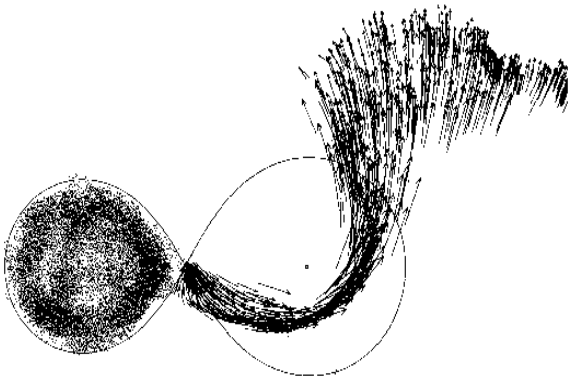

Figure 2.10: The outflow of the propeller according to the Wynn, King & Horne (1997) simulation. On the left is the lobe filled secondary, which loses mass through the L_1 funnel. The effect of the propeller action can be seen from the mass of arrows that represent the velocity vectors of gas blobs.

$\sim k_\circ(r/r_\circ)^{-n}$ where $k_\circ$, n and $r_\circ$ are constants. An estimate of $l_b \sim 10^9$ cm and a density $\rho_b \sim 10^{-11}$ g cm^{-3} is used, but the magnetic field is not estimated *a priori*. The value of k(r) is determined by setting n = 2 and changing $k_\circ$ in order to get a good agreement between the simulated Hα tomogram and the observed one. A representative value of $k_\circ$ is 10^{-5} s^{-1}, which means that for the parameters used, B $\approx$ 60-130 G at $r_\circ$. This would indicate a polar strength of $B_* \geq 10^6$ G for a white dwarf with radius $r_* = 5 \times 10^8$ cm.

A simulated flow from the propeller shows that the gas stream is ejected from the system having reached a maximum velocity of $v_{esc} > 1000$ km s^{-1} at the closest approach to the white dwarf ($r_\circ \sim 10^{10}$ cm) and leaving the system with a velocity of $v_\infty \sim 300$ km s^{-1}. The power carried away by the ejected mass $\dot{M}$ (Eracleous & Horne 1996) is of the order of $L_{esc} \sim \dot{M}v_{esc}^2/2 \sim$ few $\times 10^{33}$ erg s^{-1}, which compares well with the spin down power of the white dwarf. Figure 2.10 shows the outflow of gas as the consequence of the acceleration of the magnetospheric propeller.

WKH also considers the fate of the expelled blobs, assuming that the blobs remain intact during the interaction with the magnetosphere. They however comment that the interaction does involve a large shear which can lead to instabilities like the Kelvin-Helmholtz instability. Such effects may lead to disruption of the blobs, but the simulation suggests that the blobs do remain intact until ejection. The blobs spiral outward and the spirals are estimated to merge at a distance of r $\sim 10a$ from the system (see Figure 2.11). A low density component may also be part of the mass ejected. This gas could be the source of line-emission as reported by Eracleous & Horne (1996).

2.6.3 Critique

In this section two main points of criticism regarding the diamagnetic magnetospheric drag model, as applied to AE Aqr, will be presented. This is done in order to better illuminate the contribution of this study. The first point concerns emission expected from the mass flow propelled by the magnetospheric drag effect and observations that discounts this effect. The second point concerns the time-scale of acceleration of an idealized highly efficient drag model compared to the dynamical and viscous time-scales of the interaction of the mass flow with the magnetosphere.

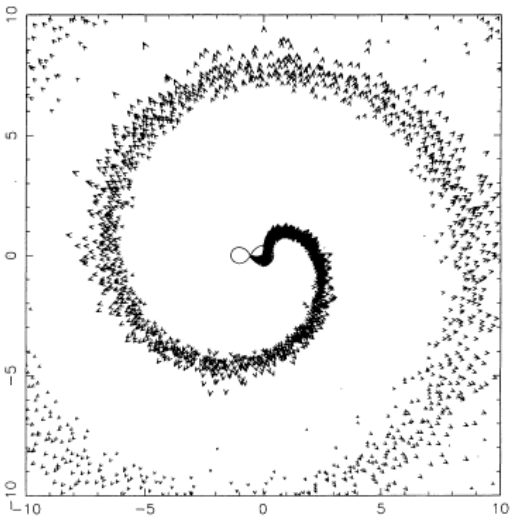

Figure 2.11: The ejected gas spirals outward (Wynn, King & Horne 1997).

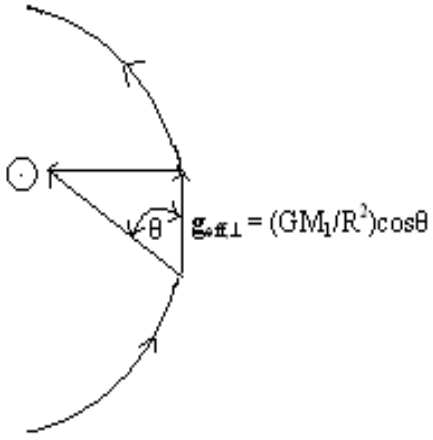

Figure 2.12: A top view of the path of the transfer stream, partly encircling the white dwarf in the orbital plane.

Blob propulsion and Current dissipation

Consider the motion of a ballistic stream of large diamagnetic blobs from the L1 point through the magnetosphere of the white dwarf. The dynamics of these large blobs across the magnetic field is determined by

$$\frac{d\mathbf{v}_\perp}{dt} = \mathbf{g}_{\rm eff,\perp} - \left(\frac{\sigma B^2}{\rho c^2}\right)(\mathbf{v}_\perp - \mathbf{w}). \tag{2.43}$$

In this analysis we consider the blobs to be large, confined mostly to the equatorial plane, and falling through the magnetosphere, which is assumed to be dipolar. As a result of the dipolar magnetospheric field configuration, there will be a significant non-zero magnetic field component perpendicular to the path the blobs follow in the equatorial plane. As a result of the orbital motion of the binary system, the fragmented stream will not fall radially to the white dwarf, but will follow a ballistic path, passing the white dwarf at the radius of closest approach, which is close to the circularization radius (Wynn, King & Horne 1997).

The diamagnetic blobs are under the influence of the white dwarf's effective gravity and magnetospheric field, and so the blobs will experience a mechanical force along their ballistic path, i.e. the component of the effective gravity drives the material along its path perpendicularly to the dipolar field. This component of the effective gravity (see Figure 2.12) can be approximated by

$$\mathbf{g}_{\rm eff,\perp} \approx \left(\frac{GM_1}{R^2}\right)\cos\theta\hat{e}_\perp, \tag{2.44}$$

with $0 < \theta < 90^\circ$ between the L1 point and the distance of closest approach, and $\theta > 90^\circ$ after the distance of closest approach. The value $\theta \to 0$ corresponds to blobs positioned close to the line of centres, i.e. just after they have left the L1 region. At this point of the ballistic trajectory, the blobs experience the full radial acceleration of gravity towards the central white dwarf. The Coriolis force will however deflect the beam sideways resulting in an arc-shaped trajectory. Along this trajectory, one can see that before the distance of closest approach has been reached, i.e. for $0 < \theta < 90^\circ$, $g_{\rm eff,\perp} > 0$, resulting in an acceleration of the blobs along their path as they plunge deeper into the potential well of the white dwarf. Alternatively, for $\theta > 90^\circ$, $g_{\rm eff,\perp} < 0$, corresponding obviously to blobs having passed the distance of closest approach, decelerating as they try to escape from the gravitational field of the white dwarf.

Conservation of mechanical energy inside the critical Roche surface surrounding the white dwarf, demands zero velocity at the critical surface if gravity alone is responsible for the propulsion of the blob. However, the presence of the second term on the RHS of eq. (2.43) may result in an additional acceleration if $w - v_\perp > 0$, which may result in blobs reaching velocities exceeding the escape velocity. The equation of motion across the field, along the flow then is

$$\frac{dv_\perp}{dt} = \frac{GM_1}{R^2}\cos\theta + \left(\frac{\sigma B^2}{\rho c^2}\right)(w - v_\perp). \tag{2.45}$$

The electrodynamic drag on a diamagnetic blob moving through a magnetic field is determined in effect by the magnitude of $(w - v_\perp)$ and the drag coefficient $K_d = (\sigma B^2/\rho c^2)$, which depends on the magnitude of the electrical conductivity of the fluid, the magnitude of the magnetic field sweeping across the blobs, and inversely on the blob density. The drag coefficient portrays the nature of the interaction between the field and the fluid, since it depends on the magnitude of the electrical conductivity of the fluid. A higher electrical

conductivity, in conjunction with a strong magnetic field sweeping across the fluid, induces a significant drag, resulting in a propulsion of the fluid across the field if $w - v_\perp > 0$. The magnitude of the drift speed of the electron guiding centres, i.e. the speed of the field moving through the surface layers of a large diamagnetic blob, is

$$w = \left(\frac{E_\mathrm{i}}{B}\right) c \tag{2.46}$$

where E_i represents the magnitude of the induced electric field screening the fluid against changing magnetic flux through the surface layer. It can be shown that in the region of the magnetosphere, before the distance of closest approach has been reached, the blobs can be propelled across the field, i.e. $\frac{dv_\perp}{dt} > 0$, if the following condition is satisfied, namely

$$\frac{GM_1}{R^2}\cos\theta + \left(\frac{\sigma B^2}{\rho c^2}\right)(w - v_\perp) > 0. \tag{2.47}$$

This implies that

$$w > v_\perp - \left(\frac{\rho c^2}{\sigma B^2}\right)\frac{GM_1}{R^2}\cos\theta,$$

resulting in the induction of electric fields on the surface of the blob with magnitude

$$E_\mathrm{i} > \left(\frac{B}{c}\right)\left\{v_\perp - \left(\frac{\rho c^2}{\sigma B^2}\right)\frac{GM_1}{R^2}\cos\theta\right\} \tag{2.48}$$

where σ represents the electrical conductivity of the gas. The conductivity of the gas is represented by $\sigma \approx 10^9\ T^{3/2}$ e.s.u., for a weakly ionized gas, and $\sigma \approx 6 \times 10^6\ T^{3/2}$ e.s.u., for a fully ionized gas (e.g. Lang 1998, p. 209-210). The eddy currents driven by this field will be such that the increasing or decreasing flux experienced by the blob will be opposed - in principle simply Lenz's law. One can see from this expression that the contribution of the screening fields as a result of the magnetic flux variations across the blobs will decrease if a strong gravitational field component accelerates the blobs continuously. For typical parameters relating to the blobs in cataclysmic variables in regions close to the circularization radius, the induction field can be estimated by using typical values for the blob conductivity, the magnetic field sweeping across the blob, as well as the blob density. Meintjes (2004) showed that the electrical conductivity in blobs with initial temperatures $T_\mathrm{blob,i} \sim 4000$ K is approximately $\sigma \sim 2.5 \times 10^{14}(T_\mathrm{blob}/4000\,\mathrm{K})^{3/2}$ e.s.u., and the density of the blobs is typically $\rho_\mathrm{blob} \sim (\langle m_\mathrm{p}\rangle n_\mathrm{p}) \sim 2 \times 10^{-8}(n_\mathrm{p}/10^{16}\mathrm{cm}^{-3})$ g cm^{-3}. From the equation above it can be seen that the maximum contribution to the propulsion, from forces other than the gravity, will occur at the distance of closest approach ($\theta \to 90^\circ$) where the component of gravity along the flow direction reaches a local minimum. Hence, at the distance of closest approach the maximum contribution to the effective acceleration of blobs across field lines has to be provided by the magnetic drag. In this limit ($\sigma \to \infty$) it can be seen that the second term in Eq. 2.48 is negligible and thus,

$$E_\mathrm{i,max} > \frac{B}{c}\, v_\perp \tag{2.49}$$

since $w > v_\perp$. In AE Aqr the fast rotating magnetosphere sweeping across the blobs may actually result in $w \gg v_\perp$. Therefore, for effective magnetospheric propulsion in the ideal MHD limit ($\sigma \to \infty$), the constraint above at least provides a lower limit on the induced surface electric fields.

In contrast to the high conductivity case above, if $\sigma \to 0$, the diamagnetic blob perspective is significantly altered. The magnetic field now readily diffuses into the blobs and a mechanical energy transfer may dominate

the interaction. As seen from Eq. 2.48, the induced electric fields are weaker and it is therefore not expected that the blobs will be significantly heated. This non-electrodynamic mechanical interaction, which is the topic under investigation in this study, may therefore lead to a cool propeller in contrast to the magnetospheric propeller.

The lower limit on the induced surface fields may in fact allow the constraint of the surface current dissipation and resultant Ohmic heating of the blobs. Since $E_{\rm i,max} \propto Bv_{\perp}$, the magnetospheric field and flow velocity at the radius of closest approach needs to be determined.

The magnetospheric field at the distance of closest approach, e.g. $R_{\rm circ} \sim 10^{10}$ cm, is approximately

$$B \sim 125 \left(\frac{R_{\rm wd}}{5\times10^{8}\,{\rm cm}}\right)^{3} \left(\frac{R_{\rm circ}}{10^{10}\,{\rm cm}}\right)^{-3} {\rm G}, \tag{2.50}$$

and if the velocity of the blob stream at the distance of closest approach exceeds the escape velocity, i.e.

$$\begin{aligned} v_{\perp} &\sim \sqrt{\left(\tfrac{2GM_1}{R^2}\right)} \\ &\sim 1.55\times10^{8} \left(\tfrac{M_1}{0.9\,M_{\odot}}\right)^{1/2} \left(\tfrac{R_{\rm circ}}{10^{10}\,{\rm cm}}\right)^{-1/2} {\rm cm\ s^{-1}}, \end{aligned} \tag{2.51}$$

the maximum value of the surface induced screening fields is

$$E_{\rm i,max} \sim 194 \left(\frac{B}{125\,{\rm G}}\right) \left(\frac{v_{\perp}}{1.55\times10^{8}\,{\rm cm\ s^{-1}}}\right) {\rm V\ cm^{-1}}. \tag{2.52}$$

The rate of current dissipation per unit volume, i.e. the heating rate per unit volume, is given by the following equation

$$\begin{aligned} \langle \tfrac{dq}{dt} \rangle &= \langle \mathbf{J}.\mathbf{E} \rangle \\ &= \langle \sigma \mathbf{E}^2 \rangle\ {\rm erg\,s^{-1}\,cm^{-3}} \\ &= \langle \tfrac{\mathbf{J}^2}{\sigma} \rangle\ {\rm erg\,s^{-1}\,cm^{-3}} \end{aligned} \tag{2.53}$$

where $\mathbf{J} = \sigma\mathbf{E}$, with σ and $\mathbf{E}$ representing the conductivity and the induced eddy field strength respectively. The skin depth of these generated eddy currents on the surface of the diamagnetic blobs (e.g. Landau & Lifshitz 1960, p. 190; Jackson 1975, p. 298) can in general be expressed in terms of the conductivity (σ) of the medium, as well as the frequency (ω) with which the magnetic field changes through the conductor, i.e.

$$\delta l = \frac{c}{\sqrt{2\pi\sigma\omega}}. \tag{2.54}$$

The average integrated Ohmic heat flux generated in the dissipation layer can be represented by

$$\begin{aligned} \langle F \rangle &= \tfrac{dq}{dt}\delta l \\ &= \langle \sigma \mathbf{E}^2 \rangle \delta l\ {\rm erg\,s^{-1}\,cm^{-2}}. \end{aligned} \tag{2.55}$$

By assuming black body radiation, the surface temperature of these blobs ploughing through the magnetosphere can be estimated using the Rayleigh-Jeans law. Therefore, from

$$\sigma_{sb} T^4 = \langle F \rangle, \tag{2.56}$$

where $\sigma_{sb} = 5.669\times10^{-5}$ erg cm^{-2} s^{-1} K^{-4} (e.g. Lang 1981, p.22) represents the Stefan-Boltzmann constant, we can readily get

$$T_{\rm surf} > 4\times10^{5} \left(\frac{\langle \mathbf{E}^2 \rangle}{\sqrt{\omega}}\right)^{4/13} {\rm K}. \tag{2.57}$$

The maximum contribution of the effective magnetic drag resulting in the acceleration of a diamagnetic blob from the binary system requires that $\langle \mathbf{E}^2 \rangle \rightarrow E^2_{\rm i,max}$, and if the average frequency of magnetic field variation through the surface layers is approximately equal to the angular frequency of the corotating magnetosphere ($\omega = (2\pi/P_1)$, we get

$$T_{\rm surf,max} > 2.7 \times 10^5 \left(\frac{\langle \mathbf{E} \rangle}{E_{\rm i,max}} \right)^{8/13} \left(\frac{P_1}{33\,{\rm s}} \right)^{2/13} {\rm K}. \tag{2.58}$$

This simplistic argument shows that current dissipation as a result of magnetic drag can indeed raise the average surface temperature substantially, since the initial temperature of the blobs is expected to be substantially lower than this value, i.e. approximately $T_{\rm phot} \approx 4000$ K.

It can be seen that the effective magnetospheric propulsion of large diamagnetic blobs in the ideal MHD limit, implies significant current dissipation and resultant heating to temperatures T $> 10^5$ K when the blobs reach the radius of closest approach. A magnetospherically propelled mass transfer stream at such temperatures at r_{cl}, would have a noticeable observational signature that would have been revealed by the optical tomograms. However, the tomograms clearly indicate that optical flaring occurs mainly outside the Roche lobe of the white dwarf, hours after the ballistic stream has slipped silently through the white dwarf's magnetosphere, propelled to velocities exceeding the escape velocity.

In an attempt to reconcile the delayed optical flaring with the propeller outflow, it has been proposed that the flaring may result from the collision of blobs with different terminal velocities, outside the Roche lobe of the white dwarf (Pearson, Horne & Skidmore 2003). Although this may be a viable scenario, it will be shown that the inherent turbulence associated with a Kelvin-Helmholtz driven magnetospheric propeller, may manifest in a delayed release of a large reservoir of thermal energy in the propeller outflow. This reconciles the delayed optical flaring, as inferred from the tomograms, with a cool propeller process.

Effective time-scales

Based upon magnetospheric drag, blobs orbiting the white dwarf will lose or gain mechanical energy depending on the relative velocity of the field with respect to the highly conducting blobs. It has been shown that low earth-orbiting satellites lose mechanical energy as a result of their motion across the slower rotating magnetic field of the earth (Drell et al. 1965). The motion of the blobs through the magnetosphere is then modified by a surface drag, and the effective magnetospheric propulsion of the blobs is then (e.g. Wynn et al. 1997) $g_{mag} = -k[v - v_f]_\perp$, where k $\sim 1/{\rm t}_{drag}$ (slow) is the effective magnetospheric drag coefficient in the slow rotator limit. If the drag (propulsion) time-scale is similar to the time-scale for the loss of mechanical energy via the excitation of Alfvén waves (Drell et al. 1965) in the slow rotator limit, it can be approximated by (${\rm t}_{drag} \sim 1/{\rm k}$), i.e.

$$\begin{aligned} t_{drag} &= \frac{c_A M_{blob}}{B^2 l^2} \\ &= 2.18 \times 10^6 \left(\frac{\rho_{blob} l}{B} \right) {\rm s} \end{aligned} \tag{2.59}$$

where c_A, M_{blob}, B and l represent the Alfvén speed in the interblob plasma, blob mass, magnetospheric field and blob dimension, respectively. The constant in this expression is calculated by using an average value for the reported interblob plasma number density, which for AE Aquarii is ${\rm n}_{ib} \sim 10^9$ - 10^{11} cm^{-3}

(Eracleous & Horne 1996; Wynn et al. 1997; Pearson et al. 2003). A detailed study of the densities of the gas blobs from the secondary star in AM Her was carried out by Beardmore & Osborne (1997) who described the variability in the hard X-rays as the result of the inhomogeneous accretion of blobs with typical densities between $n_{blob} \sim 10^{15}$ - 10^{17} cm^{-3}, and sizes similar to the dimension of the white dwarf. However, in AE Aquarii, a careful mass conservation analysis in the stream interacting with a B $\sim$ 300 G magnetospheric field at the radius of closest approach revealed an average stream (blob) density of the order of $\langle n_{blob} \rangle = (\langle \rho_{blob} \rangle / m_p) \sim$ few $\times 10^{14}$ cm^{-3} (Meintjes & Venter 2005), which is consistent with the inferred blob densities driving the optical flares when blobs collide in the exit fan (Pearson et al. 2003). Using these estimates, it can be shown (Wynn et al. 1997) that the average drag time-scale for blobs is of the order of

$$t_{drag} \sim \ 1.3 \times 10^3 \left(\frac{\mathrm{B}_{circ}}{300\mathrm{G}} \right)^{-1} \left(\frac{n_{blob}}{10^{14}\mathrm{cm}^{-3}} \right) \left(\frac{l}{10^9\mathrm{cm}} \right) \mathrm{s} \tag{2.60}$$

compared to earlier estimates of $t_{drag} \sim 10^5$ s (Wynn et al. 1997) using the Beardmore & Osborne (1997) blob density estimates. Such a long drag time-scale is difficult to reconcile with the rapid outflow these authors proposed. The typical viscous time-scale, which determines disc formation, is of the order of $t_{visc} \sim 10^5$ s (e.g. King 1993), which is still significantly larger than the magnetospheric drag time-scale in the slow rotator limit. Furthermore, it has been shown (Wynn et al. 1997) that the radius of closest approach of the stream to the white dwarf is of the order of R $\sim 10^{10}$ cm. The dynamical time-scale, i.e. the time taken by blobs to orbit the white dwarf in this region, is

$$t_{dyn} = 2\pi \left(\frac{\mathrm{GM}_1}{R^3} \right)^{-1/2} \sim 600 \left(\frac{\mathrm{M}_1}{0.9\mathrm{M}_\odot} \right)^{-1/2} \left(\frac{R}{10^{10}\mathrm{cm}} \right)^{-3/2} \mathrm{s} \tag{2.61}$$

which is significantly smaller than viscous time-scales. It can be seen that the drag time-scale is consistent with the dynamical time-scale. The comparative long viscous time-scale implies that the acceleration can occur before the material settles in a ring or a disc. These estimates emphasize the strength of magnetospheric drag to explain the propulsion of large diamagnetic blobs through the magnetosphere. However, the propulsion is based upon applying ideal magnetohydrodynamics (MHD), applicable in the slow rotator regime, to the fast rotator AE Aquarii, and furthermore quantifying a rather complicated process through a single drag coefficient.

It is therefore evident that the magnetospheric drag approach to describing the propeller in AE Aqr is insufficient in its description of the detailed physics involved in the interaction of the magnetosphere and the mass flow and the consequences of this process. The effective propelling of blobs from the binary system depends on the generation of significant surface currents that will heat the blobs to temperatures $T_{surf} \sim 10^5$ K within a short time-scale, which will have definite observable consequences related to the optical flaring given the drag time scale $t_{drag} \sim 1000$ s ($\sim t_{dyn}$). The effectiveness of the propeller process, combined with the lack of observational evidence (as suggested by the tomograms) linking the flaring directly to the magnetospheric drag propeller, calls into question whether magnetospheric drag is the only driving mechanism behind the propeller in AE Aqr. In fact, the observational evidence supports the notion of a "cool" propeller process, operating over time-scales $t_{prop} < t_{drag}$. Notwithstanding, the WKH model and simulation of the propeller mechanism in AE Aqr is of great interest in as far as it predicts a trajectory for

the gas stream leaving the system. This result will be used in the following chapter where an alternative acceleration mechanism for the propeller in AE Aqr is presented.

The discussion of the alternative propeller process in AE Aqr will be presented as follows : In Chapter 3 a detailed discussion of the KH instability and associated generation of turbulence in the flow is presented in Sections 3.1 and 3.2. Section 3.3 presents a qualitative description of the MHD power driving the KH instability, turbulence and resultant propeller outflow from the magnetosphere. In a series of three papers, i.e. Meintjes & Venter 2005 (Section 3.4.1), Venter & Meintjes 2006a (3.4.2), Venter & Meintjes 2006b (3.4.3), these results are presented as an alternative unifying model to integrate the propeller of AE Aqr with the total reservoir of thermal and non-thermal emission.

Chapter 3

Instabilities, Turbulence and mass outflow

As described in the previous chapter, the fragmented, inhomogeneous mass transfer from the secondary follows a ballistic trajectory, falling towards the white dwarf primary. The trajectory is only negligibly influenced by the magnetosphere on its way to the radius of closest approach, $r_{cl} \sim 10^{10}$ cm (Reinsch & Beuermann 1994). At this radial distance the magnetosphere and the flow is expected to interact the most efficiently, since the field strength is highest.

In this study it assumed that the accretion flow and the rotating white dwarf magnetosphere may be described as two fluids in relative motion. The motion is along the interface which can be approximated as an infinite plane surface. Since the flow follows a ballistic trajectory to r_{cl}, its velocity, at r_{cl}, is approximately $v_{ff}(\text{free-fall}) = v_{esc} = \left(\frac{2GM_1}{r_{cl}}\right)^{1/2} \approx 1550 \text{ km s}^{-1}$. In contrast, the velocity of the corotating magnetosphere, at r_{cl}, is $v_{\phi,m} = r_{cl}\Omega_* \sim 20000 \text{ km s}^{-1}$. The fast rotating magnetosphere mimics a high velocity wind blowing across a denser fluid (the ballistic stream). The velocity shear between the two fluids may be susceptible to the initiation of the Kelvin-Helmholtz instability, which is an extremely efficient momentum transfer mechanism and may also lead to the creation of turbulence in the gas flow.

Instabilities are an integral part of any dynamical system. Such a physical system adjusts, or tries to adjust, itself so as to find an equilibrium state. Equilibrium states may however be unstable, i.e. a small disturbance can cause the system to move to a new equilibrium. Instabilities in fluids, stationary or in motion relative to some boundary surface and under the influence of a gravitational potential, are examples of instabilities that are widely applicable in astrophysical systems.

3.1 The Kelvin-Helmholtz instability

In his book Chandrasekhar(1961) discusses hydrodynamic and magnetohydrodynamic stability. Two basic hydrodynamic instabilities are the Rayleigh-Taylor instability, driven by the buoyancy force in a stratified fluid medium, and the Kelvin-Helmholtz(KH) instability driven by a velocity shear. That is when different

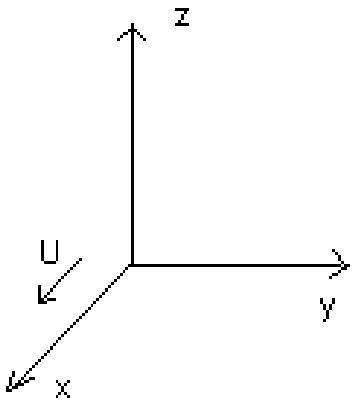

Figure 3.1: Axis system showing the direction of the velocity U

layers of stratified heterogeneous fluid are in relative motion, the kinetic energy of the velocity difference may be used to mix different layers of the fluid as a result of the growth of small perturbations. The special case of two superposed fluids flowing one over the other with a relative horizontal velocity at a plane interface may be subject to the KH instability.

The discussion that follows will be based on the comprehensive treatment in Chandrasekhar(1961). To investigate the KH instability, an equilibrium of a stratified heterogeneous fluid is considered. An initial stationary state is examined for stability of the equilibrium. This stability analysis is done by considering small perturbations of the initial state and linearizing in the amplitude of the perturbations, i.e. to neglect terms that contain multiplication of the small perturbations. This analytical approach satisfactorily describes the stability conditions of such a system, but the inherent non-linearity of the dynamics that describe the growth of the perturbations, does require a numerical approach.

It is assumed that the fluid is incompressible and inviscid. Other than the simplest, purely hydrodynamic case, the influence of magnetic fields present in the fluid will be the main variation discussed. Surface tension, which is absent in astrophysical plasmas, is appropriately neglected in the analysis. The analysis is performed on an interface (in the x-y plane) between two fluids with the fluids arranged in strata. The motion is tangential with respect to the interface and chosen to be along the x-direction. The pressure p and density ρ are functions of the coordinate z, which is perpendicular to the interface. Figure 3.1 indicates the orientation of the coordinate system.
The system is slightly perturbed and the evolution of the disturbances on the interface will indicate if the system is stable or unstable against linear perturbations.

The density at point (x, y, z), as a result of a perturbation is $\rho + \delta\rho$. The perturbation also produces a pressure perturbation δp. The equation of motion for the unperturbed fluid is

$$\rho\left(\frac{\partial \mathbf{v}}{\partial t} + (\mathbf{v}\cdot\nabla)\mathbf{v}\right) = -\nabla p - \nabla\Phi \tag{3.1}$$

where Φ is the gravitational potential. In an alternative notation the equation is

$$\rho\left(\frac{\partial u_i}{\partial t} + u_j\frac{\partial u_i}{\partial x_j}\right) = -\frac{\partial p}{\partial x_i} - g\rho\lambda_i \tag{3.2}$$

where $\boldsymbol{\lambda}$ is a unit vector in the z-direction. The continuity equation $\frac{\partial \rho}{\partial t} = -\nabla \cdot (\rho \mathbf{v})$ reduces to $\nabla \cdot \mathbf{v} = 0$ for an incompressible fluid. To ensure a constant density for a particle as it is followed along with its motion, we have

$$\frac{\partial}{\partial t}\delta\rho + u_i \frac{\partial \rho}{\partial x_i} = 0. \tag{3.3}$$

Now the components of the velocity in the perturbed state may be written as U + u, v and w, where u, v and w are small. The perturbed quantities (velocities, density and pressure) are substituted into the equations, the equilibrium equations are subtracted and nonlinear terms in the small variables are neglected. The result is a set of equations, including the equations of motion for the three directions:

$$\begin{aligned}
\rho\frac{\partial u}{\partial t} + \rho U\frac{\partial u}{\partial x} + \rho w\frac{dU}{dz} &= -\frac{\partial}{\partial x}\delta p, & (3.4)\\
\rho\frac{\partial v}{\partial t} + \rho U\frac{\partial v}{\partial x} &= -\frac{\partial}{\partial y}\delta p, & (3.5)\\
\rho\frac{\partial w}{\partial t} + \rho U\frac{\partial w}{\partial x} &= -\frac{\partial}{\partial z}\delta p - g\delta\rho, & (3.6)\\
\frac{\partial}{\partial t}\delta\rho + U\frac{\partial}{\partial x}\delta\rho &= -w\frac{d\rho}{dz}, & (3.7)\\
\frac{\partial}{\partial t}\delta z_s + U_s\frac{\partial}{\partial x}\delta z_s &= w(z_s), & (3.8)\\
\frac{\partial u}{\partial x} + \frac{\partial v}{\partial y} + \frac{\partial w}{\partial z} &= 0. & (3.9)
\end{aligned}$$

In equation (3.8), z_s indicates a vertical coordinate where a discontinuity in the density may occur. If the fluids are perturbed, the z-velocity at z_s would be $w(z_s) = w_s = \frac{d}{dt}\delta z_s$. The equation thus specifies the z-velocity w at z_s as due to the displacement of a point on the interface, i.e. the z-velocity at the discontinuity in terms of the displacement and convection with the flow. At such a discontinuity, boundary conditions will be applied to solve for the evolution of perturbations in the different strata. The disturbances are supposed normal modes with x, y and t dependence given by

$$\exp[i(k_x x + k_y y + nt)]. \tag{3.10}$$

This approach simplifies the analytical analysis significantly, especially in regards to determining the conditions under which the system would be unstable.

With the substitution of Fourier solutions of this form, equations 4-9 become

$$\begin{aligned}
i\rho(n + k_x U)u + \rho(DU)w &= -k_x\delta p, & (3.11)\\
i\rho(n + k_x U)v &= -ik_y\delta p, & (3.12)\\
i\rho(n + k_x U)w &= -D\delta p - g\delta\rho, & (3.13)\\
i(n + k_x U)\delta\rho &= -wD\rho, & (3.14)\\
i(n + k_x U_s)\delta z_s &= w_s, & (3.15)\\
i(k_x u + k_y v) &= -Dw, & (3.16)
\end{aligned}$$

where D ≡ d/dz.

Multiply (3.11) and (3.12) by $-ik_x$ and $-ik_y$, respectively, add the resulting equations and eliminate the $(k_x u + k_y v)$ term using (3.16). This gives

$$i\rho(n + k_x U)Dw - i\rho k_x (DU)w = -k^2 \delta p, \tag{3.17}$$

where $k^2 = k_x^2 + k_y^2$.
By combining (3.13) and (3.14) (eliminating $\delta\rho$) we get

$$i\rho(n + k_x U)w = -D\delta p - ig(D\rho)\frac{w}{n + k_x U}. \tag{3.18}$$

We now eliminate δp between (3.17) and (3.18), which results in

$$D\{\rho(n + k_x U)Dw - \rho k_x (DU)w\} - k^2\rho(n + k_x U)w = gk^2(D\rho)\frac{w}{n + k_x U}. \tag{3.19}$$

Expanding this equation results in

$$(n + k_x U)(D^2 - k^2)w - k_x(D^2 U)w - gk^2\frac{D\rho}{\rho}\left(\frac{w}{n + k_x U}\right) = 0. \tag{3.20}$$

This equation describes the effects of perturbations in a single fluid where the density is continuous. If the fluid is confined in some geometry and if discontinuities in the density distribution (or interfaces between different fluids) are present, boundary conditions need to be specified. Consider the fluid to be confined between the two planes at z = 0 and z = d. Then the solutions to (3.19, 20) must satisfy the boundary condition

$$w = 0, \text{ at } z = 0 \text{ and } z = d, \qquad \text{cond(1)}.$$

At an interface between two fluids, $z = z_s$, we require the continuity of the velocity w. However, if the horizontal velocity U is discontinuous across $z = z_s$, the normal displacement of any point on the interface must be unique. In view of Eq. 3.15, both of these requirements are fulfilled by the condition

$$w/(n + k_x U) \text{ must be continuous at an interface within the fluid,} \qquad \text{cond(2)}.$$

Now by integrating (3.19) over the discontinuity, a relation that must hold at the boundary interface, is

$$\Delta_s\{\rho(n + k_x U)Dw - \rho k_x (DU)w\} = gk^2\Delta_s(\rho)\left(\frac{w}{n + k_x U}\right)_s, \tag{3.21}$$

where $\Delta_s(f) = f_{z=z_s+0} - f_{z=z_s-0}$ is the jump in the quantity f at $z = z_s$ and f_s is the value of f at $z = z_s$.

3.1.1 The case of two uniform fluids in relative horizontal motion

Let two fluids have a plane interface at z = 0. The densities of the fluids are such that the upper fluid is less dense than the bottom fluid or $\rho_1 < \rho_2$. In the absence of any streaming the configuration is stable. Now let each fluid have a constant streaming velocity U_1 and U_2. Then in each region

$$(D^2 - k^2)w = 0. \tag{3.22}$$

A general solution of the equation would be linear combination of e^{+kz} and e^{-kz}. This condition forces the amplitude of the vertical velocity perturbations to zero for large $|z|$ (above and below the interface), i.e. the

KH instability is strictly a surface phenomenon. Since the velocity w cannot increase exponentially on either side of z = 0 and w/(n + k_xU) must be continuous on the surface, we may choose solutions of the form

$$w_1 = A(n + k_x U_1)e^{+kz}, \tag{3.23}$$

$$w_2 = A(n + k_x U_2)e^{-kz}. \tag{3.24}$$

Now applying the condition (3.21) to the solutions, results in a characteristic equation:

$$\rho_2(n + k_x U_2)^2 + \rho_1(n + k_x U_1)^2 = gk(\rho_1 - \rho_2) \tag{3.25}$$

Let $\alpha_i = \frac{\rho_i}{\rho_1+\rho_2}$, Eq. (3.25) then becomes

$$\alpha_2(n + k_x U_2)^2 + \alpha_1(n + k_x U_2)^2 - gk(\alpha_1 - \alpha_2) = 0. \tag{3.26}$$

Expanding this equation gives

$$n^2 + 2k_x(\alpha_1 U_1 + \alpha_2 U_2)n + k_x^2(\alpha_1 U_1^2 + \alpha_2 U_2^2) - gk(\alpha_1 - \alpha_2) = 0. \tag{3.27}$$

The roots of this equation are given by

$$n = -k_x(\alpha_1 U_1 + \alpha_2 U_2) \pm [gk(\alpha_1 - \alpha_2) - k_x^2 \alpha_1 \alpha_2 (U_1 - U_2)^2]^{1/2}. \tag{3.28}$$

As seen from eq. (3.10), n may be thought of as the growth rate of the perturbations; it depends on the wave number k and the relative velocity of the fluids flowing over one another.

If $k_x = 0$ (or k = k_y) ,

$$n = \pm[gk(\alpha_1 - \alpha_2)]^{1/2}.$$

Since $\alpha_1 > \alpha_2$ we see that perturbations transverse to the direction of streaming are unaffected by the streaming's presence.

In other directions the perturbations will be unstable if n has a non-zero imaginary component. This condition, the instability condition, is given in terms of wave number by

$$k_x^2 \alpha_1 \alpha_2 (U_1 - U_2)^2 > gk(\alpha_1 - \alpha_2). \tag{3.29}$$

For a given (U_1 - U_2) and a direction of **k**, instability occurs for all wave numbers

$$k > \frac{g(\alpha_1 - \alpha_2)}{\alpha_1 \alpha_2 (U_1 - U_2)^2 \cos^2\theta} \tag{3.30}$$

where θ is the angle between **k** and **U**. In the special case of $\theta = 0$, k has a minimum, k_{min}. Thus for, k > k_{min} instability will be present i.e. sufficiently small wavelength perturbations will grow exponentially. The smaller (U_1 - U_2), the smaller the unstable wavelengths are. The growth rate and condition for instability will discussed further in Section 3.1.4.

3.1.2 The influence of a magnetic field

As seen from the above discussion, perturbations along the direction of streaming are the most susceptible to the KH instability. Now, if a uniform magnetic field is present in the fluid, its direction with respect to the streaming will determine to what extent the field will stabilize the fluid, i.e. suppress the KH instability. If the field is transverse to the direction of U, then the most unstable perturbations are transverse to the field also. If on the other hand the field is in the direction of the streaming, the field may have a marked effect on the perturbations. In this case the perturbations tend to bend the field lines and a restoring force or tension in the field lines oppose the instability. The field lines act as a kind of "surface tension", damping or inhibiting the growth of linear perturbations.

In the infinite conductivity limit ($\sigma \to \infty, \eta = \frac{c^2}{4\pi\sigma} \to 0$), the evolution of the magnetic field in the fluid is determined by

$$\frac{\partial B}{\partial t} = \nabla \times (\mathbf{v} \times \mathbf{B}).$$

In alternative form the equation is

$$\frac{dB_i}{dt} = \frac{\partial B_i}{\partial t} + v_j \frac{\partial B_i}{\partial x_j} = B_j \frac{\partial v_i}{\partial x_j}$$

Now consider a horizontal magnetic field B, along the x-axis, which is also the streaming direction. The perturbation to the magnetic field is represented by $\mathbf{b} = (b_x, b_y, b_z)$ and as before the perturbation of the velocity is $\mathbf{u} = (u, v, w)$. Substitution of the equilibrium + perturbation variables into the equation and neglecting non-linear terms, yields

$$\frac{\partial \mathbf{b}}{\partial t} + U\frac{\partial \mathbf{b}}{\partial x} = B\frac{\partial \mathbf{u}}{\partial z} + \mathbf{b}\frac{dU}{dz}. \tag{3.31}$$

The Lorentz force $\mathbf{F}_L = \frac{1}{4\pi}(\nabla \times \mathbf{B}) \times \mathbf{B} = \frac{1}{4\pi}(\mathbf{B} \cdot \nabla)\mathbf{B} - \nabla(B^2/8\pi)$, must be included in the equation of motion. Incorporating the solenoidal nature of the magnetic field, $\mathbf{F}_L$ can also be written as

$$\mathrm{F}_{Li} = \frac{1}{4\pi} B_k \left(\frac{\partial B_i}{\partial x_k} - \frac{\partial B_k}{\partial x_i} \right) \tag{3.32}$$

The equation of motion takes the form

$$\rho\frac{\partial u_i}{\partial t} + \rho u_j \frac{\partial u_i}{\partial x_j} - \mathrm{F}_{Li} = -\frac{\partial}{\partial x_i} p. \tag{3.33}$$

The equations governing the perturbations, with the (x, y, t)-dependence given by (3.10), then are

$$i\rho(n + k_x U)u + \rho(DU)w = -k_x \delta p \tag{3.34}$$

$$i\rho(n + k_x U)v - \frac{B}{4\pi}(ik_x b_y - ik_y b_x) = -ik_y \delta p \tag{3.35}$$

$$i\rho(n + k_x U)w - \frac{B}{4\pi}(ik_x b_z - Db_x) = -D\delta p - g\delta\rho \tag{3.36}$$

$$i(n + k_x U)\mathbf{b} = ik_x B\mathbf{u} + b_z D\mathbf{U} \tag{3.37}$$

$$i(n + k_x U)\delta\rho = -(D\rho)w \tag{3.38}$$

The components of the field (from to Eq. 3.37) are

$$b_x = \frac{k_x B}{n + k_x U}\left(u - \frac{iDU}{n + k_x U} w \right) \tag{3.39}$$

$$b_y = \frac{k_x B}{n + k_x U} v \tag{3.40}$$

$$b_z = \frac{k_x B}{n + k_x U} w \tag{3.41}$$

Insert these components into (3.35) and (3.36)

$$i\rho(n + k_x U)v - \frac{k_x}{n + k_x U}\frac{B^2}{4\pi}\left(\zeta - \frac{k_y DU}{n + k_x U} w\right) = -k_y \delta p \tag{3.42}$$

$$i\rho(n + k_x U)w + \frac{B^2 kx}{4\pi} D\left\{\frac{1}{n + k_x U}\left(u - \frac{iDU}{n + k_x U} w\right)\right\} - \frac{ik_x^2}{n + k_x U}\frac{B^2}{4\pi} w = -D\delta p - ig\frac{D\rho}{n + k_x U} w \tag{3.43}$$

The z-component of the vorticity $\zeta = ik_x v - ik_y u$, where the vorticity $\mathbf{w}$ is defined by $\mathbf{w} = \nabla \times \mathbf{u}$.
Equations (3.34) $\times$ -ik$_y$ added to (3.42) $\times$ +ik$_x$ gives

$$\zeta = \frac{k_y DU}{n + k_x U} w \tag{3.44}$$

and so (3.42) reduces to

$$i\rho(n + k_x U)v = -ik_y \delta p. \tag{3.45}$$

Multiply (3.34) and (3.45) by $-k_x$ and $-k_y$, respectively, and add to find

$$\rho(n + k_x U)Dw - \rho k_x (DU)w = ik^2 \delta p. \tag{3.46}$$

Now write (3.43) in the form

$$ik^2 D\delta p = \rho k^2 (n + k_x U)w - \frac{k^2 k_x^2}{n + k_x U}\frac{B^2}{4\pi} w - k_x k^2 \frac{B^2}{4\pi} D\left\{\frac{1}{n + k_x U}\left(iu + \frac{DU}{n + k_x U} w\right)\right\} + gk^2 \frac{D\rho}{n + k_x U} w. \tag{3.47}$$

Eliminate u by using the relation

$$ik^2 u = -(k_x Dw + k_y \zeta) \tag{3.48}$$

which follows from equations (3.16), the relation $\zeta = ik_x v - ik_y u$ and (3.44).
Therefore we find

$$ik^2 D\delta p = \rho k^2 (n + k_x U)w - k_x^2 \frac{B^2}{4\pi}\left\{D\left(\frac{Dw}{n + k_x U}\right) + \frac{k^2 w}{n + k_x U}\right\} - k_x^3 \frac{B^2}{4\pi} D\left\{\frac{DU}{(n + k_x U)^2} w\right\} + gk^2 \frac{D\rho}{n + k_x U} w. \tag{3.49}$$

Now we can eliminate δp between (3.46) and (3.49) to obtain

$$\begin{aligned} D\{\rho(n + k_x U)Dw - \rho k_x (DU)w\} &= k^2 \rho(n + k_x U)w + k_x^2 \frac{B^2}{4\pi}\left\{D\left(\frac{Dw}{n + k_x U}\right) + \frac{k^2 w}{n + k_x U}\right\} \\ &- k_x^3 \frac{B^2}{4\pi} D\left\{\frac{DU}{(n + k_x U)^2} w\right\} + gk^2 \frac{D\rho}{n + k_x U} w. \end{aligned} \tag{3.50}$$

3.1.3 Two magnetized, uniform fluids in relative horizontal motion

Let the two fluids have densities ρ_1 and ρ_2 and be separated by the boundary at z = 0. Furthermore, let the fluids have velocities U_1 and U_2. In each region of constant density ρ and velocity U, equations (3.44) and (3.50) give

$$\zeta = 0 \tag{3.51}$$

and

$$\left[\rho(n+k_xU) - \frac{k_x^2}{n+k_xU}\frac{B^2}{4\pi}\right](D^2-k^2)w = 0. \tag{3.52}$$

Solutions in the two regions $z<0$ and $z>0$ can as before have the forms

$$w_1 = A(n+k_xU_1)e^{+kz} \quad (z<0), \tag{3.53}$$

$$w_2 = A(n+k_xU_2)e^{-kz} \quad (z>0). \tag{3.54}$$

The continuity of $w/(n+k_xU)$ and the requirements at infinity, are met by these solutions. The last boundary condition follows by integrating equation (3.50) across the interface at $z=0$. This results in

$$\Delta_0\{\rho(n+k_xU)Dw\} = k_x^2\frac{B^2}{4\pi}\Delta_0\left(\frac{Dw}{n+k_xU}\right) + gk^2\Delta_0(\rho)\left(\frac{w}{n+k_xU}\right)_0, \tag{3.55}$$

where $\Delta_0(f)$ represents the jump of f at $z=0$.

We can now apply condition (3.55) to the solutions and obtain

$$\rho_2(n+k_xU_2)^2 + \rho_1(n+k_xU_1)^2 = gk(\rho_1-\rho_2) + k_x^2\frac{B^2}{2\pi}. \tag{3.56}$$

The roots of equation (3.56) are

$$n = -k_x(\alpha_1U_1+\alpha_2U_2) \pm \left[gk(\alpha_1-\alpha_2) + k_x^2\frac{B^2}{2\pi(\rho_1+\rho_2)} - k_x^2\alpha_1\alpha_2(U_1-U_2)^2\right]^{1/2}. \tag{3.57}$$

From this equation it follows that a uniform magnetic field parallel to the direction of streaming will suppress the KH instability if

$$\alpha_1\alpha_2(U_1-U_2)^2 \le \frac{B^2}{2\pi(\rho_1+\rho_2)}. \tag{3.58}$$

That is, the field will suppress the growth of the perturbations if the relative speed is smaller than the rms Alfvén speed of the two media.

The effect of a field transverse to the streaming direction may be investigated with the following equations:

$$i\rho(n+k_xU)u + \rho(DU)w + \frac{B}{4\pi}(ik_xb_y - ik_yb_x) = -ik_x\delta p, \tag{3.59}$$

$$i\rho(n+k_xU)v = -ik_y\delta p, \tag{3.60}$$

$$i\rho(n+k_xU)w - \frac{B}{4\pi}(ik_xb_z - Db_y) = -D\delta p - g\delta\rho, \tag{3.61}$$

$$i(n+k_xU)\mathbf{b} = ik_yB\mathbf{u} + b_zD\mathbf{U}. \tag{3.62}$$

The remaining equations are unaltered. Now following the same procedure as above, (3.50) is replaced by

$$\begin{aligned} D\{\rho(n+k_xU)Dw - \rho k_x(DU)w\} &= k^2\rho(n+k_xU)w + k_y^2\frac{B^2}{4\pi}\left\{D\left(\frac{Dw}{n+k_xU}\right) + \frac{k^2w}{n+k_xU}\right\} \\ &- k_xk_y^3\frac{B^2}{4\pi}D\left\{\frac{DU}{(n+k_xU)^2}w\right\} + gk^2\frac{D\rho}{n+k_xU}w. \end{aligned} \tag{3.63}$$

This equation reduces to the hydrodynamic case, as discussed in Section 3.1.1, if $k_y=0$. Therefore the transverse field in the system does not affect the growth of the KH instability in the direction of maximal growth, i.e. the streaming direction.

3.1.4 Growth time scales

In general, the interface between two fluids in relative motion is unstable to the Kelvin-Helmholtz mode when the relative velocity is large enough that it dominates the suppressing effects of, for example, gravity and magnetic field line tension. However, the growth rate of unstable perturbations also depends on the linear size of the perturbations and the relative densities of the fluids. As seen in Section 3.1.1, the growth rate in the purely hydrodynamic case of two fluids flowing over each other is given by

$$n = -k_x(\alpha_1 U_1 + \alpha_2 U_2) \pm [gk(\alpha_1 - \alpha_2) - k_x^2 \alpha_1 \alpha_2 (U_1 - U_2)^2]^{1/2} \tag{3.64}$$

If the effective gravity is zero, the interface will be unstable for all wave vectors $\mathbf{k}$ with a component in the streaming direction. The growth rate is then given by

$$n = -k_x(\alpha_1 U_1 + \alpha_2 U_2) \pm [-k_x^2 \alpha_1 \alpha_2 (U_1 - U_2)^2]^{1/2}. \tag{3.65}$$

An equivalent growth time is defined as $\tau_{KH} = 1/n_{im}$ where n_{im} is the magnitude of the imaginary part of n. Therefore

$$\tau_{KH} = [k_x^2 \alpha_1 \alpha_2 (U_1 - U_2)^2]^{-1/2}. \tag{3.66}$$

Now we let $(U_1 - U_2) = v_{rel}$ and define a wave length $\lambda = 2\pi k_x$, which leads to (cf. Wang & Robertson 1984)

$$\begin{aligned} \tau_{KH} &= \frac{\lambda}{2\pi}(\alpha_1 \alpha_2)^{-1/2} \frac{1}{v_{rel}} \\ &= \frac{1 + \rho_1/\rho_2}{(\rho_1/\rho_2)^{1/2}} \frac{\lambda}{2\pi} \frac{1}{v_{rel}}. \end{aligned} \tag{3.67}$$

Since $\tau_{KH} \propto \frac{\lambda}{v_{rel}}$ for fixed relative density, it can be seen that small perturbations on an interface with high relative velocities grow the fastest, i.e. $\tau_{KH} \to 0$ $[\lambda \to 0, v_{rel} \to \infty]$.

The growth of linear perturbations on a two-fluid interface, accompanied by effective mixing may be a very effective angular momentum transfer mechanism. This effect was investigated by Wang & Robertson (1984, 1985), by investigating the growth of the KH instability at the interface separating a fast rotating magnetosphere and an accretion disc in X-ray binaries. Numerical simulations performed by these authors revealed that the KH instability may be a very effective mechanism explaining accretion disc propelling, but also showed that magnetic bubbles (vortex tubes) that transfer angular momentum, are also induced along the interface. This process is accompanied by episodes of magnetic reconnection, and possibly particle acceleration. Since the formation of vortex tubes, angular momentum transfer (propeller action), reconnection and particle acceleration is associated with the propeller in AE Aqr, a brief discussion of the Wang & Robertson results will be presented. This is mainly done to illustrate the process of magnetic bubble formation, which may be highly relevant in explaining the effective propeller and multi-wavelength emission in AE Aqr.

3.1.5 The Wang & Robertson investigation

In the quest to understand the observed properties of accreting X-ray sources, specifically the spindown of binary radio pulsars, Wang & Robertson (1984) investigated the interaction of a plasma with the magnetosphere of a fast rotating neutron star. The authors investigated the non-linear development of the KH

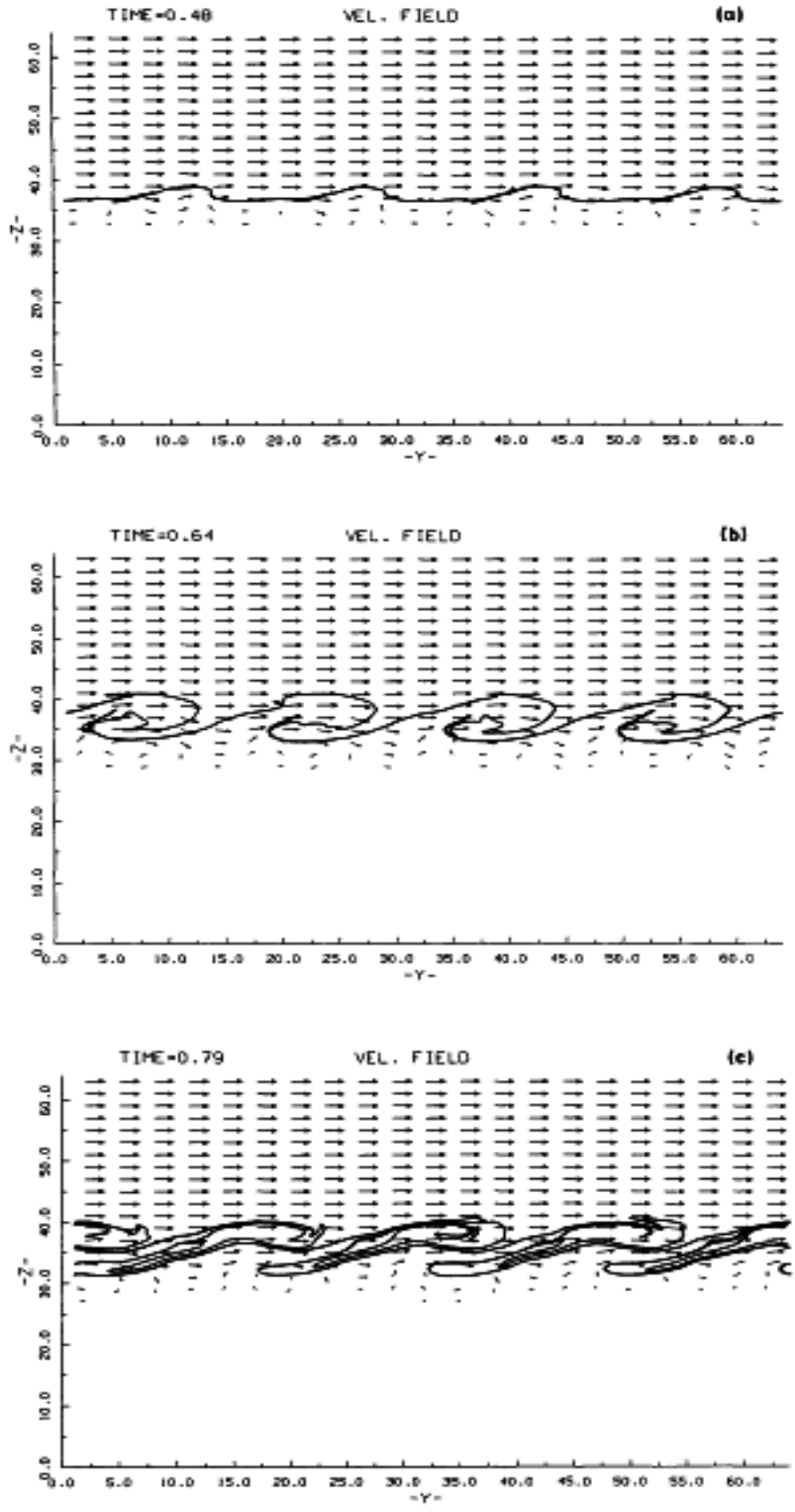

Figure 3.2: Diagrams showing the time evolution of sinusoidal disturbances due to the KH instability (Wang & Robertson 1984). The top fluid is flowing to the right while the bottom fluid is stationary. It can be seen that fluid elements of the initial interface is moved in a manner that affects the mixing of the fluids.

Figure 3.3: Photograph of Kelvin-Helmholtz instability mixing of clouds and air (B. Wong, www.cloudappreciationsociety.org)

instability numerically. The configuration they chose represented the interface between a fast rotating magnetosphere and an accretion disc. The computations are however carried out on a 2-D Cartesian grid. The system consists of two fluids, one in the upper half of the grid and one in the lower half. In the equilibrium state, the upper fluid (Medium 1) has velocity u to the right and Medium 2 is stationary. The fluids have densities ρ_1 and ρ_2, respectively. A gravitational field g, pointing downwards, could also be added to the numerical model in order to analyze the formation and growth of the Rayleigh-Taylor instability in the unstable case when $\rho_1 > \rho_2$.

The results of the simulations revealed that disturbances of a characteristic horizontal extent or wavelength $\lambda_\circ$, grow exponentially as the linear theory predicts. However, when the disturbance reaches an amplitude comparable to $\lambda_\circ$, the growth saturates, the interface rolls up generating vortex structures. Another important result is that neighboring vortices tend to coalesce and therefore large wavelength disturbances, which initially grow the slowest, ultimately dominate. Mixing of the two fluids over length scales determined by these large wavelength disturbances, may result in highly efficient angular momentum transfer. This transfer may lead to a propeller effect of the type envisaged for a rapidly spinning neutron star (Illarionov & Sunyaev 1975). The generation of magnetic vortex tubes and resultant momentum transfer to disc material due to the centrifugal expulsion of these magnetic bubbles, are illustrated in Figures 3.2, 3.4. An areal photograph of the generation of the KH instability at the interface between high altitude cirrus clouds and high velocity wind is shown in Figure 3.3. Clearly visible in the photograph is the effective mixing of the two fluids which facilitates the transfer of momentum between the denser fluid (water vapour) and the lower density, high velocity air.

The generation of large-scale MHD perturbations on the interface and the transfer of momentum to neighboring layers may result in the generation of velocity fluctuations in the fluid, i.e. turbulence. The generation of hydrodynamic turbulence in the flow will manifest in a cascade of mechanical energy, via the

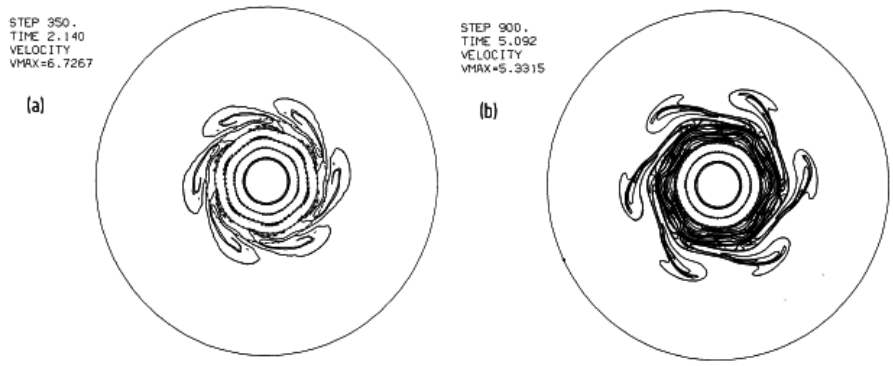

Figure 3.4: As in Figure 3.2, but in a 2-D cylindrical geometry (Wang & Robertson 1985). The simulation investigates the interaction of a fast spinning, neutron star magnetosphere and impinging gas. The magnetosphere interacts strongly with the gas and in the mixing zone, angular momentum can be transferred.

Kolmogorov process, to the dissipative regime, which results in heating and radiation. The signature of this process may in fact be the release of a vast reservoir of turbulent energy after a characteristic cascade time, determined by the Kolmogorov spectrum. This may explain the occurrence of optical flares in AE Aqr several hours after the blobs have silently glided through the magnetosphere. The possible relation between a turbulent propeller ejected flow and thermal energy release (flares) warrants a brief discussion.

3.2 Turbulence

The growth of KH instabilities in a flow is inexorably tied to the development of turbulence (Biskamp 2003), which has a severe influence on the flow profile of the fluid. The transition to a turbulent state may be described as the generation of random motions from a smooth flow. Disturbances to a fluid in motion, manifest in gradients of velocity, pressure and magnetic field. If these gradients become larger than threshold values, diffusion as transport mechanism becomes insufficient and the system becomes unstable. The growth of perturbations in the fluid leads to turbulence, which provides a more efficient, convective transport mechanism for momentum, heat and magnetic flux. Biskamp (2003) discusses three types of instability that trigger turbulence in macroscopic plasmas :

i) Kelvin-Helmholtz instability, driven by a velocity shear

ii) Rayleigh-Taylor instability, driven by the buoyancy force

iii) current-driven MHD instabilities in magnetic plasmas - in particular the tearing instability

Turbulence in a stream of fluid is a coping mechanism for dealing with too large a shear at its surface where it interacts with another fluid or a pipe wall. The onset of KH driven turbulence may result in the effective mixing of the fluids across a boundary layer. The mixing extracts mechanical energy from the relative motion of the fluids, adding to the intensity of turbulence of the flow. Hence, turbulence induces more turbulence in a flow.

The Reynolds number is often a good indication whether or not turbulence is likely to develop. The dimensionless Reynolds number $R_e = \mathrm{Lv}/\nu$, where L and v are typical length and velocity scales and ν is

the fluid viscosity, quantifies the importance of viscosity in hydrodynamics. A high value of R_e suggests that the flow of the fluid dominates the viscous dissipation of fluid motions. Experimental results indicate that flows become turbulent at values of $R_e > 10^3$ (e.g. Tritton 1977, p. 233-237, Choudhuri 1998, p. 86).

3.2.1 Turbulent energy cascade and the Kolmogorov spectrum

Turbulence is quantified in terms of a statistical description considering mean values and fluctuations.

A turbulent fluid is described as containing eddies of different sizes. The interaction of the motion on different length scales can be described in terms of these eddies. On the largest scales, eddies appear localized in the flow, but small eddies are not individually distinguishable.

The energy cascade process involves the formation of smaller eddies from larger ones. This process may be described by considering two fluid elements in a vortex tube. The two elements are likely to be displaced in different directions. Now, if the fluid is incompressible and the vorticity is conserved, the vortex tube will be stretched. If vorticity is still to be conserved, the cross-section of the tube must decrease, which suggests vorticity is transferred to smaller scales.

In most investigations it is assumed that the turbulence is isotropic and homogeneous, i.e. the turbulent motions show no preferred direction and the statistical properties have no positional dependence. Quantification in terms of a statistical description involves considering mean values and fluctuations. The velocity and pressure at each point in the fluid is written as a sum of the mean (an ensemble average) and the fluctuation about the mean,

$$\mathbf{v} = \bar{\mathbf{v}} + \mathbf{v}', \quad P = \bar{P} + P'.$$

We have that $\langle \mathbf{v}' \rangle = \frac{1}{T} \int_0^T \mathbf{v}'(t) dt \to 0$ for large T (a time long compared to the time scales of variation of $\mathbf{v}$). The mean velocity-fluctuation squared $\langle |\mathbf{v}'|^2 \rangle$ is related to the kinetic energy of the motion and is referred to as the strength or the intensity of the turbulence.

The velocity field can be analyzed in Fourier components, producing a frequency spectrum that characterizes the distribution of energy of the turbulent motions over different time scales. A spatial analysis produces a distribution in terms of wave numbers. The fluctuating part of the velocity field $\mathbf{v}'(\mathbf{x})$ (effectively the velocity fluctuation per unit volume) can be written as

$$\mathbf{v}'(\mathbf{x}) = \frac{1}{(2\pi)^3} \int_V \mathbf{v}^*(\mathbf{k}) e^{i\mathbf{k}.\mathbf{x}} d^3k \tag{3.68}$$

where $\mathbf{v}^*(\mathbf{k})$ is the Fourier transform of $\mathbf{v}'(\mathbf{x})$. If U is the total turbulent energy per unit mass, then

$$U = \frac{1}{(2\pi)^3} \frac{1}{V} \int \frac{1}{2} \langle |\mathbf{v}^*(\mathbf{k})|^2 \rangle d^3k. \tag{3.69}$$

Furthermore, if the turbulent eddies or velocity fluctuations are distributed isotropically, the energy per unit wave number per unit mass can be written as

$$U_k(k) = \frac{k^2 \langle |\mathbf{v}^*(\mathbf{k})|^2 \rangle}{4\pi^2 V}. \tag{3.70}$$

The angular brackets denote a time average over the velocity. The energy per unit mass U, may be obtained by integrating U_k over all wave numbers k. U_k may be thought of as the spectral energy density of the turbulent velocity field $\mathbf{v}'$.

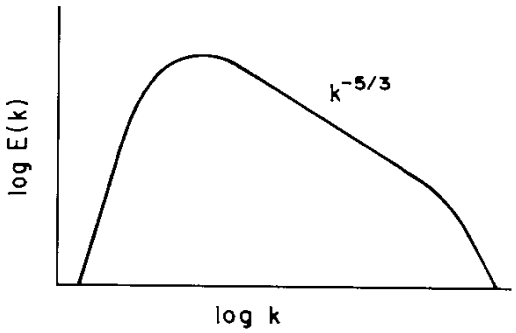

Figure 3.5: (Choudhuri 1998) A spectrum of energy density vs. wavenumber showing the typical Kolmogorov dependence, i.e. the characteristic spectrum of the inertial range ($k_{min} \ll k \ll k_{max}$). The qualitative behaviour of the turbulent spectrum outside the inertial range, is also indicated.

Back in real space, k is related to an eddy length scale as $k = 2\pi/\ell$. Let k_{min} and k_{max} denote the wave numbers of the largest and the smallest eddies, respectively. An rms turbulent turnover speed v is assumed, which corresponds with a turnover time given by $\mathrm{t} \sim \ell/v = 1/kv$. Through stretching of vortex tubes, each eddy breaks up into roughly half its size on roughly the same time scale and the energy flows from wave number k to $2k$. This cascade prevents energy from accumulating at any wave number. The cascading energy per unit mass and unit time, must then be constant and can be written as $\mathrm{Q} \sim v^2/\mathrm{t} = kv^3$ and thus $v(k) \sim (\mathrm{Q}/k)^{1/3}$. The total energy as a function of wave number is $U \sim v^2(k)$, but the energy per unit mass in an eddy of wave number k is $\sim kU_k$. The spectral energy density is therefore

$$U_k(k) = Q^{2/3}k^{-5/3} \quad , \quad k_{min} \ll k \ll k_{max} \tag{3.71}$$

where k falls in the *i*nertial range. The relation is known as the Kolmogorov spectrum of energy density (plotted in Figure 3.5) and has been verified experimentally to a high degree of accuracy in large R_e flows. It should be emphasized that the $U_k(k) \propto k^{-5/3}$ applies strictly to the inertial range where the total mechanical energy of the turbulent cells transform to smaller length scales, without dissipation into heat. Only upon reaching length scales comparative to the mean free path on molecular level, does the total turbulent reservoir dissipate as heat energy. A brief discussion is presented below.

3.2.2 Turbulent dissipation: Heat generation

As was pointed out above, the Kelvin-Helmholtz mechanism may be intimately linked to the generation of turbulence in a flow. Furthermore, it has been shown (Meintjes & Venter 2005) that the Reynolds number of the flow in the interaction region with the white dwarf magnetosphere is of the order of $R_\mathrm{e} \sim 10^9$, which is orders of magnitude higher than the limiting Reynolds numbers of $R_\mathrm{e} \sim 3000$ where laboratory flows start to exhibit turbulence (e.g. Tritton 1977, pp. 233-237). Therefore, any discussion of the Kelvin-Helmholtz instability in the boundary layer must be done in connection with associated turbulent flow.

The time needed for energy to cascade down from the largest to the smallest eddies can be estimated. For large eddies, the effects of viscosity may be neglected, but at the smallest scales viscous and inertial forces become comparable and the cascading kinetic energy is converted into heat. Hence the Reynolds number

for the smallest scales of the flow will be $\mathrm{R}_e \sim 1$. Comparing this to the turnover velocity, it is found that

$$\frac{k_{max}}{k_{min}} = R_e^{3/4} \tag{3.72}$$

where R_e here is the Reynolds number of the largest eddies in the flow. Each successive cascade occurs in a time shorter than the previous by a factor $2^{-2/3}$. Consequently the cascade time to the second largest eddies, is approximately equal to the cascade time further down to the smallest eddies. The total cascade time can therefore be approximated as $\mathrm{t}_{casc} \approx 0.74\ell/v$.

The cascade process accelerates towards shorter length scales (e.g. Landau & Lifshitz 1987, pp. 132-133) as each eddy feeds its energy to shorter scales, resulting in a total cascade time of the order of

$$\tau_{\mathrm{cas}} \approx \left(\frac{L_{\mathrm{max}}}{v_{\mathrm{rms}}}\right), \tag{3.73}$$

where L_{max} and $v_{\mathrm{rms}} \sim \alpha c_s (\alpha \sim 0.1)$ represent the maximum length scale of the turbulent cells and the associated turbulent turnover velocity, typically of the order of a fraction of the local sound speed, respectively.

For a Kolmogorov type energy cascade of turbulent eddies of initial dimension $l_{\mathrm{max,i}}$, with an average turn-over velocity $v_{\mathrm{rms,i}}$ in the inertial range, to the dissipative scale where the corresponding values are l_{d} and $v_{\mathrm{rms,d}}$ (e.g. Choudhuri 1998, pp. 165-169), we have an eventual energy dissipation rate per unit mass

$$\begin{aligned} \epsilon &= \left(\frac{v_{\mathrm{rms,i}}^3}{l_{\mathrm{max,i}}}\right) \\ &= \left(\frac{v_{\mathrm{rms,d}}^3}{l_{\mathrm{d}}}\right). \end{aligned} \tag{3.74}$$

This results in a rate of heat generation on the dissipative scale which is given by

$$\begin{aligned} \dot{u}_{\mathrm{t}} &= \rho\left(\frac{v_{\mathrm{rms}}^3}{L_{\mathrm{max}}}\right) \\ &= \rho\nu_{\mathrm{t}}\left(\frac{v_{\mathrm{rms,d}}}{l_{\mathrm{d}}}\right)^2 \ \mathrm{erg\ cm^{-3}s^{-1}}, \end{aligned} \tag{3.75}$$

where $\nu_{\mathrm{t}} = v_{\mathrm{rms,d}} l_{\mathrm{d}}$ represents the coefficient of turbulent viscosity. An upper limit on the heating rate of the gas on the scale of the smallest eddies can be obtained by assuming that the turn-over velocity of the turbulence approaching the speed of sound. This will result in an effective shock-driven process of converting the mechanical energy contained in turbulent cells into heat energy, hence quenching the turbulent flow on the molecular level. It can be shown (e.g. Choudhuri 1998, p. 166) that the size of the smallest eddies relates to the size of the largest according to

$$l_{\mathrm{d}} = \left(\frac{R_{\mathrm{e}}}{R_{\mathrm{e,crit}}}\right)^{-3/4} l_{\mathrm{max}}, \tag{3.76}$$

where R_{e} and $R_{\mathrm{e,crit}} \sim 100$ (e.g. Biskamp 2003, p. 47) represent respectively, the Reynolds number of the flow and the critical value where the largest eddy equals the size of the smallest.

Turbulence can be sustained as long as MHD power is dissipated in the boundary layer, presumably by the action of the fast rotating magnetosphere of the white dwarf. A qualitative investigation of the total MHD reservoir, driving the KH instability and turbulent outflow is presented next.

3.3 MHD dissipation

The rate of doing work by external electric and magnetic fields on a single charge q is given by $q\mathbf{v}\cdot\mathbf{E}$ where $\mathbf{v}$ is the velocity of the charge. The magnetic field does not change the energy of the charge, since the magnetic force is perpendicular to the velocity. The rate at which the fields do work in a finite volume V is

$$\frac{dW}{dt} = \int_V \mathbf{J}\cdot\mathbf{E}\, d^3x.$$

The principal effect of the work done by the fields is that it converts electromagnetic energy into mechanical or heat energy, but this process also changes the field energy inside V. (In a plasma with a high conductivity the thermal dissipation of the field energy is negligible and the bulk fluid can therefore gain kinetic energy.) The total power dissipated by the fields in a volume V can be written as

$$\int_V \mathbf{J}\cdot\mathbf{E}\, d^3x = \frac{-1}{4\pi}\int_V \left[c\nabla\cdot(\mathbf{E}\times\mathbf{H}) + \mathbf{E}\cdot\frac{\partial\mathbf{D}}{\partial t} + \mathbf{H}\cdot\frac{\partial\mathbf{B}}{\partial t}\right] d^3x. \tag{3.77}$$

Now denote the total energy density of the fields as

$$u_f = \frac{1}{8\pi}(\mathbf{E}\cdot\mathbf{D} + \mathbf{B}\cdot\mathbf{H}). \tag{3.78}$$

Then it follows that a continuity equation for the field energy of the system, i.e. the field energy density and e-m flux, is given by

$$-\int_V \mathbf{J}\cdot\mathbf{E}\, d^3x = \int_V \left[\frac{\partial u_f}{\partial t} + c\nabla\cdot(\mathbf{E}\times\mathbf{H})\right] d^3x \tag{3.79}$$

and for arbitrary V we have

$$\frac{\partial u}{\partial t} + \nabla\cdot\mathbf{S} = -\mathbf{J}\cdot\mathbf{E}, \tag{3.80}$$

where the negative sign indicates the dissipation of the fields. In this continuity equation, the vector $\mathbf{S}$ represents the energy flux, i.e. Poynting's vector,

$$\mathbf{S} = \frac{c}{4\pi}(\mathbf{E}\times\mathbf{H}).$$

Therefore the work done by the fields in V and the flux of electromagnetic energy into or out of V, manifests in the change in the energy density of the fields.

Charged particles gain energy from the work done by the fields in V. Poynting's theorem can now describe the conservation of energy of the combined system of particles and fields. Now, if E_{mech} is the total mechanical energy of the particles in the volume V, we have

$$\frac{dE_{mech}}{dt} = \frac{dW}{dt} = \int_V \mathbf{J}\cdot\mathbf{E}\, d^3x. \tag{3.81}$$

For the combined field and particle system, Poynting's theorem now gives

$$\frac{dE}{dt} = \frac{d}{dt}(E_{mech} + E_{field}) = -\oint_S \mathbf{S}\cdot\mathbf{n}\, da \tag{3.82}$$

where the total field energy is given by

$$E_{field} = \int_V u\, d^3x = \frac{1}{8\pi}\int_V (\mathbf{E^2} + \mathbf{B^2})\, d^3x.$$

Equation (3.82) relates the rate of change of the total energy to the electromagnetic flux crossing the boundary of the fluid. Hence, a flux of electromagnetic energy across the surface of a conducting fluid volume, can change the mechanical and field energy within the volume.

In a conducting fluid with finite resistivity, the electric field is given by (Parker 1976)

$$E_{\perp} = -\frac{\mathbf{v}}{c} \times \mathbf{B} \left[1 + \left(\frac{1}{R_{\rm m}} \right) \left(\frac{Lv}{c} \right) \left(\frac{\nabla \times \mathbf{B}}{\mathbf{B} \times \frac{\mathbf{v}}{c}} \right) \right], \tag{3.83}$$

where R_m represents the magnetic Reynolds number (e.g. Meintjes & Venter 2005). For highly conducting fluids $R_m \rightarrow \infty$ (i.e. $\sigma \rightarrow 0$) and the electric field reduces (in the non-relativistic limit) to

$$\mathbf{E} + \frac{1}{c}(\mathbf{v} \times \mathbf{B}) = 0. \tag{3.84}$$

The electric field is therefore determined by the magnetic field and the relative velocity between the fluid and the field.

When this velocity $\mathbf{v} = \mathbf{v_{rel}}$, is perpendicular to the field $\mathbf{B}$, Poynting's vector is a maximum and is given by

$$\begin{aligned} \mathbf{S} &= \frac{1}{4\pi}[\mathbf{B} \times (\mathbf{v_{rel}} \times \mathbf{B})] \\ \text{and} \quad |\mathbf{S}| &= \frac{1}{4\pi} v_{rel} \mathrm{B}^2. \end{aligned} \tag{3.85}$$

The Poynting flux is therefore a useful way of quantifying or constraining the total MHD power dissipated in the flow. It has been shown (Eq. 3.82) that the Poynting flux will result in a transfer of mechanical energy to the fluid, which is in fact the driving mechanism of the MHD propeller in AE Aqr. Furthermore, Eq. 3.85 indicates that $|\mathrm{S}| \rightarrow \infty$ for ($\mathrm{v}_{\perp}$, B) $\rightarrow \infty$.

It was mentioned earlier that $\frac{v_{\phi,m}}{v_{ff}} \gg 1$, and thus $\mathrm{v}_{rel} \rightarrow v_{\phi,m} \approx 20000$ km s^{-1}. If the white dwarf field is assumed to have a dipolar configuration with $\mathrm{B}_* \sim 10^6$ G, then B(r_{cl}) $\sim$ 300 G. It is therefore evident that a significant reservoir of MHD energy exists, which can drive the propeller process in AE Aqr.

The discussion presented in the above sections, have been integrated in a unified model connecting the propeller mechanism and the peculiar multi-wavelength emission in AE Aqr. This is now presented in a series of three papers.

3.4 A unified model explaining the peculiar multi-wavelength emission of AE Aqr in terms of a KH driven MHD propeller

3.4.1 The diamagnetic blob propeller in AE Aquarii and non-thermal radio to mid-infrared emission

MNRAS 360, 573 (2005)

P.J. Meintjes, L.A. Venter

Abstract

This paper presents a qualitative investigation of the propeller mechanism in AE Aquarii within the framework of the magnetohydrodynamic interaction between the fast rotating magnetosphere of the white dwarf and a blobby mass flow stream from the secondary star. It has been shown that the denser part of the mass flow can penetrate the fast rotating magnetosphere of the white dwarf to the circularization radius, before it is ejected from the system. It has been shown that the total magnetohydrodynamic power dissipated on a volume of material equivalent to an orbiting ring of cross-sectional radius $R_{\rm stream} \sim 10^9$ *cm, at the circularization radius, is* $P_{\rm mhd} \sim 10^{34}$ *erg* s^{-1}*, which is of the same order of magnitude than the inferred spin down power of the white dwarf. Mixing of the magnetospheric field with a turbulent gas stream due to turbulent diffusion and Kelvin-Helmholtz instabilities, creating magnetic vortices in the flow, results in a transfer of mechanical energy to the stream, accelerating it like a slingshot to velocities exceeding the escape velocity over time scales far too short for viscous spreading of the material into a disc. The diffusion of the field into the turbulent gas probably results in stripping of the magnetospheric field through fast reconnection as a result of the huge differential rotation, resulting in the creation of magnetized plasma clouds with fields of* $B_{\rm cloud} \geq 300$ *G. It has been shown that the interaction of the white dwarf field with the magnetized blob can accelerate electrons to energies of at least* $\epsilon_{\rm e,} \sim 130$ *MeV within the dominant energy loss time scales, which is high enough to account for the maximum electron energies of* $\epsilon_{\rm max} \sim 80$ *MeV, inferred from the latest detection of possible non-thermal emission at frequencies* $\nu \sim 17\,000$ *GHz and 25 000 GHz, using the Keck I telescope in Hawaii. It has been shown that the efficiency of the mhd propeller in converting thermal electrons to relativistic electrons, energetic enough to drive the total observed non-thermal emission in AE Aquarii, is probably of the order of* ~ 0.1 *%. This is consistent with the ratio (*$\beta \sim 0.1\%$*) of the total observed radio to mid-infrared synchrotron emission to the total spin down power of the white dwarf. Based upon energy arguments, it has been shown that magnetized synchrotron emitting clouds with fields of* $B_{\rm eq} \sim 300$ *G, which is similar to the magnetospheric field at the main interaction zone, i.e. the circularization radius, can confine a population of relativistic electrons that are able to power the total observed non-thermal radio to mid-infrared emission with luminosity* $L_{\rm r-ir} \sim 10^{31}$ *erg* s^{-1}*.*

keywords

accretion - binaries: general - stars: white dwarf - processes: mass transfer, outbursts.

1. INTRODUCTION

AE Aquarii is a peculiar nova-like variable star, consisting of a fast rotating white dwarf primary star, with a rotation period of $P_{\rm spin} \approx 33$ s (Patterson 1979), orbiting a K4 type secondary star about the common centre of mass (CM) with an orbital period of $P_{\rm orb} \sim 9.88$ h (Joy 1954). The inferred distance to AE Aquarii is approximately $D \sim 100$ pc (Welsh, Horne & Gomer 1995; Friedjung 1997). This enigmatic system has been studied intensively over 18 decades in energy, and displays a host of peculiar emission properties from radio waves (e.g. Bookbinder & Lamb 1987; Bastian, Dulk & Chanmugam 1988) to possibly TeV gamma-rays (Meintjes et al. 1992, 1994; Meintjes & de Jager 2000).

It has been shown (Meintjes 2002; Schenker et al. 2002) that AE Aquarii evolved into the cataclysmic variable phase after a history of high thermal time scale mass transfer from the K4 secondary star, and resultant high mass accretion onto the surface of an initially slowly rotating white dwarf. It has been pointed out that the initial rotation period of the magnetized white dwarf during the phase of high mass accretion could have been in the order of $P_{1,i} \sim 1$ hour (Wynn, King & Horne 1997). By investigating the evolution of AE Aquarii, it has been shown (Meintjes 2002) that the current short $P_1 = P_{\rm spin} \approx 33$ s spin period of the white dwarf and the long $P_{\rm orb} = 9.88$ h orbital period is reconcilable with a history of very high, run-away mass accretion onto the white dwarf, which probably lasted for a period of approximately $t_{\rm acc} \approx 10^4$ - 10^5 years (Meintjes 2002; Schenker et al. 2002). In this high mass transfer phase AE Aquarii could have been a super soft x-ray source (Meintjes 2002; Schenker et al. 2002). The high mass accretion rate onto the surface of the white dwarf resulted in the white dwarf being spun-up to a period close to $P_1 = P_{\rm spin}$. It has been shown (Meintjes 2002) that the high mass transfer phase in AE Aquarii probably terminated at a critical mass ratio of $q_{\rm crit} \leq 0.73$ assuming the secondary is slightly evolved, which seems to be the case (e.g. Wynn, King & Horne 1997; Eracleous & Horne 1996; Pearson, Horne & Skidmore 2003). Optical (Welsh, Horne & Gomer 1995, 1998) and ultraviolet (Eracleous et al. 1994) spectroscopic observations using the *HST* reveal, in conjunction with a pulse timing analysis of the 33 s spin period (de Jager, Meintjes, O' Donoghue & Robinson 1994), that the current mass ratio of the system is probably between $q = (M_2/M_1) \approx 0.64$-$0.67$. The rapid mass transfer in the thermal mass transfer phase rapidly eroded the mass of the secondary star from values probably in excess of $M_{2,\rm i} \sim 1\ M_\odot$, to a value $M_2 < 1\ M_\odot$ before $\rm q_{crit}$ was reached. Meintjes (2002) showed for $q \leq \rm q_{crit}$ mass transfer proceeded at a much lower rate, driven by magnetic braking of the secondary star.

The system shows rapid flaring in optical wavelengths (e.g. Patterson 1979) with the optical intensity varying between $m_v = 10$ - 12 on a regular basis. These flares were initially associated with enhanced mass accretion onto the magnetic poles of the white dwarf from an accretion disc. However, there is a peculiarly weak correlation between the amplitude of the 33 s oscillation and the increased intensity during optical outbursts (e.g. Patterson 1979; O' Donoghue et al. 1995), refuting the idea of enhanced mass accretion onto the poles of the white dwarf as being the source of the optical outbursts. This has been confirmed by *HST* observations of AE Aquarii during outbursts (Eracleous et al. 1994), showing no correlation between the amplitude of the 33 s period and the increased brightness during flares. These findings, combined with the absence of double peaked emission lines in the spectrum which are the signature of an accretion disc (e.g. Horne 1991), indicate that no accretion disc facilitates mass accretion onto the white dwarf in quiescence

and flares.

Cropper (1986), and later Beskrovnaya et al. (1995), reported circular polarization at the level of (0.05 ± 0.01) % and (0.10 ± 0.03) % respectively in optical frequencies, which, if produced by cyclotron emission, may indicate a magnetic field in excess of $B_1 \sim 10^6$ G (Chanmugam & Frank 1987). It has been pointed out (Patterson 1994) that the fast rotating magnetosphere of the white dwarf will act as a propeller, ejecting the mass flow from the system before it can settle in a well defined disc. It has been pointed out that the mass transfer in cataclysmic variables is most probably blob-like (e.g. King 1993; Wynn & King 1995), and that the observed outbursts in AE Aquarii are a result of less dense blobs overtaking denser and heavier blobs that have been ejected by the propeller from regions closer to the white dwarf (Welsh 1999; Horne 1999; Pearson, Horne & Skidmore 2003). In this model, the magnetospheric propeller acts as a blob sorter. The denser, heavier blobs penetrate deep into the magnetosphere, exiting with lower terminal velocity than less dense blobs which are more easily penetrated by the field and ejected further out, exiting with higher terminal velocity (e.g. Wynn, King & Horne 1997; Horne 1999; Pearson, Horne & Skidmore 2003). The result is a collision between less dense blobs overtaking heavier blobs, resulting in shocks and flares. Detailed simulations of the dynamics of magnetically propelled blobs indicate that they cross in an arc-shaped region of the exit stream, in just the right place to account for the orbital kinematics inferred from the Doppler tomography of the emission lines (Welsh, Horne & Gomer 1998; Welsh 1999; Horne 1999; Ikhsanov, Neustroev & Beskrovnaya 2004).

It has been shown (Wynn, King & Horne 1997) that the ballistic stream consisting of the denser diamagnetic blobs passes the white dwarf at the distance of closest approach, which is of the order of the circularization radius, i.e. $R_{\rm circ} \sim 10^{10}$ cm. This means that the interaction between the magnetosphere and the blob stream takes place far outside the corotation radius, which is of the order of $R_{\rm cor} \sim 2 \times 10^9$ cm. Therefore, the interaction between the fast rotating white dwarf magnetosphere and the fragmented mass flow from the secondary star exerts a spin-down torque on the white dwarf. This has been confirmed by a 13 year study of the phase-coherence of the 33 s white dwarf spin period, revealing that the white dwarf is indeed spinning down at a rate of $\dot{P} \sim 5.6 \times 10^{-14}$ s s^{-1} (de Jager, Meintjes, O' Donnoghue & Robinson 1994). This spin-down implies an inferred spin-down power of $P_{\rm sd} = I\Omega\dot{\Omega} \sim 10^{34}$ erg s^{-1}. The inferred spin-down power is approximately a factor of 500 higher (e.g. Meintjes & de Jager 2000) than the observed accretion induced luminosity, i.e. $L_{\rm acc} \sim 2 \times 10^{31}$ erg s^{-1}, derived from *HST* ultra-violet (uv) and X-ray data (e.g. Eracleous, Halpern & Patterson 1991; Eracleous & Horne 1996). This implies an accretion rate onto the poles of the white dwarf of the order of $\dot{M} \sim 10^{14}$ g s^{-1}. It has been pointed out (Eracleous & Horne 1996; Wynn, King & Horne 1997), that in order to explain the emission lines, the propeller driven mass outflow rate of material from the white dwarf has to be of the order of $\dot{M}_{\rm out} \approx 5 \times 10^{17}$ g s^{-1}. The ratio of the inferred accretion rate to the inferred mass transfer corresponds to a fraction of approximately $\sim$ 0.01-0.02 %, suggesting an extremely effective propeller. This is confirmed by the inferred rate of outflow of mechanical energy from the system which is at least

$$\begin{aligned} L_{\rm mech} &= \tfrac{1}{2}\dot{M_{\rm out}} v_{\rm esc}^2 \\ &\approx 5 \times 10^{33} \left(\tfrac{\dot{M}_{\rm out}}{5\times10^{17}\ {\rm g\ s^{-1}}}\right) \\ &\quad \left(\tfrac{v_{\rm esc}}{1.55\times10^{8}\ {\rm cm\ s^{-1}}}\right)^2 {\rm erg\ s^{-1}}. \end{aligned} \tag{3.86}$$

This is of the order of the inferred spin-down power of the white dwarf, implying that nearly the entire reservoir of rotational kinetic energy drives the mass outflow from the system. This propeller effect contributes to the uniqueness of AE Aquarii among the magnetic cataclysmic variables. Another aspect contributing to the uniqueness of AE Aquarii is the highly variable optical as well as non-thermal radiation.

It has been mentioned that the uniqueness of AE Aquarii is most probably the propellering of material from the system and the nearly continuous thermal and non-thermal outbursts. A recent paper (Pearson Horne & Skidmore 2003) establishes the relation between the thermal optical flares and the propeller outflow of material in terms of less dense blobs colliding with slower moving, denser blobs, in the outflow. The main emphasis of this paper will be the investigation of the energetics of the magnetohydrodynamic propeller in AE Aquarii and the consequences for the continuous non-thermal flaring. By investigating the propeller ejection of a blob-like mass flow from the magnetosphere, important constraints can be placed on the non-thermal emission processes. This paper will be structured as follows. In Section 2 an overview of the observed non-thermal radio to mid-infrared emission from AE Aquarii is presented. In Section 3 the basic energetics of the magnetohydrodynamic interaction between the white dwarf magnetosphere with clumpy mass flow is investigated. In Section 4, a qualitative discussion relating to the energy the propeller mechanism channels into particle acceleration and possible non-thermal emission is presented, followed by the discussion in Section 5.

2. RADIO FLARES

AE Aquarii displays peculiar non-thermal radio to infrared (IR) variability (Bastian, Dulk & Chanmugam 1988; Abada-Simon et al. 1993, 1995a, 1995b, 1998), and possibly also transient VHE gamma-ray emission (e.g. Meintjes et al. 1992, 1994, Meintjes & de Jager 2000). Radio measurements with the *VLA* at 1.5 GHz, 4.9 GHz, 15 GHz and 22.5 GHz reveal nearly continuous radio synchrotron outbursts superimposed on a weak quiescent background emission (Bastian, Dulk & Chanmugam 1988), mimicking Cyg X-3, just on a lower scale. This variable radio emission was interpreted as non-thermal (10^9 K $< T_B < 10^{12}$ K) incoherent flares involving relativistic electrons radiating in expanding magnetized clouds ($B_\circ \sim$ 300-1000 G) with energies $\gamma \leq$ 3 - 30 (Bastian, Dulk & Chanmugam 1988). The general time averaged shape of the radio spectrum up to 15 GHz resembled a self-absorbed power law $S_\nu \sim S_\circ \nu^\alpha$ with an index $\alpha = 0.3$ - 0.4 (Bastian, Dulk & Chanmugam 1988). More recent radio and infrared (IR) observations (Abada-Simon et al. 1993, 1995a,b, 1999, 2002) extending to $\nu \sim$ 3333 GHz revealed similar outbursts, confirming the self-absorbed spectrum extending to $\nu \sim$ 3333 GHz. However, the authors cautioned that the measured flux level at 3333 GHz is also consistent with the optically thin part of the radio spectrum after the turning point. The detection at 3333 GHz (90 microns) corresponds to a measured flux level (at 5 sigma level) of $S_\nu \sim$ 113 mJy (Abada-Simon et al. 2002), different from their earlier reports (Abada-Simon et al. 1999), which put the detection at the 3.1 σ significance level and a flux close to $S_\nu \sim$ 180 mJy. It is anticipated that the detection of the 3333 GHz emission must be very close to the turning point of the self-absorbed spectrum, since *IRAS* only obtained three $\sim$ 200 mJy upper limits (Abada-Simon et al. 2002) at 12, 25 and 60 μm respectively (i.e. 25 000 GHz, 11 538 GHz and 5000 GHz). The time averaged spectrum up to 3333 GHz is approximately $S_\nu = S_1 \, (\frac{\nu}{1 GHz})^{0.5}$, with $S_1 \approx$ 3.15 mJy (Abada-Simon et al. 1999, 2002). A recent mid-infrared campaign

at 11.7 μm ($\nu \sim 25000$ GHz) and 17.7 μm ($\nu \sim 17000$ GHz), using the Keck I telescope (Dubus et al. 2004) detected variable emission at average flux levels of $S_{11.7\mu\mathrm{m}} = 24.1 \pm 1.0$ mJy and $S_{17.7\mu\mathrm{m}} = 26.8 \pm 5.5$ mJy respectively. This results in an average electron spectral index of approximately $\delta \sim 1.55$ which is close to the canonical $\delta = 2$. These flux levels are perfectly consistent with the predicted non-thermal optically thin mid-infrared flux (e.g. Abada-Simon et al. 1999; Meintjes & Venter 2003). This may be in fact the first direct detection of the optically thin part of the non-thermal spectrum of AE Aquarii. Unfortunately, the long integration time with Keck I destroyed any information regarding time variability of the observed emission.

The variability of the observed radio emission and the resultant spectrum can be explained in terms of a superposition (Bastian Dulk & Chanmugam 1988) of optically thick expanding magnetized synchrotron emitting clouds (van der Laan 1963,1966). *VLBI* observations of AE Aquarii during a radio flare indicate that the radio source expands with a velocity of the order of $\mathrm{v}_{exp} \sim 0.01$ c, with c the speed of light (A.E. Niell, personal comm.), reaching sizes of ~ 4 orbital radii during large flares. As these plasmoids expand they become optically thin to the synchrotron emission, showing a spectrum $\mathrm{S} \propto \nu^{-(\delta-1)/2}$, with δ the electron spectral index. The frequency at which the spectrum turns over from optically thick to optically thin, i.e. ν_m, corresponds to the maximum flux density $\mathrm{S}_\circ$ which is related to the initial blob size $\mathrm{r}_\circ$ and magnetic field $\mathrm{B}_\circ$ of these plasmoids (van der Laan 1966; Bastian, Dulk & Chanmugam 1988).

No information regarding the nature of the flaring is obtained from the latest detection at 90 microns (3333 GHz), or the Keck I data (Dubus et al. 2004). However, the non-thermal spectrum (see Abada-Simon et al. 1999, 2002; Meintjes & Venter 2003) indicates that the flux density is not compatible with flux densities obtained in the *J*, *H*, *K*, *L* band (Tanzi, Chincarini & Tarenghi 1981) corresponding to the spectrum of the secondary star (Abada-Simon et al. 1999,2002). This evidence, complemented with the latest mid-infrared detections (Dubus et al. 2004) strengthens the conjecture of the non-thermal nature of the observed radio emission. The total integrated non-thermal flux is obtained by integrating over the whole non-thermal spectrum (Meintjes & Venter 2003), between $\nu = (1 - 10^5)$ GHz, resulting in an integrated flux of $S = \int S_\nu d\nu \approx 10^{-11}$ erg cm^{-2}s^{-1}. Assuming a spherical source, the total integrated flux implies a non-thermal radio to mid-infrared luminosity of approximately

$$L_{r-ir} \approx 10^{31} \left(\frac{\Omega}{4\pi}\right) \left(\frac{S}{10^{-11}\,\mathrm{erg\ cm^{-2}s^{-1}}}\right) \left(\frac{D}{100\,\mathrm{pc}}\right)^2 \mathrm{erg.s^{-1}}. \tag{3.87}$$

This maximum non-thermal radio luminosity inferred from the radio spectrum of AE Aquarii is several orders of magnitude lower than the spin-down power of the magnetized white dwarf, i.e.

$$\beta \quad \sim \quad 10^{-3} \left(\frac{I\Omega\dot{\Omega}}{10^{34}\,\mathrm{erg.s^{-1}}}\right)^{-1} \left(\frac{L_{r-ir}}{10^{31}\,\mathrm{erg.s^{-1}}}\right), \tag{3.88}$$

implying that only a small fraction ($\sim 0.1\%$) of the spin-down power is converted into non-thermal synchrotron emission.

Since the magnetic propeller is probably the mechanism driving the non-thermal emission in AE Aquarii, a qualitative investigation has been made of its basic energetics. In the next section, the basic equations relating to the magnetohydrodynamic power, as well as the influence it may have on the clumpy mass flow from the secondary star, is presented.

3. ENERGETICS AND MASS FLOW

3.1 The basic equations

The energetics of the magnetohydrodynamic interaction between the fast rotating magnetosphere and diamagnetic blobs plunging through the magnetosphere may be explained by Poynting's theorem, which states that the rate of change of the mechanical and field energy per unit volume equals the negative of the divergence of the field energy flux into a certain volume element, i.e.

$$\frac{d}{dt}(u_{\rm mech}+u_{\rm field})=-\nabla.\left(\frac{c}{4\pi}(\mathbf{E}\times\mathbf{B})\right). \tag{3.89}$$

In terms of standard electrodynamics, the rate of change of the mechanical and field energy densities are represented by

$$\frac{du_{\rm mech}}{dt}=\mathbf{j}.\mathbf{E} \tag{3.90}$$

$$\frac{du_{\rm field}}{dt}=\frac{1}{8\pi}\frac{d}{dt}(E^2+B^2) \tag{3.91}$$

Integrating the equation above over a volume occupied by a conducting fluid interacting with the magnetosphere, using the divergence theorem, results in

$$\frac{d}{dt}(U_{\rm mech}+U_{\rm field})=-\int_S\frac{c}{4\pi}(\mathbf{E}\times\mathbf{B}).d\mathbf{A} \tag{3.92}$$

where the $\mathbf{E}\times\mathbf{B}$ term on the right represents the so-called Poynting flux. The electric field depends on the resistivity (η) of the gas through its dependence on the on the magnetic Reynolds number ($R_{\rm m}\propto 1/\eta$). Standard magnetohydrodynamics gives (e.g. Parker 1976)

$$E_\perp=-\frac{\mathbf{v}}{c}\times\mathbf{B}\left[1+\left(\frac{1}{R_{\rm m}}\right)\left(\frac{Lv}{c}\right)\left(\frac{\nabla\times\mathbf{B}}{\mathbf{B}\times\frac{\mathbf{v}}{c}}\right)\right]. \tag{3.93}$$

Since the magnetic Reynolds number for a most astrophysical plasmas is high, the second term can safely be ignored. A qualitative check regarding its contribution in relation to the specific case under consideration, even in the presence of turbulence, confirmed this conjecture.

In the equation above the velocity $\mathbf{v}$ represents the relative velocity of the magnetic field with respect to the flow. In this paper the interaction between the fast corotating poloidal field of the white dwarf with a clumpy flow in the equatorial plane is investigated. In such a scenario it is anticipated that the relative velocity between the corotating poloidal magnetic field and the free falling ballistic stream, will be azimuthally in the equatorial plane, i.e. perpendicular to the poloidal field in the equatorial plane, i.e. $\mathbf{v}=\mathbf{v}_{\rm rel,\perp}=\mathbf{v}_{\phi,*}-v_{\rm ff}$. Therefore the electric field can be expressed as

$$\mathbf{E}_\perp=-\frac{1}{c}(\mathbf{v}_{\rm rel,\perp}\times\mathbf{B}). \tag{3.94}$$

The corresponding expression for the Poynting flux then is

$$\begin{aligned}\mathbf{S} &= \tfrac{1}{4\pi}(\mathbf{B}\times(\mathbf{v}_{\rm rel,\perp}\times\mathbf{B}))\\ &= \tfrac{1}{4\pi}\mathbf{v}_{\rm rel,\perp}B^2.\end{aligned} \tag{3.95}$$

The equation above quantifies the energetics of the azimuthal energy transfer per unit surface area on orbiting material, resulting in acceleration of the material to velocities that may exceed the escape velocity from the system, i.e. the propeller effect. Although the equation above provides a vehicle quantifying the energetics involved, it depends obviously on effective and quick mixing of the magnetospheric field with the flow, enabling effective transfer of mechanical energy. Some ideas relating to this aspect have been proposed in the next section.

The azimuthal velocity of the corotating magnetosphere at the radius of closest approach of the ballistic stream, i.e. around the circularization radius $R_{\rm circ} \sim 10^{10}$ cm (i.e. $R_{\rm circ} \approx 10R_{\rm cor}$), is of the order ($\mathbf{v}_{\phi,*} = R_{\rm circ}\Omega_{\phi,*} \sim 2 \times 10^9\,{\rm cm\ s^{-1}}$). This exceeds the free fall velocity of the flow in the same region by at least an order of magnitude, compelling us to believe that most of the propellering of material probably occurs close to the circularization radius (e.g. Wynn, King & Horne 1995, 1997). This implies that the azimuthal velocity of the corotating magnetosphere will be by far the dominant contributor to the perpendicular component of the relative velocity, hence $\mathbf{v}_{{\rm rel},\perp} \approx \mathbf{v}_{\phi,*}$. The total power transferred to a stream of material is obtained by integrating the Poynting flux over the whole surface area of the fluid exposed to the magnetohydrodynamic flux. The total power transferred to the material in the magnetosphere may result in the increase in the mechanical energy of the material and possibly also particle acceleration. In the next section the properties of the magnetosphere and the gas stream are investigated, enabling the quantifying of the mechanical energy transfer responsible for the propeller outflow.

3.2 The magnetospheric properties

In the previous paragraph it has been shown that the mechanism driving the propeller outflow is most probably the result of the fast rotating magnetosphere interacting with the flow. This interaction forms the basis of the magnetospheric propeller effect. To allow an investigation of the magnetospheric propellering process, the magnetospheric field profile that is interacting with the flow, has to be investigated.

As mentioned earlier, the reported circular polarization may indicate a white dwarf surface magnetic field in excess of $B_{1,*} \sim 10^6$ G (Chanmugam & Frank 1987). An independent estimate relating to the magnetic field of the white dwarf can be obtained by inverting the discless accretion argument (Wickramasinghe, Wu & Ferrario 1991; Warner 1995) used to determine the possible existence of an accretion disc in intermediate polars. This implies that in the earlier high mass transfer phase an accretion disc, most possibly responsible for the rapid spin-up of the white dwarf to a period close to $P \sim 33$ s, could develop if the magnetic moment of the white dwarf did not exceed (Meintjes 2002)

$$\mu_{1,32} \leq 3 \left(\frac{P_{\rm orb,i}}{8.5\,{\rm h}}\right)^{7/6} \left(\frac{M_1}{0.9\,M_\odot}\right)^{5/6} \left(\frac{-\dot{M}_{2,i}}{10^{20}\,{\rm g\ s^{-1}}}\right)^{1/2} {\rm G\ cm^3}\,, \tag{3.96}$$

expressed in units of 10^{32} G cm^3. This estimated magnetic moment is in excellent agreement with the magnetic moments ($\mu_{1,32} \sim 2$) of the other DQ Her stars (Warner & Wickramasinghe 1991). This allows an independent estimate of the surface magnetic field strength of the white dwarf ($B_{1,*} \sim \mu/R_{1,*}^3$) if its radius is known. By adopting the Hamada & Salpeter (1961) white dwarf mass-radius relation, the white dwarf radius is approximately $R_1 \sim 5 \times 10^8\,(M_1/0.9\,M_\odot)^{-0.8}$ cm (see also Eracleous & Horne 1996), resulting in a

white dwarf surface field of

$$B_{1,*} \leq 2.4 \times 10^6 \left(\frac{\mu_{1,32}}{3}\right) \left(\frac{R}{R_1}\right)^{-3} \text{ G}, \tag{3.97}$$

which is in perfect agreement with an estimated magnetic field strength of $B_{1,*} \sim 10^6$ G inferred from circular polarization measurements (Cropper 1986; Beskrovnaya et al. 1995; Chanmugam & Frank 1987).

A fast rotating magnetosphere of this magnitude will most probably have a very significant influence on the mass flow dynamics of large diamagnetic blobs in the stream from the secondary star. To investigate the magnetospheric effect on the flow, the energetics of the flow can be compared to that of the magnetosphere through which they plunge. The average flow density through the L1 funnel (Meintjes 2004) is of the order of

$$\begin{aligned} \langle \rho_{\rm L1} \rangle \quad &\sim \quad 2 \times 10^{-8} \left(\tfrac{\dot{M}_2}{4\times 10^{17}\ \text{g s}^{-1}}\right) \times \\ &\left(\tfrac{T}{4000\,\text{K}}\right)^{-3/2} \left(\tfrac{P_{\rm orb}}{9.88\,\text{hr}}\right)^{-2} \text{ g cm}^{-3}. \end{aligned} \tag{3.98}$$

Since the secondary star has a temperature of approximately $T_{\rm surf,2} \sim 4000$ K (Meintjes 2004), the isothermal flow across the L1 point enters the Roche lobe of the white dwarf with the speed of sound, i.e.

$$c_{\rm s} \geq 5.8 \times 10^5 \left(\frac{\mu_{\rm w}}{1}\right)^{-1/2} \left(\frac{T}{4000\,\text{K}}\right)^{1/2} \text{ cm s}^{-1}, \tag{3.99}$$

with $\mu_{\rm w} < 1$ representing the mean molecular weight of the gas in AE Aquarii. Using energy conservation arguments, the radius of the funnel is determined to be of the order of $R \sim (c_{\rm s}/\Omega_{\rm orb}) \sim 2 \times 9\,$cm (Meintjes 2004). This results in a mass transfer rate through the L1 funnel which is approximately

$$\begin{aligned} \dot{M}_2 \quad &= \quad \langle \rho_{\rm L1} \rangle A_{\rm L1} c_{\rm s} \\ &\approx \quad 3 \times 10^{17} \left(\tfrac{\langle \rho_{\rm L1} \rangle}{2\times 10^{-8} \text{g cm}^{-3}}\right) \\ &\quad \left(\tfrac{c_{\rm s}}{10^6\ \text{cm s}^{-1}}\right) \left(\tfrac{A_{\rm L1}}{1.25\times 10^{19}\ \text{cm}^2}\right) \text{ g s}^{-1}. \end{aligned} \tag{3.100}$$

Detailed modelling of the stream (Wynn, King & Horne 1995; 1997) shows that the stream follows a ballistic trajectory, interacting very strongly with the white dwarf magnetospheric field at the radius of closest approach, which is close to the co-called circularization radius (e.g. Frank, King & Raine 2002, Chapt. 4, p 60), given by

$$R_{\rm circ} = (1+q) \left(\frac{b_1}{a}\right)^4 a. \tag{3.101}$$

The value of the circularization radius for AE Aquarii is approximately

$$R_{\rm circ} \sim 10^{10} \left(\frac{M_1}{0.9\,M_\odot}\right)^{1/3} \left(\frac{P_{\rm orb}}{9.88\,\text{hr}}\right)^{2/3} \text{ cm}. \tag{3.102}$$

The acceleration of the inhomogeneous blob stream into the fast rotating magnetosphere of the white dwarf, through a spray of accelerated gas stripped off the surface of blobs, as well as viscous heating as a result of the stream having to punch through the magnetospheric field, most probably result in a steady increase in the surface temperature of these blobs to values of the order of $\text{T}_{\rm stream} \sim 10^5$ K, which is required to explain the line emitting plasma (Jameson, King & Sherrington 1980). Conservation of mass between the L1 region and the circularization radius, i.e.

$$\langle \rho_{\rm L1} \rangle A_{\rm L1} v_{\rm L1} = \langle \rho_{\rm stream} \rangle A_{\rm stream} v_{\rm stream}, \tag{3.103}$$

allows the estimation of the free-fall stream density at the circularization radius, provided the cross-sectional area of the stream is known. An independent calculation shows that the condition of hydrostatic equilibrium of the stream at the radius of closest approach, with respect to the ambient magnetic field, results in a required particle concentration at T $\sim 10^5$ K, of

$$\begin{aligned} \rho_{\rm stream} &= \left(\frac{m_{\rm p} B^2}{8\pi k T}\right) \\ &\approx 4\times10^{-10}\left(\frac{B}{300{\rm G}}\right)^2\left(\frac{T_{\rm stream}}{10^5\,{\rm K}}\right)^{-1}\,{\rm cm}^{-3} \end{aligned} \tag{3.104}$$

Using the principle of mass conservation, the cross-sectional radius of the stream at the region of closest approach can be estimated to be of the order of

$$\begin{aligned} R_{\rm stream} &= \left(\frac{\dot{m}}{\pi\rho_{\rm stream}\,v_{\rm ff}}\right)^{1/2} \\ &\approx 1.2\times10^9\left(\frac{\dot{m}}{3\times10^{17}\,{\rm g\ s^{-1}}}\right)^{1/2}\times \\ &\quad \left(\frac{\rho_{\rm stream}}{4\times10^{-10}\,{\rm g\ cm^{-3}}}\right)^{-1/2}\times \\ &\quad \left(\frac{v_{\rm ff}}{1.55\times10^8\,{\rm cm\ s^{-1}}}\right)^{-1/2}\,{\rm cm}. \end{aligned} \tag{3.105}$$

This result is consistent with the principle of mass conservation between the L1 point and the radius of closest approach, if the average stream density at the circularization radius is

$$\begin{aligned} \langle\rho_{\rm stream}\rangle &\approx \left(\frac{\langle\rho_{L1}\rangle A_{\rm L1}\,v_{\rm L1}}{A_{\rm stream}\,v_{\rm stream}}\right) \\ &\approx 4\times10^{-10}\left(\frac{\rho_{\rm L1}}{2\times10^{-8}{\rm g\ cm^{-3}}}\right) \\ &\quad \left(\frac{R_{\rm L1}}{2\times10^9\,{\rm cm}}\right)^2\left(\frac{R_{\rm stream}}{1.2\times10^9\,{\rm cm}}\right)^{-2} \\ &\quad \left(\frac{v_{\rm L1}}{c_{\rm s}}\right)\left(\frac{v_{\rm stream}}{v_{\rm ff}}\right)^{-1}\,{\rm g\ cm^{-3}}, \end{aligned} \tag{3.106}$$

confirming the previous estimate. In the expression above, $v_{\rm ff} \approx 1.55 \times 10^8$ cm s^{-1} represents the free-fall velocity of the flow at the radius of closest approach, i.e. close to the circularization radius, with $v_{\rm L1} = c_{\rm s} \sim 10^6$ cm s^{-1}.

It can be shown that the required magnetospheric field significantly influencing the ballistic free falling stream, at the circularization radius, can be estimated through pressure balance arguments, resulting in a required magnetospheric field strength of

$$\begin{aligned} B_{\rm eq,circ} &= \sqrt{4\pi\rho v^2} \\ &= 10^4\left(\frac{\rho}{4\times10^{-10}\,{\rm g\ cm^{-3}}}\right)^{1/2}\left(\frac{v}{v_{\rm ff}}\right)\,{\rm G}. \end{aligned} \tag{3.107}$$

This is orders of magnitude larger than the magnetospheric field strength at the circularization radius, which is of the order of

$$B_{\rm circ} \sim 300\left(\frac{B}{B_{1,*}}\right)\left(\frac{R_{\rm wd}}{5\times10^8\,{\rm cm}}\right)^3\left(\frac{R_{\rm circ}}{10^{10}\,{\rm cm}}\right)^{-3}\,{\rm G}, \tag{3.108}$$

confirming that the ballistic nature of the blob stream may be preserved up to the radius of closest approach, justifying the selection of the free fall velocity ($v_{\rm ff}$) as representative of the bulk stream velocity through the magnetosphere. Since the field strength drops off as B $\propto$ R^{-3}, the field pressure will be too weak to

significantly influence the stream at radii significantly outside the circularization radius. It is therefore anticipated that the bulk of the flow probably penetrates the magnetosphere to a region around the circularization radius unhindered by the magnetic field. The less dense material may however be stripped off the surface of the stream and accelerated away from the system outside the circularization radius, colliding with slower denser blobs being ejected from deeper into the Roche lobe of the white dwarf, exiting with lower terminal velocities, producing the optical flares (Horne 1999; Pearson, Horne & Skidmore 2003).

Provided effective mixing can occur between the fast rotating field and the blobby stream, the bulk of the stream may be accelerated azimuthally and propelled out of the system from the circularization radius. The effective gravity of orbiting material close to the white dwarf, in the orbital plane is

$$\begin{aligned} \mathbf{g}_{\rm eff} &= -\nabla\Phi_{\rm eff} \\ &= -\left(\tfrac{GM_1}{R^2}\right)\,\hat{\mathbf{e}}_{\rm R} + \Omega_K^2 R\,\hat{\mathbf{e}}_{\rm R}, \end{aligned} \tag{3.109}$$

where R represents the radial distance of the blob in the orbital plane, measured from the centre of the white dwarf, and $\hat{\mathbf{e}}_{\rm R}$ points away from the centre of the white dwarf. For pure Keplerian flow the $g_{\rm eff} \rightarrow 0$. If the flow is accelerated, or alternatively, decelerated azimuthally as a result of magnetospheric drag (e.g. Drell, Foley & Ruderman 1965; King 1993; Wynn & King 1995; Wynn, King & Horne 1997), the effective gravity the flow experiences will be $\mathbf{g}_{\rm eff} > 0$ (propeller) and $\mathbf{g}_{\rm eff} < 0$ (towards white dwarf) respectively.

If the propulsion time scale is shorter than the viscous time scale, i.e. the time scale required ($t_{\rm visc} \sim 3 \times 10^5$ s) for viscous spreading of the ring into an accretion disc (e.g. King 1993), the propeller effect may be effective enough to prevent accreting onto the white dwarf. This seems to be supported by observational evidence suggesting extremely low mass accretion onto the surface of the white dwarf. In the next section the energy transfer from the fast rotating magnetosphere to a blobby accretion stream orbiting the white dwarf at the circularization radius will be investigated.

3.3 Magnetosphere-stream interaction

The mechanism responsible for the dramatic propeller outflow from AE Aquarii is the mechanical interaction between the fast rotating magnetosphere with the inhomogeneous flow, and relies on the proper mixing of the magnetospheric field with the flow. This is achieved if the fast rotating magnetosphere can penetrate the flow over sufficiently short time scales, allowing maximum momentum transfer and resultant acceleration. The Reynolds number ($R_{\rm e} = (\rho_{\rm stream} v R_{\rm stream}/\mu)$) (e.g. Rai Choudhuri 1998, p.85) of the flow at the radius of closest approach, assuming funnel-like flow as a result of the equipartition between the gas and surrounding magnetospheric pressures, and smooth kinematic viscosity given by $\mu = 0.02(T/10^5\,{\rm K})^{1/2}{\rm g\ cm^{-1}s^{-1}}$ (e.g. Lang 1998, p. 209), is of the order of

$$R_{\rm e} \sim 3.6 \times 10^9 \left(\frac{\rho_{\rm stream}}{4 \times 10^{-10}\,{\rm g\ cm^{-3}}}\right)\left(\frac{v}{v_{\rm ff}}\right)\left(\frac{R_{\rm stream}}{1.2 \times 10^9\,{\rm cm}}\right)\left(\frac{\mu}{0.02\,{\rm g\ cm^{-1}s^{-1}}}\right)^{-1}. \tag{3.110}$$

Reynolds numbers of these magnitudes are most probably inducive to the onset of turbulence in the flow (e.g. Tritton 1977, p. 233-237; Rai Choudhuri 1998, p. 85-87), resulting in a dramatic decrease in the electrical conductivity (σ) of the stream, and a corresponding dramatic increase of the magnetic diffusivity ($\eta = (c^2/4\pi\sigma)$) allowing rapid diffusion of the magnetospheric field into the turbulent flow. An order

of magnitude estimate of the turbulent magnetic diffusion time scale can be obtained from the magnetic induction equation. Dimensional analysis of the conduction equation (e.g. Jackson 1975, Chapter 10, p. 472) shows that the rate of diffusion (over length scales $\sim L$) of the field (of strength B) into a conducting fluid moving with velocity v is determined by the second term on the right hand side in the equation below, which is

$$\frac{B}{t} \approx \frac{vB}{L} - \frac{1}{R_{\rm m}}\frac{vB}{L}, \tag{3.111}$$

where $R_{\rm m} = (Lv/\eta) = (4\pi Lv\sigma/c^2)$ represents the magnetic Reynolds number. Turbulent diffusion (e.g. Campbell 1997, p. 43) of the magnetospheric field into a turbulent ballistic stream of radius $\rm R_{stream} \sim 10^9$ cm, at the radius of closest approach, results in a diffusivity $\eta_{\rm tur} \sim \epsilon c_{\rm s} R_{\rm stream} \sim 10^{16}(\epsilon/1)\,(c_{\rm s}/5\times10^6\,{\rm cm\ s^{-1}})$ $(R_{\rm stream}/1.2\times10^9\,{\rm cm})\ {\rm cm^2 s^{-1}}$. A magnetic diffusivity of this magnitude results in a diffusion time scale (e.g. Meintjes 2004) which is of the order of

$$\begin{aligned} \tau_{\rm diff} &= \left(\frac{L^2}{\eta_{\rm tur}}\right) \\ &\sim 30\left(\frac{L}{0.5R_{\rm stream}}\right)^2 \left(\frac{\eta_{\rm tur}}{10^{16}\,{\rm cm^2 s^{-1}}}\right)^{-1}\ {\rm s} \end{aligned} \tag{3.112}$$

This result shows that turbulent diffusion results in the magnetospheric field sufficiently penetrating the flow over time scales of the order of one rotation period, resulting in an effective transfer of momentum and resultant azimuthal acceleration to velocities above the escape velocity. Another possibility is the onset of magnetohydrodynamic instabilities like the so-called Kelvin-Helmholtz instability. The condition for the triggering of growing unstable modes (Wang & Robertson 1985) is $B^2/4\pi \sim \langle\rho_{\rm mag}\rangle v^2_{\phi,*}$, i.e. the average magnetospheric energy density being similar to the kinetic energy density of trapped plasma corotating with the magnetospheric field. Since the average plasma density in the magnetosphere will be significantly lower than the average density in the stream, unstable modes of the MHD perturbations can grow in amplitude nearly everywhere in the magnetospheric field, without being ironed out by the trapped flow. This condition is already satisfied if the average trapped magnetospheric plasma density near the radius of closest approach is $n_{\rm mag} \leq 10^9\ {\rm cm^{-3}}$, or $\rho_{\rm mag} \sim 10^{-15}\,{\rm g\ cm^{-3}}$, which is similar to the inferred average interblob plasma density in the ballistic stream plunging through the fast rotating magnetosphere. The triggering of the Kelvin-Helmholtz instability leads to growing unstable modes that may penetrate the flow, especially in the presence of turbulence in the flow. The Kelvin-Helmholtz instability results in the generation of magnetic vortices, resulting in the effective mixing of fluid and field (e.g. Wang & Robertson 1985), facilitating the effective transfer of mechanical energy to the orbiting gas. These magnetized vortices may decouple from the stream through fast magnetic reconnection, given the high fluid resistivity in the presence of turbulence. This may result in the generation of magnetized plasma bubbles that are magnetically pumped and accelerated by the fast rotating magnetospheric field sweeping across it. Trapped electrons in these bubbles may in fact drive the observed non-thermal radio to mid-infrared synchrotron emission. This will be discussed in greater detail in a later section. Since it is believed that the propeller process is effective enough to prevent the build-up of a dense gas envelope in the magnetosphere, the triggering of Rayleigh-Taylor instabilities is possibly avoided.

The high spin-down rate of the white dwarf, in conjunction with the low mass accretion of the white dwarf in comparison to the higher mass transfer from the secondary star, infer a very effective propeller

process. Since the propeller is most probably too effective allowing material to settle into an orbiting ring at the radius of closest approach, i.e. the circularization radius, the total mass outflow from the fast rotating magnetosphere is probably accelerated over a very short fraction of a circular orbit at the circularization radius. In order to make an estimation of the propeller outflow, it can be shown that the total MHD power transmitted across the surface of a volume of gas, equivalent to the content of a ring of cross-sectional radius $R_{\rm stream}$, with surface area $A_{\rm stream} \sim (2\pi R_{\rm stream})(2\pi R_{\rm circ})$, is of the order of

$$\begin{aligned} P_{\rm mhd} &= \left(\tfrac{v_{\rm rel,\perp} B^2 A_{\rm stream}}{4\pi}\right) \\ &\approx 10^{34} \left(\tfrac{v_{\rm rel,\perp}}{2\times10^9\,{\rm cm\ s^{-1}}}\right) \left(\tfrac{B_{\rm circ}}{300\,{\rm G}}\right)^2 \\ &\quad \left(\tfrac{A_{\rm stream}}{5\times10^{20}\,{\rm cm^2}}\right)\ {\rm erg\ s^{-1}}. \end{aligned} \tag{3.113}$$

This does not imply that a ring of material would be orbiting the white dwarf, but it allowed an estimation of the required mass that would be driven out from the magnetosphere, explaining the inferred outflow luminosity (Wynn, King & Horne 1997). This estimate of the MHD power is exactly the same as the total inferred spin down power of the white dwarf which is sufficient to drive the inferred mass outflow from the white dwarf as well as the thermal and non-thermal emission from AE Aquarii. The corresponding magnetospheric energy input per unit volume into such a stream, is

$$\begin{aligned} \dot{q} &= \left(\tfrac{P_{\rm mhd}}{2\pi^2 R_{\rm stream}^2 R_{\rm circ}}\right) \\ &\approx 3.5\times10^4 \left(\tfrac{P_{\rm mhd}}{10^{34}\,{\rm erg\ s^{-1}}}\right) \left(\tfrac{R_{\rm stream}}{1.2\times10^9\,{\rm cm}}\right)^{-2} \\ &\quad \left(\tfrac{R_{\rm circ}}{10^{10}\,{\rm cm}}\right)^{-1}\ {\rm erg\ cm^{-3} s^{-1}}, \end{aligned} \tag{3.114}$$

resulting in an acceleration of the material

$$\begin{aligned} \langle \dot{v}_\phi \rangle &= \left(\tfrac{\dot{q}}{\langle\rho\rangle v_{\rm stream}}\right) \\ &\approx 5.6\times10^5 \left(\tfrac{\dot{q}}{3.5\times10^4\,{\rm erg\ cm^{-3} s^{-1}}}\right) \\ &\quad \left(\tfrac{\rho}{\langle\rho_{\rm stream}\rangle}\right)^{-1} \left(\tfrac{v_{\rm stream}}{v_{\rm ff}}\right)^{-1}\ {\rm cm\ s^{-2}}. \end{aligned} \tag{3.115}$$

Using ordinary Newtonian mechanics, it can be shown that this magnetohydrodynamic acceleration can propel the stream at the circularization radius to velocities ($v_\phi = v_{\rm ff} + \dot{v}_\phi\ {\rm t}$), reaching values of the order $v_\phi \approx 1.7\times10^8\,{\rm cm\ s^{-1}}$, within one rotation of the white dwarf. This effective outward gravity that the azimuthally accelerated material experiences is of the order of $|g_{\rm eff}| \sim 1.7\times10^4\,{\rm m\ s^{-2}}$, in comparison to the effective gravity material accelerated to the escape velocity experiences, which is $|g_{\rm eff}| \sim 1.2\times10^4\,{\rm m\ s^{-2}}$. Therefore it can be seen that the dissipation of magnetohydrodynamic power transfers sufficient energy to the flow to propel it azimuthally to velocities exceeding the escape velocity within one rotation of the field. It is anticipated that dense blobs accelerate less than the less dense blobs, probably resulting in collisions between blobs of different speeds after their encounter with the rapidly rotating magnetosphere. This may explain the optical flares observed from AE Aquarii (e.g. Pearson, Horne & Skidmore 2003).

It has been shown that the transfer of mechanical energy from the fast rotating magnetospheric field to the fragmented stream via turbulent diffusion and magnetic vortices generated by Kelvin-Helmholtz instabilities is most probably the physical mechanism responsible for the propeller ejection of material from the binary system. It has been showed that unstable modes of the Kelvin-Helmholtz instability can grow

everywhere in the magnetosphere where the magnetospheric tension is not dominated by the ram pressure of trapped plasma corotating with the flow (Wang & Robertson 1985). The possible turbulent nature of the gas also favors fast reconnection, allowing the magnetized cells to be stripped from the flow. Without accepting any specific model for particle acceleration, the energy required for the observed non-thermal radio to mid-infrared emission will be determined within this framework.

4 PARTICLE ACCELERATION

If the propeller effect and resultant magnetic reconnection is instrumental in the creation of a magnetized plasma with magnetic fields of the order of the magnetospheric field, i.e. $\mathrm{B_{mag}} \sim 300$ G, being propelled from the magnetosphere, the interaction between these magnetized bubbles and the fast rotating magnetosphere sweeping across them may have interesting consequences. It can be shown that the Lorentz interaction between a magnetized conducting fluid experiencing a fast moving magnetic disturbance propagating through a gas with the Alfvén velocity $\mathbf{v}_\mathrm{A}$, and a thermal electron moving with a velocity $\mathbf{v}_\mathrm{e}$ in the plasma, anchored to the frozen-in ambient field (e.g. Parker 1976), is

$$\frac{d\epsilon_\mathrm{e}}{dt} = -\mathrm{e}(\mathbf{E}_\perp + \frac{\mathbf{v}_\mathrm{e}}{c} \times \mathbf{B}). \tag{3.116}$$

It can be seen that both the perpendicular component of the electric field, and the magnetic Lorentz interaction can result in the acceleration of charged particles like electrons perpendicular to a presumably chaotic (H. Spruit 2003, personal communication) field configuration inside the blobs. The acceleration will result in an effective transfer in energy from the field to thermal electrons, which is

$$\begin{aligned} \tfrac{d\epsilon_\mathrm{e}}{dt} &= (\tfrac{-\mathrm{e}}{c})[(-\mathbf{v}_\mathrm{e} - \mathbf{v}_\mathrm{A}) \times \mathbf{B}].\mathbf{v}_\mathrm{e} \\ &= (\tfrac{-\mathrm{e}}{c})\mathbf{v}_\mathrm{A}.(\mathbf{v}_e \times \mathbf{B}) \\ &= \mathbf{v}_\mathrm{A}.\mathbf{F}_\mathrm{L}. \end{aligned} \tag{3.117}$$

These electrons will experience a push from the Lorentz force, resulting in a sudden increase in energy (e.g. Parker 1976). It is in fact a Fermi mechanism or magnetic pumping. Therefore, thermal electrons in the fluid will be scattered up in energy through a head-on interaction with the Lorentz force, as a result of magnetic disturbances propagating along the chaotic twisted field lines. If the typical initial velocities of thermal electrons are of the order of the sound speed $v_\mathrm{e} \sim 3 \times 10^6 (T_\mathrm{blob}/10^5\,\mathrm{K})^{1/2} \mathrm{cm\ s^{-1}}$, and the Alfvén velocity is of the order of $v_\mathrm{A} \sim 4 \times 10^6 (B_\mathrm{blob}/300\,\mathrm{G})(\rho/\langle\rho_\mathrm{bstream}\rangle)^{-1/2}\,\mathrm{cm\ s^{-1}}$, then the upper limit of the rate at which energy is being transferred to thermal electrons in the blob is

$$\frac{d\epsilon_\mathrm{e}}{dt} \approx 37 \left(\frac{T_\mathrm{surf}}{10^5\,\mathrm{K}}\right)\left(\frac{B}{300\,\mathrm{G}}\right)\ \mathrm{MeV\ s^{-1}}. \tag{3.118}$$

The total accelerating time scale will determine the energy the particles will reach, but the synchrotron radiation and adiabatic cooling rate in expanding blobs result in rapid losses, limiting the maximum energy electrons can obtain in the pumping process. The acceleration time scale will be of the order of the time a single magnetospheric pressure wave, traveling at the local Alfvén velocity, traverses a magnetized cloud, which is

$$\begin{aligned} t_\mathrm{a} &\sim \tfrac{dl}{v_\mathrm{A}} \\ &\sim 250\,(\tfrac{l_\mathrm{blob}}{10^9\,\mathrm{cm}})\,(\tfrac{v_\mathrm{Al}}{10^8\,\mathrm{cm\ s^{-1}}})^{-1}\ \mathrm{s}, \end{aligned} \tag{3.119}$$

However, the initial synchrotron and adiabatic loss time scales are respectively

$$t_{\rm s} = 4 \left(\frac{\gamma}{2000}\right)^{-1} \left(\frac{B_{\rm blob}}{300\,{\rm G}}\right)^{-2} {\rm s} \tag{3.120}$$

and

$$\begin{aligned} t_{\rm ad} &= \left(\frac{l_{\rm blob}}{v_{\rm exp}}\right) \\ &\approx 3 \left(\frac{l_{\rm blob}}{10^9\,{\rm cm}}\right) \left(\frac{v_{\rm exp}}{0.01\,c}\right)^{-1} {\rm s}. \end{aligned} \tag{3.121}$$

In the second equation the velocity of the expanding synchrotron emitting clouds corresponds to the a *VLBI* observation of an expanding synchrotron source at a speed of $v_{\rm exp} \sim 0.01c$, where c represents the speed of light. It can be seen that this mechanism can accelerate electrons to energies reaching at least $\gamma_e \sim 250$ ($\epsilon_{\rm e} \sim 130$ MeV) within the dominant energy loss time scales.

The calculation above shows that thermal electrons in the dissipation region can be scattered up to energies of the order of $\epsilon_{\rm e} \sim 130$ MeV over the dominant energy loss time scales. It has been shown (Meintjes & Venter 2003) that only moderate electron energies ($\gamma_e < 20$) are required to explain the non-thermal emission in gas clouds with magnetic fields between $B_{\rm cloud} \sim 2000$ - 3000 G. If the clouds contain magnetic fields of the order of the magnetospheric field, then the maximum electron energy explaining the total non-thermal emission, including the latest measurements at frequencies $\nu \sim 17000$ GHz and 25000 GHz (Dubus et al. 2004), is of the order of

$$\gamma_{\rm e,max} \sim 150 \left(\frac{\nu_{\rm max}}{25000\,{\rm GHz}}\right)^{1/2} \left(\frac{B_\perp}{300\,{\rm G}}\right)^{-1/2} \tag{3.122}$$

Therefore it can be seen that magnetic pumping in these magnetized bubbles is effective enough to pump-up electrons to high enough energies explaining the total observed non-thermal emission from AE Aquarii. It has been pointed out (Bastian, Dulk & Chanmugam 1988) that the number density of relativistic particles in single flare events, resulting from expanding synchrotron emitting clouds, is given by

$$n_\circ = A_3 \left[\frac{\delta+2}{\delta-1} \left(\frac{\epsilon_{\rm e}}{1\,{\rm MeV}}\right)^{-(\delta-1)} \left(\frac{B_\circ^{2\delta+9}}{r_\circ}\right)\right]^{\frac{1}{\delta+5}} \tag{3.123}$$

where δ represents the power index of the accelerated electrons, which is approximately $\delta \sim 1.55$ (Dubus et al. 2004), and where $A_3 = [3.2 \times 10^4 \times 2^{\delta/2} (10^{11})^{1/(\delta+4)}]^{(\delta+4)/(\delta+5)}$. It can be shown that the number density of mildly relativistic electrons required to explain the non-thermal flares in AE Aquarii is of the order of

$$\begin{aligned} n_\circ &\sim 8 \times 10^8 \left(\tfrac{\gamma}{150}\right)^{-0.9} \left(\tfrac{B_{\rm blob}}{300\,{\rm G}}\right)^{1.85} \\ &\quad \left(\tfrac{r_\circ}{10^9\,{\rm cm}}\right)^{-0.15} {\rm cm}^{-3}. \end{aligned} \tag{3.124}$$

Here it has been assumed the initial size of these magnetized blobs is $r_\circ \sim 10^9$ cm, imposed by the width of the stream into which the magnetospheric field penetrate via turbulent diffusion and Kelvin Helmholtz instabilities. It can be shown that particle acceleration in magnetized blobs with thermal particle densities exceeding $\langle n_{\rm p} \rangle \geq 10^{12}\,{\rm cm}^{-3}$ require a conversion efficiency of thermal particles to the required population of relativistic particles that can drive the non-thermal radio to mid-infrared synchrotron emission from AE Aquarii, is $e \leq 0.1$ % in a single blob. This is consistent with the overall conversion ratio ($\beta \sim 0.1\%$) of the spin down power to the total observed non-thermal emission, as has been mentioned earlier. The combined

radio to mid-infrared emission from AE Aquarii can then be explained in terms of a superposition of these synchrotron radiating bubbles, in various stages of their expansion after propeller ejection from the system (e.g. Bastian Dulk & Chanmugam 1988; Meintjes & Venter 2003).

The required magnetic field supporting the relativistic electron pressure capable of driving the maximum radio to mid-infrared synchrotron emission in expanding blobs with initial size $r_\circ \sim 10^9$ cm, can be calculated by assuming equipartition between the field and relativistic particles (e.g. Pacholczyk 1970). This results in

$$\begin{aligned} B_{\rm min} &= \left[\tfrac{3}{4}\,8\pi C_e(\delta)\tfrac{L_{\rm r-ir}}{V_{\rm source}}\right]^{2/7} \\ &\sim 300\left(\tfrac{L_{\rm r-ir}}{10^{31}\,{\rm erg\ s^{-1}}}\right)^{2/7}\left(\tfrac{r_\circ}{10^9{\rm cm}}\right)^{-6/7}\ {\rm G}, \end{aligned} \tag{3.125}$$

with $C_e(\delta) \sim 10^5$ (for $\delta \sim 1.55$) , with $V_{\rm source}$ representing the initial source volume. This inferred field strength is similar to the magnitude of the magnetospheric field at the circularization radius. This result supports the conjecture that a very effective process of magnetization of the stream occurs, possibly at the circularization radius where the flow interacts most severely with the magnetospheric field. Turbulent diffusion and possibly Kelvin-Helmholtz instabilities may result in the creation of magnetized vortices in the stream, being stripped off through fast turbulent reconnection as a result of the large differential velocity between the magnetospheric field and the flow, resulting in magnetized synchrotron emitting bubbles being ejected from the magnetosphere. Magnetic fields of this magnitude are also remarkably similar to the inferred blob fields from radio flares in earlier observations (Bastian, Dulk & Chanmugam 1988).

These estimates definitely indicate that the MHD interaction between the fast rotating magnetosphere and a clumpy fragmented flow around the circularization radius provides a very interesting vehicle to explain the non-thermal radio to mid-infrared emission from AE Aquarii. This may also indicate that the nearly continuous flaring activity observed from AE Aquarii, may in fact be the signature of the violent magnetospheric interaction.

5 CONCLUSIONS

The purpose of this study is not to provide a detailed model for the MHD processes involved in the propeller ejection of a fragmented stream from the AE Aquarii system by the fast rotating magnetosphere, but rather to provide a qualitative description of the required energetics assuming standard magnetohydrodynamics. From an energetics point of view the results look rather promising. It has been shown that turbulent diffusion and Kelvin-Helmholtz instabilities result in the fast rotating magnetosphere diffusing into the fragmented stream of material over time scales comparable to the white dwarf spin period. This fast diffusion of magnetic field into the mass transfer stream allows an effective transfer of mechanical energy into the flow, that will propel it out of the binary system. It has been shown that the amount of MHD power pumped into a volume of gas equivalent to the volume of a ring of material that could orbit outside the circularization radius, if allowed to do so, is of the order of $P_{\rm mhd} \sim 10^{34}\,{\rm erg\ s^{-1}}$, which is sufficient to drive the total inferred propeller ejected mass flow ($L_{\rm mech} \sim P_{\rm mhd}$) from the binary system. The efficiency of the propeller mechanism is most probably the result of very effective mixing between the field and the flow resulting in the formation of magnetized bubbles of plasma being ejected from the fast rotating magnetosphere. Magnetic pumping may result in a fraction of the thermal electron population to be accelerated to energies

of the order of $\gamma_e \sim 150$, which is required to explain the non-thermal radio to mid-infrared synchrotron emission from AE Aquarii. It has been pointed out that the efficiency of the particle acceleration process inside individual magnetized blobs can be of the order of $e \sim 0.1$ %. The efficiency of the acceleration process in magnetized plasma bubbles is also of the same order of magnitude to the inferred conversion rate of the white dwarf's rotational kinetic energy to non-thermal emission, i.e. $\beta \sim 0.1$ %. This confirms the distribution between mechanical and non-thermal power as is inferred from observational data. It has been pointed out that magnetic fields frozen into the magnetized plasma bubbles is of the order of a few hundred Gauss, i.e. the magnetospheric field at the circularization radius, which may have been stripped-off through reconnection into the gas in the interaction layer. These magnetized gas bubbles, or synchrotron sources, have the required energy density to confine a whole population of relativistic electrons with energies that can reach $\gamma_e \sim 150$. This is sufficient to drive the total radio to mid-infrared emission from the system from 1 - 25000 GHz. This proposed model of the magnetospheric propulsion of blobs in AE Aquarii provides an interesting framework to evaluate the non-thermal emission in the system. The continuous non-thermal activity observed in AE Aquarii may in fact just be the signature of the processes described in the previous sections.

ACKNOWLEDGEMENTS

The author wishes to thank the National Research Foundation (NRF) in South Africa for the research grant leading to a sabbatical month at the Paris-Meudon observatory where the research presented in this paper was initiated. The author would also like to express his appreciation to the Paris-Meudon observatory for their hospitality towards the author during his month-long stay there, as well as towards the CNRS for funding the author's attendance of a conference in Strasbourg. The author also want to express his appreciation to Prof. Eugene Parker for valuable discussions surrounding the work presented in this paper.

3.4.2 Kelvin-Helmholtz driven propeller in AE Aquarii: A unified model for thermal and non-thermal flares

Mon. Not. R. Astron. Soc. 366, 557 (2006)
L.A. Venter, P.J. Meintjes*

Abstract

In this paper an attempt is made to integrate the propeller ejection of material by the fast rotating white dwarf in AE Aquarii with the highly transient thermal and non-thermal emission in a single unifying model. It has been shown that the violent interaction between the fast rotating magnetosphere and a clumpy fragmented stream, in AE Aquarii specifically, may result in the growth of unstable modes of the Kelvin-Helmholtz instability and associated turbulence over length scales comparable to the stream radius on time-scales $\tau_{\rm K-H} \sim t_{\rm dyn}$ *(*$\sim 600\,s$*). For all conversion efficiencies of MHD power to mechanical energy* $\epsilon \geq 0.1$ *these instabilities results in the effective azimuthal acceleration of the gas parcels to the escape velocity over time-scales* $t_{\rm acc} \leq 1000$ *s (*$\sim t_{\rm dyn}$*). Further, it has been shown that the turbulence in the flow will cascade down to the dissipative level over time-scales* $\tau_{\rm cas} \sim 3$ *hours. If released through dissipative shocks, this reservoir can drive a luminosity of* $L \sim 10^{33}\,erg\,s^{-1}$*, which can significantly contribute to the total emission when blobs collide in the exit stream, resulting in shock heating and associated flares. During the propeller process particles can also be accelerated to high energies, which may be the driving mechanism behind the non-thermal radio to mid-infrared emission. The confluence of these ejected magnetized clouds may result in radio remnant surrounding AE Aquarii which is optically thin between frequencies* $\nu \geq 100$ *MHz - 1 GHz.*

keywords

accretion - binaries: general - stars: white dwarf - processes: mass accretion, turbulence, dwarf nova eruptions.

1. INTRODUCTION

The enigmatic nova-like cataclysmic variable AE Aquarii has been intensively studied over many decades in frequency, ranging from radio to very high energy ($\epsilon_\gamma > 1$ TeV) γ-rays (e.g. Bastian Dulk & Chanmugam 1988; Patterson 1979; Meintjes et al. 1992, 1994; e.g. Meintjes & de Jager 2000; Meintjes 2002; Meintjes & Venter 2003, 2005 for discussions). The system consists of a $\sim$0.9 $M_\odot$ highly magnetic white dwarf with a surface field of approximately $B_{1,*} \sim 10^6$G (e.g. Meintjes 2002) orbiting a lobe-filling ~ 0.6 $M_\odot$ K4-5 secondary red dwarf about the common centre of mass. The orbital period of the system is approximately $P_{\rm orb} \approx 9.88$ hours, implying a rather wide binary system. Optical (e.g. Patterson 1979) and X-ray (e.g. Patterson et al. 1980) observations reveal $P_{1,*} \sim 33$ s pulsations in the lightcurves which can only be associated with the spin period of the white dwarf. A detailed study of the stability of the spin period of the white dwarf over a base line of 14 years (de Jager, Meintjes O' Donoghue & Robinson 1994) reveals a steady spin-down $\dot{P} \sim 5.65 \times 10^{-14}$ s s^{-1}, implying a spin-down power of approximately $\dot{E}_{\rm rot} = I\Omega\dot{\Omega} \sim 10^{34}$ erg s^{-1} (e.g. Meintjes & de Jager 2000).

AE Aquarii is characterized by low mass accretion and highly variable emission over a very wide range of frequencies from radio to X-ray and transient TeV gamma ray radiation (Bastian Dulk & Chanmugam 1988; Patterson 1979; Patterson et al. 1980; O'Donoghue et al. 1995; Eracleous & Horne 1996; Meintjes et al. 1992, 1994). It is believed that a magnetic propeller is operating in the system and that this process is the origin of the mechanisms driving the observed emission (Eracleous & Horne 1996; Wynn King & Horne 1997; Horne 1999; Meintjes & de Jager 2000; Meintjes & Venter 2003,2005; Pearson Horne & Skidmore 2003, 2004). It has been shown (Meintjes & Venter 2005) that the total magnetohydrodynamic power dissipated in the interaction region between the fast co-rotating magnetosphere and the gas stream from the secondary star, is $L_{\rm mhd} \sim 10^{34}\,{\rm erg\,s^{-1}}$, which is compatible with the spin-down power of the white dwarf, and may be the driving mechanism behind the transient multi-wavelength emission of AE Aquarii. Observations in optical/uv and IR/radio wavelengths show nearly continuous variability, superimposed on a varying average emission. In terms of our current understanding the short time-scale variations or flares can best be explained in terms of a fragmented (e.g. King 1993; King & Regev 1994; Wynn & King 1995; Meintjes 2004) and colliding propeller driven outflow resulting in the collision between blobs of various mass and velocity ejected by the fast rotating magnetosphere (Pearson Horne & Skidmore 2003,2004). It has been shown that fragmentation of a stream can occur through growing Rayleigh-Taylor instabilities when the mass flow from a secondary star interacts with a magnetosphere of an accreting compact object (e.g. Arons & Lea 1976; Hameury, King & Lasota 1986; Aly & Kuijpers 1990). However, Meintjes (2004) showed that magnetic viscosity in the funnel between a magnetic secondary star and the compact white dwarf, where the flow crosses the L1 region, can also fragment the mass flow, which can account for the expected inhomogeneous or granular nature of the mass flow from the secondary star in AE Aquarii, as well as other cataclysmic variables.

The propeller outflow in T Tauri stars (e.g. King & Regev 1994) and AE Aquarii (Wynn, King & Horne 1995; 1997) have been described previously in terms of a magnetospheric drag force (Drell Foley & Ruderman 1965) exerted on large diamagnetic blobs by a rotating magnetosphere. The underlying physics behind this mechanism is the inability of the magnetosphere to penetrate the moving blobs as a result of the high surface conductivity (King & Regev 1994), resulting in a surface drag. Depending on the relative motion of the magnetosphere with respect to the blob, the drag can either decelerate the blob, e.g. like the decaying orbits show of low earth orbiting satellites crossing the earth's magnetic field (Drell Foley & Ruderman 1965), or propel the blobs, when faster moving fields intercept the blobs, i.e. the magnetospheric propeller (e.g. King & Regev 1994). It has been shown (King & Regev 1994) that the conducting properties of typical diamagnetic blobs in most close binaries may be of the order of $\sigma \sim {\rm few} \times 10^{15}\,(T/1000\,{\rm K})^{-1/2}{\rm s}^{-1}$, which implies very effective screening from magnetic fields for all realistic blob parameters, even if they are largely neutral (King & Regev 1994). However, it has been shown (Meintjes & Venter 2005) that the mass flow in AE Aquarii may be turbulent, i.e. having Reynolds numbers of the order of $R_{\rm e} \sim {\rm few} \times 10^9$. Apart from this, it has been shown (Meintjes & Venter 2005) that the shear layer between the magnetosphere and the flow in AE Aquarii is most likely subjected to unstable modes of the Kelvin-Helmholtz instability, which is a significant independent source of turbulence in the gas (e.g. Biskamp 2003, pp. 33-65). The fact that the Kelvin-Helmholtz and turbulence operate in tandem in the shear layer where the magnetosphere interacts with the flow, implicates a significantly lower conductivity of the flow in general, and hence, less

effective screening against magnetic fields. For example, it has been shown that for AE Aquarii a turbulent driven diffusivity of $\eta_{\rm tur} \sim 10^{16}\,{\rm cm^2 s^{-1}}$ results in a diffusion time-scale of $\tau_{\rm tur} \sim 30\,{\rm s}$ for magnetic field through large blobs with dimensions $l_{\rm blob} \sim 10^9\,{\rm cm}$ (Meintjes & Venter 2005). Under this assumptions, the propeller outflow of material in AE Aquarii in particular cannot readily be explained in terms of a surface drag, applicable to the slow rotator regime where ideal magnetohydrodynamics holds.

According to the magnetospheric drag model, applied to AE Aquarii (Wynn King & Horne 1995; 1997) the associated time-scales of the magnetospheric drag and associated acceleration are summarized briefly for comparison with the equivalent calculations presented in Section 2, based upon the Kelvin-Helmholtz and turbulence driven propeller.

1.1 Effective time-scales

Based upon magnetospheric drag blobs orbiting the white dwarf will lose or gain mechanical energy depending on the relative velocity of the field with respect to the highly conducting blobs. It has been shown that low earth-orbiting satellites lose mechanical energy as a result of their motion across the slower rotating magnetic field of the earth (Drell Foley & Ruderman 1965). The motion of the blobs through the magnetosphere is then modified by a surface drag, and the effective magnetospheric propulsion of the blobs is then (e.g. Wynn King & Horne 1997)

$$g_{\rm mag} = -k\,[\mathbf{v} - \mathbf{v}_{\rm f}]_{\perp}, \tag{3.126}$$

where $k \sim 1/t_{drag}$ (slow) is the effective magnetospheric drag coefficient in the slow rotator limit.

If the drag (propulsion) time-scale is similar to the time-scale for the loss of mechanical energy via the excitation of Alfvén waves (Drell, Foley & Ruderman 1965) in the slow rotator limit, it can be approximated by ($t_{\rm drag} \sim 1/k$), i.e.

$$\begin{aligned} t_{\rm drag} &= \left(\tfrac{c_{\rm A} M_{\rm blob}}{B^2 l^2}\right) \\ &= 2.18 \times 10^6 \left(\tfrac{\rho_{\rm blob}\, l}{B}\right)\,{\rm s}, \end{aligned} \tag{3.127}$$

where c_A, $M_{\rm blob}$, B and l represent the Alfvén speed in the interblob plasma, blob mass, magnetospheric field and blob dimension respectively. The constant in this expression is calculated by using an average value for the reported interblob plasma number density, which for AE Aquarii, is $n_{\rm ib} \sim 10^9$ - 10^{11} cm^{-3} (Eracleous & Horne 1996, Wynn, King & Horne 1997, Pearson, Horne & Skidmore 2003). A detailed study of the densities of the gas blobs from the secondary star in AM Her was carried out by Beardmore & Osborne (1997). They described the variability in the hard X-ray observations from AM Her, made by *Ginga*, as shot noise caused by inhomogeneous accretion of blobs with typical densities between $n_{\rm blob} \sim 10^{15}$ - 10^{17} cm^{-3}, and sizes similar to the dimension of the white dwarf. However, applied to AE Aquarii in particular, a careful mass conservation analysis in the stream interacting with a $B \sim 300\,{\rm G}$ magnetospheric field at the radius of closest approach, revealed an average stream (blob) density of the order $\langle n_{\rm blob}\rangle = (\langle\rho_{\rm blob}\rangle/m_{\rm p}) \sim$ few $\times\, 10^{14}\,{\rm cm^{-3}}$ (Meintjes & Venter 2005), which is consistent with the inferred blob densities driving the optical flares when blobs collide in the exit fan (Pearson Horne & Skidmore 2003). Using these estimates, it can be shown that

the average drag time-scale for blobs is of the order of

$$t_{\rm drag} \sim 1.3 \times 10^3 \left(\frac{B_{\rm circ}}{300\,{\rm G}}\right)^{-1} \left(\frac{n_{\rm blob}}{10^{14}\,{\rm cm}^{-3}}\right) \left(\frac{l}{10^9\,{\rm cm}}\right)\,{\rm s}, \tag{3.128}$$

compared to earlier estimates of $t_{\rm drag} \sim 10^5\,{\rm s}$ (Wynn King & Horne 1997) using the Beardmore & Osborne (1997) blob density estimates. Such a long drag time-scale is difficult to reconcile with the rapid outflow these authors proposed. The typical viscous time-scale is of the order of $t_{\rm visc} \sim 10^5$ s (e.g. King 1993), which is still significantly larger than the magnetospheric drag time-scale in the slow rotator limit.

It has been shown (Wynn King & Horne 1997) that the radius of closest approach of the stream to the white dwarf is of the order of ${\rm R} \sim 10^{10}\,{\rm cm}$. The dynamical time-scale, i.e. the time it takes blobs to orbit the white dwarf in this region is

$$\begin{aligned} t_{\rm dyn} &= 2\pi \left(\tfrac{GM_1}{R^3}\right)^{-1/2} \\ &\sim 600 \left(\tfrac{M_1}{0.9\,M_\odot}\right)^{-1/2} \left(\tfrac{R}{10^{10}\,{\rm cm}}\right)^{-3/2}\,{\rm s}, \end{aligned} \tag{3.129}$$

which is significantly smaller than viscous time-scales. It can be seen that the drag time-scale is consistent with the dynamical time-scale. The comparative long viscous time-scale implies that the acceleration can occur before the material settle in a ring.

These estimates emphasize the strength of magnetospheric drag to explain the propulsion of large diamagnetic blobs through the magnetosphere. However, the propulsion is based upon applying ideal MHD, applicable in the slow rotator regime, to the fast rotator AE Aquarii, and furthermore quantifying a rather complicated process through a single drag coefficient. It has been shown (Meintjes & Venter 2005) that the propulsion of blobs can be explained rather successfully by applying a "magnetospheric drag" driven by highly unstable modes of the Kelvin-Helmholtz instability, which may be a very efficient propulsion mechanism of blobs through the magnetosphere (Parker 2004, personal communication). The associated turbulence may also allow the possibility to integrate the peculiar thermal and non-thermal emission in a unified model.

1.2 Propeller driven mass outflow

The bulk of the evidence leading to the current conjecture supporting a propeller driven outflow from AE Aquarii resulted from a large set of high time resolution UV spectra with the *HST* (Horne & Eracleous 1995; Eracleous & Horne 1996). The kinematic information contained within the observed emission lines basically provided the killing blow to any conjecture excluding a propeller driven system. The main findings related to the flares and associated kinematics of the emission lines are summarized below.

The *HST* spectra show large amplitude ultraviolet (UV) flares which are most probably the counterparts of those previously observed in the optical (Patterson 1979; van Paradijs et al. 1989). The UV spectrum during flares displays a plethora of emission lines, in agreement with earlier *IUE* observations (Jameson, King & Sherrington 1980), superposed on a prominent Balmer recombination continuum corresponding to a temperature of the order of $T \sim 10^4$ K. The UV emission lines can be associated with ionization potentials of the order of several eV. Based upon the critical densities of the observed semi-forbidden lines it has been suggested that the density of a large fraction of the line emitting gas is of the order of $n_{\rm p} \sim 10^9 - 10^{11}{\rm cm}^{-3}$,

with a mean density of the order of $n_{\rm p} \sim 10^{10}\,{\rm cm}^{-3}$. However, it has been mentioned that some of the semi-forbidden species may have in fact been emitted in a gas with density $n_{\rm p} \leq 10^9$ cm^{-3}. During flares all components of the spectrum, i.e. continuum and lines, vary together with no easily discernable time lag. The fluxes of all the lines vary proportionally to the continuum flux. The radial velocity curves of the stronger UV emission lines lead the radial velocity curve of the companion star with approximately 0.3 cycles. This behaviour, also seen in the Balmer lines, suggests that the line emission originates in a gas stream with a direction similar to that of the mass transfer stream from the companion star. The overall kinematics of the line emitting gas support the conjecture of a propeller outflow from the magnetosphere, which had been proposed earlier by (Eracleous & Horne 1996; Wynn King & Horne 1995, 1997). These authors showed that the mass transfer from the companion star is most probably highly inhomogeneous, consisting of denser regions $n_{\rm p} \sim 10^{13} - 10^{14}$ cm^{-3} with typical sizes of $l_{\rm b} \sim 10^9\,{\rm cm}$ separated by less dense regions with density $n_{\rm p} \sim 10^{10}\,{\rm cm}^{-3}$, i.e. the interblob plasma (Wynn, King & Horne 1995). The availability of time-resolved data allowed the estimation of the blob masses. The estimate was made using the photon luminosity of the Balmer continuum, combined with atomic data from Osterbrock (1989). The range of blob masses that were consistent with the H_α-emission are $M_{\rm balmer} \sim (0.09-2)\times 10^{-12} n_{10}^{-1} D_{100}^2 M_\odot$. Combining this mass estimate with the mean recurrence time-scale of flares, which is approximately 6 hours (e.g. Patterson 1979; van Paradijs et al. 1989; Bruch 1991), a mean mass transfer was estimated which is of the order of $\langle \dot{\rm M}_2 \rangle \sim 4 \times 10^{17} {\rm n}_{10}^{-1} {\rm D}_{100}^2\,{\rm g\ s}^{-1}$. The ratio of the inferred accretion rate to the inferred mass transfer corresponds to a fraction of approximately $\sim$ 0.01-0.02 %, suggesting an extremely efficient propeller. This is confirmed by the inferred rate of outflow of mechanical energy from the system (Wynn King & Horne 1997) which is at least

$$\begin{aligned} L_{\rm mech} &= \tfrac{1}{2} \dot{M_{\rm out}} v_{\rm esc}^2 \\ &\approx 5 \times 10^{33} \left(\tfrac{\dot{M}_{\rm out}}{5\times 10^{17}\ {\rm g\ s^{-1}}} \right) \\ &\quad \left(\tfrac{v_{\rm esc}}{1.55\times 10^8\ {\rm cm\ s^{-1}}} \right)^2 {\rm erg\ s^{-1}}. \end{aligned} \tag{3.130}$$

This is of the order of the inferred spin-down power of the white dwarf, implying that nearly the entire reservoir of rotational kinetic energy drives the rapid mass outflow from the system. This propeller effect contributes to the uniqueness of AE Aquarii among the magnetic cataclysmic variables. Another aspect contributing to the uniqueness of AE Aquarii is the highly variable optical as well as non-thermal radiation.

The nature of the flares seem to support the conjecture that it originates in the propeller driven outflow. These flaring states typically last from several minutes to hours. Balmer lines (Welsh Horne & Gomer 1998) indicate that the new light appearing during a flare can have emission lines shifted from the line centroid and are somewhat narrower. Individual flares therefore occupy only a part of the entire emission-line region. The correct velocity amplitude and direction occur in the exit fan just outside the Roche lobe of the white dwarf (Horne 1999). The nagging question at the time was why the flares are ignited here, several hours after the gas slipped silently through the magnetosphere (Pearson Horne & Skidmore 2003). Within this framework, the flares in AE Aquarii has been modelled in terms of colliding blobs (e.g. Pearson Horne & Skidmore 2003,2004) in the exit stream. In a detailed analysis these authors showed that the flares can be explained in terms of collisions between blobs of different densities, ejected from the magnetosphere with different velocities, producing isothermal, shock heated, $T \sim 18000$ K fireballs that cool radiatively after

collisions in the exit fan (Horne 1999; Pearson Horne & Skidmore 2003).

The model proposed in this paper describes (e.g. also Meintjes & Venter 2005) the propeller outflow in terms of a Kelvin-Helmholtz driven magnetospheric drag and associated energy transfer from the fast rotating magnetosphere to the slower mass flow from the secondary. The global energetics of the Kelvin-Helmholtz driven propeller in AE Aquarii has been presented by Meintjes & Venter (2005). This paper will focus specifically on a more quantitative investigation of the Kelvin-Helmholtz instability in the shear layer between the magnetosphere and the flow, and the resulting consequences. It will be shown that much of the peculiar thermal and non-thermal emission associated with AE Aquarii can be explained within this framework. The paper will be structured as follows: In Section 2 the Kelvin-Helmholtz instability and associated generation of turbulence will be discussed in terms of their contribution to the propeller mechanism and thermal emission. Section 3 focuses on the production of non-thermal radio to mid-infrared (mid-IR) emission within the same model. The discussion is presented in Section 4.

2. THE K-H DRIVEN PROPELLER

2.1 The magnetosphere-flow interaction

The flow can be described as a ballistic stream of gas clumps falling from close to rest at the L_1 point towards the WD (e.g. Meintjes 2004), being propelled by the effective gravity in the Roche lobe of the white dwarf. The conservation of angular momentum will cause the stream to pass the compact object at the distance of closest approach (Lubow & Shu 1975, cf. Reinsch & Beuermann 1994), which is given by the expression $\mathrm{R_{cl}} = 1.4 \times 10^7 \mathrm{P_{orb}}(s)^{2/3}\mathrm{M_1^{1/3}}$ cm $= 1.5 \times 10^{10}\,(P_{\rm orb}/9.88\,{\rm hr})^{2/3}(M_1/M_\odot)^{1/3}$ cm, with $\mathrm{M_1}$ the mass of the white dwarf in solar units. This is consistent with the results of Wynn, King & Horne (1997) and it is anticipated that the bulk of the acceleration will take place in this region. The speed of the gas at the closest approach, relative to the white dwarf, is of the order of ~ 1000 kms^{-1}, slightly below the escape velocity which is $v_{\rm esc} \sim 1550$ km s^{-1}. To effectively escape from the binary system the gas has to be accelerated to velocities exceeding the escape velocity. This variation in density along the stream is an important factor influencing the interaction with the magnetosphere on smaller length scales, as well as the triggering of magnetohydrodynamic instabilities in the magnetosphere-gas interface. The trajectory of the mass transfer flow at closest approach is predominantly in the azimuthal direction, i.e. the gas thus skirts the magnetosphere like a pebble skipping over a pond. Efficient interaction between the fast rotating magnetosphere and the gas stream will result in the transfer of momentum which is required to propel the stream through the magnetosphere to velocities exceeding the escape velocity (Meintjes & Venter 2005).

The magnetosphere of the white dwarf is assumed to consist of a dipole magnetic field corotating with the WD and dragging with it a trapped very low density magnetospheric plasma. The Poynting flux $\mathrm{S} = \frac{1}{4\pi} v_{\rm rel}\mathrm{B^2} \propto \mathrm{r^{-5}}$ (with r the radial distance from the WD), where $v_{\rm rel}$ represents the relative velocity between the fast rotating field and the slower stream. The energy is transferred per unit surface area perpendicular to the velocity, $\mathrm{v_{rel}}$(the relative velocity of the flow and the field). Such a scenario was considered by Wang & Robertson (1984,1985)(WR84,85) for the development of Kelvin-Helmholtz instabilities in the interface between the fast rotating magnetosphere of a neutron star and the surrounding slower mov-

ing accretion disc.These authors showed that the Kelvin-Helmholtz instability results in the generation of vorticity in the interface as the field attempts to force the gas into corotation. The high level of differential motion will result in reconnection in regions of opposing magnetic polarity, resulting in magnetic bubbles that will float outward, transferring angular momentum to the gas. This process forms the basis of the MHD propeller, resulting in the propulsion of material away from the gravitating compact object at the expense of the rotational kinetic energy of the compact object. These authors also showed that the magnitude of the spindown torque exerted on the neutron star is sufficient to account for the long periods of many of the observed binary X-ray pulsars.

The scenario under consideration in AE Aquarii may be very similar to the interaction between a fast rotating neutron star magnetosphere and an accretion disc outside the corotation radius. The growing Kelvin-Helmholtz instabilities mixes the field with the flow, propelling blobs through the magnetosphere at the expense of the rotational kinetic energy of the white dwarf.

2.2 Kelvin-Helmholtz instabilities

The Kelvin-Helmholtz instability is a phenomenon occuring at the interface between fluids moving with different speeds with respect to one another (e.g. Chandrasekhar 1961, pp. 481-514; Choudhuri 1998, pp. 141-148). A shear layer may form in which the velocity changes less abruptly from the one fluid to the other. The stability of an equilibrium between the fluids depends on the relative velocity, the densities and the nature of the perturbation of the interface.

In the case under investigation the two fluids under consideration are the less dense, fast rotating magnetosphere, sweeping across the denser slower moving stream of material punching through the magnetosphere. Numerical simulations (WR84) showed that disturbances (velocity perturbations perpendicular to the flow direction) to an initial equilibrium state, grow at the rate predicted by a linear analysis of the MHD equations (cf. Landau & Lifshitz 1961, p. 228). The linear growth rate is given by

$$n = [k_{\mathrm{x}}^2 \alpha_1 \alpha_2 U^2]^{1/2}, \tag{3.131}$$

with $\alpha_1 = \rho_1/(\rho_1 + \rho_2)$. The growth time is

$$\tau_{\mathrm{KH}} = \frac{1 + \rho_1/\rho_2}{(\rho_1/\rho_2)^{1/2}} \frac{\lambda}{2\pi} \frac{1}{v_{rel}}, \tag{3.132}$$

where $\lambda_\circ$ is the wavelength of the disturbance. The Mach number of the flow is $\mathrm{M} = \mathrm{U}/\mathrm{c_{s1}}$, with U the relative velocity between the two fluids and c_{s1} the sound speed in fluid 1. Maximum growth occurs for perturbations with wave vectors in the direction of the streaming. As can be seen from the equation, the growth rate of the instability depends on the relative velocity of the two fluids and their respective densities. A uniform magnetic field in one of the fluids does not affect the growth if its orientation stays perpendicular to the flow direction. The instability develops as if the field is absent. An instability criterion for the scenario described above is $\mathrm{U} < (c_{\mathrm{s1}}^{2/3} + c_{\mathrm{s2}}^{2/3})^{3/2}$, or if fluid 2 has a magnetic field, c_{s2} can be replaced by the magnetosonic speed $(c_{\mathrm{s2}}^2 + v_{\mathrm{A2}}^2)^{1/2}$ (WR85). Thus the interface is unstable if the streaming motion is subsonic or sub-Alfvénic in one of the fluids. WR84 showed that a perturbed quantity like the velocity or shear layer thickness grows like $\exp(t/\tau_{\mathrm{KH}})$ and thus the amplitude of the disturbance grows for a time t, to $\mathrm{t} = 10\tau_{\mathrm{KH}}$

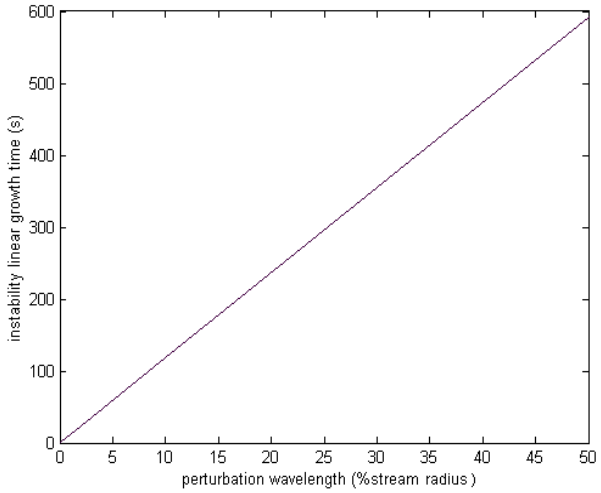

Figure 1: Growth times of perturbations of the interface as a function of the wavelength in the streaming direction with the stream density(fluid 1), $n_{\rm b} \sim 5 \times 10^{14}$ cm^{-3} and magnetosphere (fluid m), $n_{\rm m} = 10^{7}$ cm^{-3}

while the shear layer broadens. Non-linear effects then become important and saturation occurs. Following from this linear instability analysis, the expected growth times for instabilities in the interface between two fluids is represented in Figure 1. The two fluids are considered to be the stream (i.e. fluid 1) $n_1 \sim 10^{14}\,{\rm cm}^{-3}$ (Meintjes & Venter 2005) and the trapped magnetospheric plasma(fluid 2). The density of the trapped plasma is assumed to be between the upper limit, given by equipartition with the field (Meintjes & Venter 2005) $n \sim 5 \times 10^{8}\,{\rm cm}^{-3}$, and the Goldreich-Julian (1969) density $\rho_{\rm G-J} = ({\rm B}_{*}\Omega_{*}/2\pi{\rm ec}) \approx 2 \times 10^{3}$ cm^{-3}. A value of $n_2 \sim 10^{7}\,{\rm cm}^{-3}$, closer to the expected upper limit, was used in the calculations. For comparison, the growth rate of the Kelvin-Helmholtz instability at the interface between the magnetospheric plasma and the low density interblob plasma, where the fluid density is approximately $n_1 \approx 10^{10}\,{\rm cm}^{-3}$ (Eracleous & Horne 1996; Wynn King & Horne 1997) is displayed in Figure 2.

It is clear from Figure 1 that in the denser regions of the inhomogeneous stream ($n_{\rm p} \sim 10^{14}\,{\rm cm}^{-3}$) MHD perturbations with dimensions up to $\lambda \leq R_{\rm stream}$ ($R_{\rm stream} \sim 10^{9}\,{\rm cm}$) can be triggered over time-scales $\tau_{\rm KH} \leq 600$ s, which corresponds to the dynamical time-scale $t_{\rm dyn} \sim 600\,{\rm s}$ in the region of closest approach of the stream. Compared to this, KH instabilities of dimensions similar to the stream radius $\lambda \leq R_{\rm stream}$ can be triggered on time-scales of seconds $\tau_{\rm KH} \leq 5\,{\rm s}$ in the interface between the magnetosphere and the less dense parts of the stream, i.e. the interblob plasma where the particle densities are of the order of $n_{\rm p} \sim 10^{10}\,{\rm cm}^{-3}$ (e.g. Eracleous & Horne 1996; Wynn King & Horne 1997). These results are promising in the sense that large scale Magnetohydrodynamic perturbations in every part of the flow, i.e. the densest and less dense regions, can be triggered over time-scales $\tau \leq \tau_{\rm dyn}$. This growth of large magnetohydrodynamic instabilities of scales comparable to the stream width over these time-scales may in fact be the mechanism driving the bulk propeller outflow in AE Aquarii, since the fast growth of such instabilities mixes the flow and results in the gas being driven by a magnetospheric wave, accelerating it to velocities that can exceed the escape velocity over relatively short time-scales (Meintjes & Venter 2005), assuming a efficient conversion of magnetohydrodynamic to mechanical power in the process.

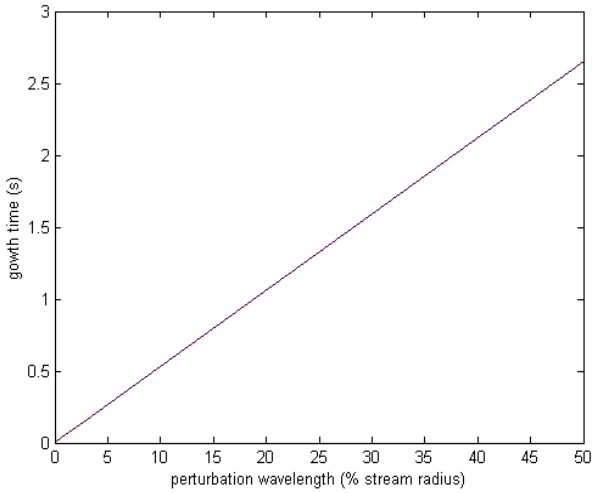

Figure 2: As figure 1, but with the density of the stream material that of low the density component of the line emission plasma, $n_{\rm low} \sim 10^{10}$ cm^{-3} and $n_{\rm m} \sim 10^{7}$ cm^{-3}

From an energetics point of view, it can be shown that the average rate of magnetohydrodynamic energy injection per unit volume into the stream is of the order of

$$\begin{aligned} \dot{q} &= \mathbf{f}_{{\rm mag},\phi}.\mathbf{v} \\ &= \langle \rho_{\rm stream} \rangle \dot{v}_{\phi} v_{\phi}. \end{aligned} \tag{3.133}$$

Depending on the conversion efficiency of magnetohydrodynamic power to mechanical energy (ϵ), the energy transfer results in an azimuthal acceleration of

$$\dot{v}_{\phi} = \left(\frac{\epsilon \dot{q}}{\langle \rho_{\rm stream} \rangle v_{\phi}} \right). \tag{3.134}$$

It has been shown (Meintjes & Venter 2005) that the volume rate of injection of MHD energy into the stream is of the order of $\dot{q} \sim 4 \times 10^{4}$ erg cm^{-3}s^{-1}, which if converted entirely to mechanical power ($\epsilon = 1$), results in an azimuthal acceleration of the gas of

$$\begin{aligned} \dot{v}_{\phi} \sim\ & 5 \times 10^{5} \left(\frac{\epsilon}{1} \right) \left(\frac{\dot{q}}{4 \times 10^{4}\,{\rm erg\ cm^{-3}s^{-1}}} \right) \\ & \left(\frac{\rho}{\langle \rho_{\rm stream} \rangle} \right)^{-1} \left(\frac{v_{\phi,{\rm stream}}}{v_{\rm ff}} \right)^{-1} {\rm cm\ s^{-2}}. \end{aligned} \tag{3.135}$$

This means that accelerated fluid elements can reach the escape velocity within a time-scale of

$$t_{\rm acc} = \left(\frac{v_{\rm esc} - v_{\phi,{\rm i}}}{\dot{v}_{\phi}} \right). \tag{3.136}$$

If $v_{\rm esc} \sim 1.6 \times 10^{8}\,{\rm cm\ s^{-1}}$ and $v_{\phi,{\rm i}} = v_{\rm ff} \approx 1 \times 10^{8}\,{\rm cm\ s^{-1}}$ (Meintjes & Venter 2005), then $\delta v_{\phi} = v_{\phi} - v_{\phi,{\rm i}} \approx 5 \times 10^{7}\,{\rm cm\ s^{-1}}$, implying that in the most optimistic scenario ($\epsilon = 1$) individual fluid elements can reach the escape velocity within a time

$$t_{\rm acc} \sim 100 \left(\frac{\delta v_{\phi}}{5 \times 10^{7}\,{\rm cm\ s^{-1}}} \right) \left(\frac{\dot{v}_{\phi}}{5 \times 10^{5}\,{\rm cm\ s^{-2}}} \right)^{-1} {\rm s}. \tag{3.137}$$

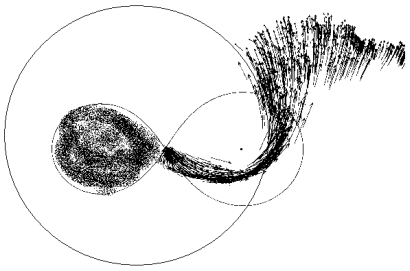

Figure 3: Simulation of gas ejected by the magnetic propeller (Wynn, King & Horne 1997)

This result shows that, assuming $\epsilon = 1$, the acceleration time-scale of regions of the stream with density $\langle n_{\rm stream} \rangle \sim 10^{14}\,{\rm cm}^{-3}$ (Meintjes & Venter 2005) is similar to the growth time-scale of Kelvin-Helmholtz instabilities with dimensions of the order of $l_{\rm K-H} \sim 0.1 R_{\rm stream}$ in regions of the same density, implying effective acceleration of the surface with skin depth of 10 % of the stream. Based upon these estimates it can be seen that with an efficiency of only $\epsilon \sim 0.1$, the fluid can still be accelerated to the escape velocity within $\tau_{\rm acc} \sim 1000$ s, which is similar to the inferred drag time-scales in the slow rotator limit and still of the order of $t_{\rm dyn} \sim 600$ s. This clearly emphasizes the efficiency of the K-H instability as a mechanism explaining the propeller outflow in AE Aquarii. The outflow dynamics of a K-H driven propulsion is certainly compatible with the flow dynamics reported by Wynn King & Horne (1997) which is shown in Figure 3.

2.3 Turbulence

It has been mentioned earlier that growth of Kelvin-Helmholtz instabilities in the flow is accompanied by the injection of turbulence into the flow (e.g. Biskamp 2003, pp. 33-65). One of the properties of turbulence (e.g. Choudhuri 1998, pp. 158 - 175) is that large turbulent cells in the ejected outflow will divide into smaller cells, resulting in a Kolmogorov type energy cascade down to the shortest length scales where the turbulent energy can be dissipated into heat. The cascade process accelerates towards shorter length scales (e.g. Landau & Lifshitz 1987, pp. 132-133) as each eddy feeds its energy to shorter scales in a time that is a factor $2^{-2/3}$ shorter than the previous, resulting in a total cascade time of the order of

$$\tau_{\rm cas} \quad = \quad \left(\frac{l_{\rm max}}{v_{\rm rms}} \right), \tag{3.138}$$

where $l_{\rm max}$ and $v_{\rm rms}$ represent respectively the maximum length scale of the turbulent cells and the associated turbulent turnover velocity, typically of the order of a fraction of the local sound speed. Using the same parameters as above, it can be shown that the upper limit for the turbulence cascade time-scale, i.e the time for the largest possible turbulent perturbations of initial dimension $l_{\rm max} \sim R_{\rm stream}$ to cascade down with a velocity of the order of $v_{\rm rms} \sim \alpha c_{\rm s}$, with $\alpha \sim 0.1$ (e.g. Campbell 1997, pp. 43, 64), is of the order of

$$\tau_{\rm cas} \quad \sim \quad 10000 \left(\frac{l_{\rm max}}{R_{\rm stream}} \right) \left(\frac{v_{\rm rms}}{0.1\, c_{\rm s}} \right)^{-1} {\rm s}, \tag{3.139}$$

with $c_{\rm s} \sim 10^6 (T/10^4\,{\rm K})^{1/2}\,{\rm cm\ s}^{-1}$. This cascade time-scale ($\tau_{\rm cas} \sim 3\,$hours) represents the time delay before the energy contained in turbulence manifests in heating the gas. Therefore, it is expected that a certain

fraction of the magnetohydrodynamic reservoir, driving the propeller and the associated Kelvin-Helmholtz instabilities, will be dissipated in the heating of the propeller outflow as the turbulent perturbations reach the dissipative scale. Since the Kelvin-Helmholtz instability growth time-scales, which is probably determines the rate at which turbulence is fed into the accelerated gas, is of the order of seconds to minutes, depending on the density of the stream (e.g. Figure 1,2), the associated turbulence in the outflow will eventually cascade down to the dissipative scale long after the gas has silently slipped though the magnetosphere. It is then proposed that the turbulence may in fact be a prominent contributer towards the heating of the outflow, i.e contributing to the heating of the line emitting gas and possibly even contributing to the optical flares when blobs in the outflow collide.

For a Kolmogorov type energy cascade of turbulent eddies of initial dimension $l_{\rm max,i}$, with an average turn-over velocity $v_{\rm rms,i}$ in the inertial range, to the dissipative scale where the corresponding values are $l_{\rm d}$ and $v_{\rm rms,d}$ (e.g. Choudhuri 1998, pp. 165-169), results in an eventual energy dissipation rate per unit mass

$$\begin{aligned} \epsilon &= \left(\frac{v_{\rm rms,i}^3}{l_{\rm max,i}}\right) \\ &= \left(\frac{v_{\rm rms,d}^3}{l_{\rm d}}\right). \end{aligned} \tag{3.140}$$

This results in a rate of heat generation on the dissipative scale which is given by

$$\begin{aligned} \dot{u}_{\rm t,d} &= \rho\left(\frac{v_{\rm rms,d}^3}{l_{\rm d}}\right) \\ &= \rho\nu_{\rm t,d}\left(\frac{v_{\rm rms,d}}{l_{\rm d}}\right)^2 \ {\rm erg\ cm^{-3}s^{-1}}, \end{aligned} \tag{3.141}$$

where $\nu_{\rm t,d} = v_{\rm rms,d} l_{\rm d}$ represents the coefficient of turbulent viscosity on the dissipative scale.

It can be shown (e.g. Choudhuri 1998, p. 166) that the size of the smallest eddies relates to the size of the largest according to

$$l_{\rm d} = \left(\frac{R_{\rm e}}{R_{\rm e,crit}}\right)^{-3/4} l_{\rm max}, \tag{3.142}$$

where $R_{\rm e}$ and $R_{\rm e,crit} \sim 100$ (e.g. Biskamp 2003, p. 47) represent respectively, the Reynolds number of the flow and the critical value where the largest eddy equals the size of the smallest. Since the typical Reynolds numbers of the flow is of the order of $R_e \sim 10^9$ (Meintjes & Venter 2005) and the largest eddies probably have dimensions of the order of $l_{\rm max} \sim 10^9\,{\rm cm}$ at the interface between the magnetosphere and the interblob plasma, the smallest eddies dissipating turbulent energy in the gas is of the order of

$$l_{\rm d} \sim 5 \times 10^3 \left(\frac{R_{\rm e}}{10^9}\right)^{-3/4} \left(\frac{R_{\rm e,crit}}{100}\right)^{3/4} \left(\frac{l_{\rm max}}{10^9\,{\rm cm}}\right)\ {\rm cm}. \tag{3.143}$$

The typical gas temperatures that can explain the optical flares (Pearson Horne & Skidmore 2003) and the UV line emission (Jameson, King & Sherrington 1980) are between $1 \times 10^4\ {\rm K} < T_{\rm lines} < 8 \times 10^4\ {\rm K}$.

If on the dissipative scale $v_{\rm rms,d} \rightarrow c_{\rm s} \sim 10^6 (T/10^4\,{\rm K})^{1/2}\,{\rm cm\ s^{-1}}$, the turbulence dissipation rate in the ejected plasma with density range between $n_{\rm p} \sim 10^{10}\,{\rm cm^{-3}}$ (interblob-plasma) and denser blobs $n_{\rm p} \sim 10^{13}\ {\rm cm^{-3}}$

involved in flare production if they collide (Pearson Horne & Skidmore 2003), is of the order

$$\dot{u}_{\rm t,d}({\rm i\text{-}b}) \sim 3 \left(\frac{n_{\rm p}}{10^{10}\,{\rm cm}^{-3}}\right) \left(\frac{\nu_{\rm t,d}}{10^{10}\,{\rm cm}^2{\rm s}^{-1}}\right) \left(\frac{v_{\rm rms}}{c_{\rm s}}\right)^2 \left(\frac{l}{l_{\rm d}}\right)^{-2} {\rm erg\ cm}^{-3}{\rm s}^{-1} \tag{3.144}$$

$$\dot{u}_{\rm t,d}({\rm blob}) \sim 3000 \left(\frac{n_{\rm p}}{10^{13}\,{\rm cm}^{-3}}\right) \left(\frac{\nu_{\rm t,d}}{10^{10}\,{\rm cm}^2{\rm s}^{-1}}\right) \left(\frac{v_{\rm rms}}{c_{\rm s}}\right)^2 \left(\frac{l}{l_{\rm d}}\right)^{-2} {\rm erg\ cm}^{-3}{\rm s}^{-1}. \tag{3.145}$$

It has been shown that the cascade time-scale for turbulence to the dissipative scale is of the order of $t_{\rm cas} \sim 10^4$ s ($\sim$ 3 hours). During this time the colliding propeller ejected blobs, expanding at the speed of sound ($v_{\rm exp} \sim c_{\rm s} \sim 10^6\,{\rm cm\ s}^{-1}$), can reach radii of the order of $R_{\rm cloud} \sim 10^{10}\,{\rm cm}$. Therefore the total dissipation luminosity $L_{\rm t,d} \sim \dot{u}_{\rm t,d} R^3_{\rm blob}$ in this ejected gas with density $n_{\rm p} \sim (10^{10} - 10^{13})\,{\rm cm}^{-3}$ can be between

$$L_{\rm t,d}({\rm i\text{-}b}) \sim 10^{31} \left(\frac{\dot{u}_{\rm t,d}}{3\,{\rm erg\ cm}^{-3}{\rm s}^{-1}}\right) \left(\frac{R_{\rm i-b}}{10^{10}\,{\rm cm}}\right)^3 {\rm erg\ s}^{-1} \tag{3.146}$$

$$L_{\rm t,d}({\rm blob}) \sim 10^{33} \left(\frac{\dot{u}_{\rm t,d}}{3000\,{\rm erg\ cm}^{-3}{\rm s}^{-1}}\right) \times \left(\frac{R_{\rm blob}}{10^{10}\,{\rm cm}}\right)^3 {\rm erg\ s}^{-1} \tag{3.147}$$

This is of the same order of magnitude as the luminosities inferred from the UV emission lines (Jameson, King & Sherrington 1980; Eracleous & Horne 1996), emitted in a gas with density $n_{\rm p} \sim 10^{10}\,{\rm cm}^{-3}$, and optical flares (van Paradijs Kraakman & van Amerongen 1989) originating from denser colliding blobs in the outflow (Pearson Horne & Skidmore 2003). The estimations presented above assume in fact that the shocks generated when blobs collide in the outflow drives $v_{\rm rms} \rightarrow c_{\rm s}$, creating a channel for the conversion of the turbulent reservoir in the blobs to heat energy, transferred through the gas over length scales comparable to the turbulent dissipation length scale ($l_{\rm d} \sim$ few $\times\, 10^3\,{\rm cm}$), which is orders of magnitude larger than the particle mean free path in a thermal plasma (Frank King & Raine 2002, p. 31), e.g. $\lambda \sim 1\,(\ln\Lambda/10)^{-1}(n_{\rm blob}/10^{13}\,{\rm cm}^{-3})^{-1}(T/10^4\,{\rm K})^2\,{\rm cm}$. This implies a rapid heat transfer, which may be the driving mechanism behind the optical flares.

The model proposed in this paper is promising since it provides a vehicle to integrate the optical flares and UV emission line emission associated with the rapid propeller outflow. It has been mentioned earlier that the turbulence generated in the outflow results in a rapid diffusion of magnetic field through the magnetosphere-gas interface. The rapid diffusion through this region of high differential motion may then result in highly sheared fields and resultant reconnection and associated particle acceleration (e.g. Parker 1976). Within this frame work, the enigmatic non-thermal radio to mid-IR flaring in AE Aquarii can be evaluated.

3. RADIO FLARES

The radio and mid-IR emission (Bastian Dulk & Chanmugam 1998; Dubus et al. 2004) from the system is assumed to be gyro-synchrotron radiation from expanding magnetized plasma blobs (e.g. Bastian, Dulk & Chanmugam 1998; Kuijpers et al. 1997; Meintjes & Venter 2003). In a first attempt to model the radio spectrum in terms of propeller ejected bubbles it was shown that the resultant emission of a superposition of synchrotron sources in different stages of expansion can account for the entire observed non-thermal radio to infrared spectrum, i.e. between $\nu \sim 1$ - 3000 GHz (Meintjes & Venter 2003; Venter & Meintjes 2004). These first results were promising, although it was assumed that the magnetized blobs are related to the mass

transfer process from the secondary star. It has been shown (Meintjes & Venter 2003) that the secondary star may have a surface polar field of the order of $B_\circ \sim 2000$ G, which may imply that it might also have magnetically active regions in the equatorial belt which may influence, and in some cases, even magnetize the mass flow with fields reaching similar values (Meintjes & Venter 2003; Venter & Meintjes 2004). However, it has been shown (Meintjes & Venter 2005) that blobs with magnetic fields of the order of a few hundred Gauss ($B \sim 300$ G) may also be the direct result of the magnetospheric propeller in AE Aquarii via the Kelvin-Helmholtz mechanism. Based upon these new results, the radio spectrum of AE Aquarii has been simulated using an approach based upon the superposition of synchrotron emitting magnetized bubbles (van der Laan 1963, 1966; Bastian Dulk & Chanmugam 1988) with fields ranging between $\mathrm{B_{blob}} \sim 300$ - 1000 G.

The Kelvin-Helmholtz driven ejection of material from the magnetosphere implies the mixing of the slower moving (i.e. $v_{\mathrm{ff}} \sim 10^8\,\mathrm{cm\ s^{-1}}$) dense ballistic gas stream with the much faster corotating magnetosphere (i.e. $v_{\mathrm{mag}} \sim 10^9\,\mathrm{cm\ s^{-1}}$). This will result in significant shearing of the magnetic field, resulting in the generation of a significant toroidal field in the boundary layer with field strengths approaching the poloidal magnetospheric field strength (e.g. Aly & Kuijpers 1990) which is of the order of $B_{\mathrm{mag}} \geq 300$ G (Meintjes & Venter 2005). These highly sheared fields will be highly unstable and very susceptible to the tearing mode instability (e.g. Priest & Forbes 2000, pp. 177-228; Biskamp 2003, pp. 57-64) and resultant reconnection. This process most probably results in the generation of magnetized bubbles or clouds which are ejected with the rest of the flow. Within the framework proposed in this paper, the largest possible magnetized bubbles generated by the Kelvin-Helmholtz instability may have the typical dimension of the blob stream ($l_{\mathrm{K-H}} \sim 10^9\,\mathrm{cm}$). The magnetic reconnection and magnetic pumping as a result of the magnetospheric interaction with the propeller can result in the generation of a population of non-thermal electrons in these clouds, with energies reaching values of the order of $\epsilon_{\mathrm{e}} \sim 170$ MeV (Meintjes & Venter 2005) within the dominant energy-loss time-scales. The subsequent expansion and superposition of these synchrotron radiating bubbles (van der Laan 1963,1966) best explains the behaviour of the transient radio to mid-infrared emission (e.g. Bastian, Dulk & Chanmugam 1998; Meintjes & Venter 2003; Venter & Meintjes 2004).

Blobs magnetized in the propeller process with field strengths of B $\geq$ 300 G and relativistic electron populations with powerlaw distribution $n(E)dE = KE^{-\delta}dE$ with K related to N (number density of electrons with $E > E_c$), as $K = (\delta - 1)E_c^{\delta-1}N$ have been used to simulate the radio to mid-infrared spectrum in AE Aquarii based upon a superposition of expanding synchrotron bubbles in different stages of expansion. Figure 4a shows the spectrum simulated with a number of blobs with magnetic fields of the order of B $\sim$ 350 G. Using the same method described in Meintjes & Venter (2003), but taking blob dynamics closer to that which are expected for the propeller outflow, the resultant spectrum based upon the radiation of 10 blobs in different stages of expansion, with initial radii of the order of $r_{\mathrm{blob,i}} \sim 8 \times 10^8\,\mathrm{cm}$, with electron energies of the order of $\mathrm{E_i} \sim 150$ MeV (Meintjes & Venter 2005) and expanding at $\mathrm{v_{exp}} = 300\ \mathrm{kms^{-1}}$ is shown in Figure 4a. Also included in Figure 4 are a selection of observations (Dubus et al. 2004, Abada et. al. 1993,1995a,b) that show the average trend of the spectrum with a gradient of approximately $\alpha \approx 0.5$ (e.g. Dubus et al. 2004). Observations (Abada-Simon et al. 2002) indicate an upper limit at 170 μm which is lower than a detection at 90 μm. From this, the authors assume that the spectrum may peak at the frequency $\nu_p = 3300$ GHz. Mid-infrared observations made with the Keck I telescope (Dubus et al. 2004) showed excess emission above the red component of the secondary star, which may correspond to the emission of a single

blob with a field of B = 1000 G and dimension $r_{\rm blob,p} \sim 10^9$ cm, with an electron component with energy ranging to $E_{\rm c} = 10$ MeV. The peak is in fact slightly below $\nu_{\rm p} = 3300$ GHz, which is illustrated in Figure 4c. However, the spectrum is expected to be highly variable, especially in the mid-IR and in the frequency range around the turnover. Figure 4b shows the result if the blob size is $r_{\rm blob,i} \sim 1.5 \times 10^9$ cm, B $\sim$ 450 G and $\rm v_{exp} = 600$ kms^{-1}. All three scenarios of Figure 4 are compatible with the general Kelvin-Helmholtz interaction model that is expected to produce magnetized bubbles with populations of relativistic electrons. It seems probable that the fields mixed into these blobs would have magnitudes between B = 300 - 1000 G since parts of the gas stream may have a slightly different trajectory at its L_1 origin, it may fall deeper into the magnetosphere and come in contact with field strength of higher magnitude.

Newly produced magnetized blobs probably emit predominantly in the infra-red, but observations show that the spectrum extends to the low GHz range. Emission at these frequencies implies larger, less dense blobs with fields B $<$ 1 G and mildly relativistic electrons. It can be shown that the synchrotron loss time $\tau_{\rm syn} \propto \gamma_e^{-1} B_{\rm blob}^{-2}$ (e.g. Lang 1980, p. 31), implying that the radiation loss time-scale increases significantly with lower energy and magnetic field strength. Blobs that expand to these large dimensions (e.g r $> 100 r_{\rm blob,i}$), with a small population of relativistic electrons, are very faint, but the synchrotron emission loss rate (see below) is very low and therefore blobs of these dimensions probably convolve, resulting in a boost of the integrated flux level. Included in the integration of the spectra in Figure 4 are three blobs of size r = 15r$_{\rm blob,i}$, six with r = 100r$_{\rm blob,i}$ and 10 with r = 500r$_{\rm blob,i}$ (for r$_{\rm blob,i} = 1.5 \times 10^9$ cm). These blobs contribute mainly at frequencies $\nu << 100$ GHz. The accumulation of expanded radio blobs is more significant towards lower frequencies and it is expected that flux levels of $S_\nu > 6$ mJy at $\nu \sim 100$ MHz may be reached. This obviously depends on the amount of magnetized blobs that emit in this frequency range. This convolution of ejected blobs in late stages of their evolution may therefore result in an optically thin $\nu \leq 1$ GHz radio remnant surrounding the AE Aquarii system.

It has been shown that with fairly modest parameter choices the trend of the observed spectrum (cf. Dubus et al. 2004, Abada et al. 1993,1995a,b) can be reproduced from radio (Bastian Dulk & Chanmugam 1998; Abada-Simon et al. 1993, 1995a,b) to mid-infrared (Dubus et al. 2004). The blob origin model for the radio-IR emission in the system is thus compatible with the propeller mechanism proposed above.

4. DISCUSSION

In this paper an attempt has been made to consolidate aspects of the peculiar multi-wavelength emission properties of AE Aquarii within the propeller model. It has been shown that the differential motion between the fast corotating magnetosphere and a much slower clumpy gas stream plunging into the Roche lobe of the white dwarf will result in Kelvin-Helmholtz instabilities with a wide spectrum of sizes ranging from $l_{\rm KH} \sim 10^7 - 10^9$ cm over time-scales ranging from $t_{\rm KH} \sim 5$ - 600 seconds in parts of the stream with densities $n_{\rm p} \sim 10^{10} - 10^{14}\,{\rm cm}^{-3}$ respectively. The associated mixing of the gas with the faster magnetospheric field will result in a very efficient magnetospheric drag that can propel blobs through the magnetosphere to the escape velocity over time-scales $\tau_{\rm acc} \leq 1000$ s, for all efficiencies $\epsilon \geq 0.1$, which is still of the order of $t_{\rm dyn} \approx 600$ s. Based upon energy arguments it has been shown that the total magnetospheric energy input into the flow is of the order of $L_{\rm mhd} \sim 10^{34}\,{\rm erg\ s}^{-1}$, which is similar to the inferred spin-down of the white dwarf. It has been

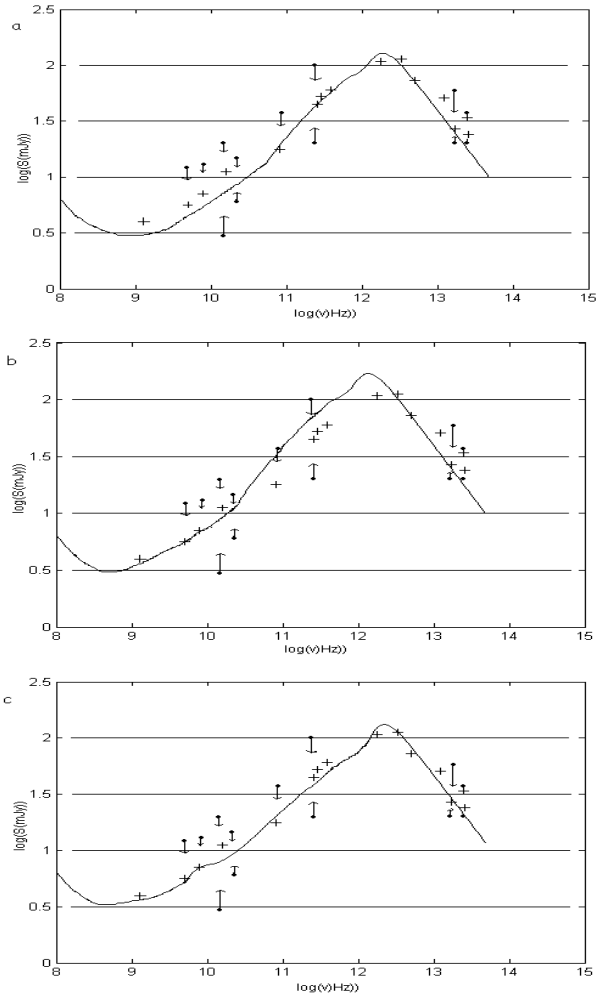

Figure 4a, b & c: Spectra (log S(ν)(mJy) vs. logν(Hz)) (a) A selection of observational averages(+) and observed minima and maxima(solid circles) and a spectrum from blobs with fields B $\sim$ 350 G and $E_c \sim$ 150 MeV; (b) The spectrum of the integrated emission from blobs with a variety of radii, field strengths $B_\circ \sim$ 450 G and $E_c \sim$ 25 MeV; (c) Like (a) and (b), but with parameters in the freshest blob, B = 1000 G and $E_c \sim$ 10 MeV (cf. Dubus et al. 2004)

shown that the growth of Kelvin-Helmholtz instabilities will be accompanied by the generation of turbulence in the flow, which may result in a turbulent Kolmogorov cascade to smaller length scales over time-scales of $t_{\rm cas} \sim 10000$ s (~ 3 hours), resulting in an additional reservoir of energy which can be released in dissipative shocks when blobs collide in the exit fan, resulting in flares. It has been shown that shock dissipation of the reservoir of turbulence in colliding blobs can drive luminosities between $L_{\rm t,d} \leq (10^{31} - 10^{33})\,{\rm erg\ s^{-1}}$, corresponding respectively to the UV line-emission (inter-blob plasma) and the optical flares (when denser blobs collide).

The Kelvin-Helmholtz interaction between the fast rotating magnetosphere and the gas stream may also be responsible for the observed non-thermal radio to mid-infrared emission. The mixing of the magnetosphere with the gas will result in a huge shear of the field, possibly triggering the tearing mode instability and resultant reconnection and associated particle acceleration. This can result in the generation of a population of magnetized bubbles that will leave the system with the rest of the propeller outflow. The superposition of the emission from a series of blobs reproduces the entire radio to mid-infrared spectrum of AE Aquarii, with fairly modest requirements in terms of particle energies and the resultant relativistic electron density. An important consequence of this process is that AE Aquarii may contain an optically thin radio remnant at frequencies $\nu \leq 1$ GHz as a result of the confluence of expanding synchrotron emitting blobs.

ACKNOWLEDGEMENTS

The authors want to thank the referee for his critical assessment and positive comments that resulted in a substantial improvement in the paper. A special word of appreciation to Prof. Eugene Parker for valuable discussions surrounding the properties of the K-H instability.

3.4.3 A tenuous X-ray corona enveloping AE Aquarii

Submitted to MNRAS (2006)
Venter L.A., Meintjes P.J.*

Abstract

In this paper we propose that the observed unpulsed X-ray emission in AE Aquarii is the result of a very tenuous hot corona associated with the secondary star, which is pumped magnetohydrodynamically (MHD) by the propeller action of the fast rotating white dwarf. It is shown that the closed coronal field of the secondary star envelopes a substantial portion of the binary system, including the fast rotating magnetized white dwarf. This implies that the propeller outflow of material in AE Aquarii is initiated inside an enveloping magnetic cavity. It has been shown that the outflow crossing the secondary dead zone field constitutes a $\beta_{\rm gen} = (8\pi\rho v_{\rm esc}^2/B^2) >> 1$ *plasma, acting as a MHD generator resulting in the induction of field aligned currents in these closed magnetospheric circuits where* $\beta_{\rm cir} = (8\pi nkT/B^2) << 1$. *It has been shown that Ohmic heating of the coronal circuit can readily account for a* $T_{\rm x} \geq 10^7\,K$ *plasma in the coronal flux tubes connecting the generator and the stellar surface. Further, it has been shown that bremsstrahlung losses of the thermal electrons in the coronal circuit can readily drive the observed unpulsed X-ray luminosity of* $L_{\rm x} \sim 10^{31}\,erg\,s^{-1}$, *which is in excellent agreement with the luminosity and relatively large source implied by recent XMM-Newton observations.*

keywords

binaries: general - stars: red dwarf - processes: heating, turbulence

1. INTRODUCTION

AE Aquarii is a binary extensively observed from radio wavelengths to TeV γ-rays (e.g. Meintjes & de Jager 2000; Meintjes & Venter 2003, 2005 and references therein). The binary has an orbital period $P_{\rm orb}$ = 9.88 hrs and the compact white dwarf has a spin period of $P_{\rm rot}$ = 33 s, probably the result of a high mass accreting history (e.g. Wynn, King & Horne 1997; Meintjes 2002). The system has an inclination $i = (55 \pm 7)^\circ$ (Welsh, Horne, & Gomer 1995). The main distinguishing feature of this cataclysmic variable is that the mass transfer from the red dwarf secondary star to the white dwarf primary is mostly not accreted, but ejected by the fast rotating primary's magnetic field, which acts as a propeller (e.g. Wynn, King & Horne 1997; Meintjes & Venter 2005; Venter & Meintjes 2006). This results in the white dwarf exhibiting a spin-down resulting in a spin-down luminosity of $P_{\rm sd} \sim 10^{34}\,{\rm erg\,s^{-1}}$ (de Jager et al. 1994; Meintjes & de Jager 2000), providing the reservoir for the majority of the emission from radio to TeV gamma-rays. The non-thermal nature of the radio-synchrotron emission has been established up to frequencies $\nu \sim 50000$ GHz (e.g. Meintjes & Venter 2003; Venter & Meintjes 2006; Dubus et al. 2004), resulting in a total non-thermal synchrotron luminosity between 1 GHz - 50000 GHz (radio to infra-red) which is of the order of $L_{\rm r-ir} \sim 10^{31}\,{\rm erg\,s^{-1}}$ (Meintjes & Venter 2003).

It has been shown (Meintjes et al. 1992; 1994) that AE Aqr exhibits events of Very High Energy (VHE) emission at energies $\epsilon_\gamma \geq 1$ TeV. These authors proposed that particle acceleration may occasionally occur, as a result of huge pulsar-like potentials being generated in the magnetosphere of the fast rotating white dwarf which is magnetically linked to a ring of gas in differential motion (Meintjes et al. 1994; Meintjes & de Jager 2000). This will result in a fraction $\gamma \sim 0.1$ % of the spin-down power of the white dwarf being channeled into non-thermal radio synchrotron emission (Meintjes & de Jager 2000; Meintjes & Venter 2005), and occasionally, $\gamma \rightarrow 1$, resulting in episodes of transient burst-like VHE γ-ray emission in AE Aquarii (Meintjes et al. 1994; Meintjes & de Jager 2000). This implies that a very effective particle accelerator may occasionally be active in AE Aquarii.

AE Aquarii was extensively studied in X-ray wavelengths (e.g. Warner 1995, p. 419; Eracleous 1999, for reviews). The system was detected in the 0.1 - 4 keV X-ray band by the *EINSTEIN* Observatory (Patterson et al. 1980; Eracleous, Patterson & Halpern 1991; Eracleous, Halpern & Patterson 1991). *EXOSAT* observations showed that the X-ray spectrum shows a multi-component structure, of which the $kT < 70$ eV component reveals a typical black body which is probably associated with accretion onto the white dwarf, and a general $kT < 1.8$ keV thermal bremsstrahlung component (Osborne 1990; Eracleous, Patterson & Halpern 1991). Follow-up *Rosat* (Clayton & Osborne 1995) and *ASCA* (Eracleous 1999) X-ray studies of AE Aquarii showed that the bremsstrahlung component typically displays properties of a two-temperature thermal plasma. It has been shown that the bremsstrahlung component of the spectrum shows properties reminiscent of those seen in coronally active systems, but with a luminosity slightly larger than the RS CVn systems containing a white dwarf (Clayton & Osborne 1995). Recent *XMM-Newton* observations (Itoh et al. 2006) indicate that the X-ray spectrum from AE Aquarii can be explained with a multi-temperature optically thin thermal plasma model with temperatures $\mathrm{T_x}$ = 1-5 $\times$ 10^7 K and an average luminosity $\mathrm{L_x} \sim 10^{31}$ erg $\mathrm{s^{-1}}$. These findings are in general agreement with earlier studies (Patterson et al. 1980; Osborne 1990; Eracleous, Halpern & Patterson 1991; Clayton & Osborne 1995; Choi, Dotani & Agrawal 1999). These latest studies (Itoh et al. 2006) imply a linear scale size of the X-ray source of $l_\mathrm{x} \sim$ (2 - 3) $\times$ 10^{10} cm, or an optically thin volume of gas, $\mathrm{V_x} \sim l_\mathrm{x}^3$. The electron density $\mathrm{n_e}$ is estimated to be of the order of $n_\mathrm{e} \sim$ few $\times$ $10^{11}\,\mathrm{cm^{-3}}$ (Itoh et al. 2006). These authors explained the unpulsed component of the X-ray emission as a result of heating of the mass transfer stream from the secondary as it plunged through the magnetospheric field in the Roche lobe of the compact white dwarf (Itoh et al. 2006).

However, in reply to the model proposed above, Ikhsanov (2006) proposed that the density of the mass transfer stream is probably several orders above the density of the X-ray emitting gas resulting in an X-ray luminosity which will exceed the observed luminosity by several orders of magnitude. As an alternative mechanism explaining the unpulsed X-ray emission, Ikhsanov (2006) proposes that the inferred spin-down power of the white dwarf in AE Aquarii (de Jager et al. 1994; Meintjes & de Jager 2000) is the result of pulsar-like magnetic dipole radiation from the fast rotating, strongly magnetized, white dwarf, and that the unpulsed X-ray source, probably outside the Roche lobe of the white dwarf, is energized by this radiation. However, this places unrealistic constraints on the magnetic field strength of the white dwarf, i.e. of the order of $B_{1,*} > 50$ MG (Ikhsanov 1998; 2001), which is significantly higher than the $B_{1,*} \approx 10^6$ G field (Chanmugam & Frank 1987), suggested by the levels of circular polarization, i.e. $\sim 0.05 \pm 0.01$ % (Cropper 1986) and 0.06 ± 0.03 % (Beskrovnaya et al. 1995). These levels of circular polarization are in general

consistent with earlier upper limits in the circular polarization of 0.06 % reported by Stockman et al. (1992). Further, it has been suggested that circular polarization at levels $< 1\%$ infer surface fields < 5 MG (Stockman et al. 1992). The field strength suggested by the level of circular polarization is also perfectly consistent with the inferred field which emerged from a study of the possible spin-up history of the white dwarf (Meintjes 2002), which shows the short spin period of the white dwarf in AE Aquarii is consistent with the system evolving through a high mass transfer phase, where the white dwarf was spun-up by a well developed accretion disc. It has been shown (Meintjes 2002), based upon disc-discless accretion scenarios in the intermediate polars (Wickramasinghe, Wu & Ferrario 1991; Warner 1995), that in the high mass transfer phase an accretion disc could develop if the magnetic moment of the white dwarf is of the order $\mu_{32} \leq 3(\dot{M}_2/10^{20}\,\mathrm{g\,s^{-1}})^{1/2}(P_{\mathrm{orb,i}}/8.5\mathrm{h})^{7/6}\,\mathrm{G\,cm^3}$, in units of $10^{32}\,\mathrm{G\,cm^3}$. Here $\dot{M}_2$ and $P_{\mathrm{orb,i}}$ represent respectively the mass transfer rate and orbital period of the binary system in a run-away mass transfer phase when the white dwarf in AE Aquarii was spun-up by a well developed accretion disc (Meintjes 2002). This estimated magnetic field is in excellent agreement with the inferred magnetic moments of other DQ Her stars ($\sim \mu_{32}/2$) (Warner & Wickramasinghe 1991). Based upon the familiar Hamada & Salpeter (1961) white dwarf mass-radius relation, i.e. $R_{1,*} \sim 5\times10^8(M_1/0.9\,M_\odot)^{-0.8}\,\mathrm{cm}$ (e.g. also Eracleous & Horne 1996), these magnetic moments imply a white dwarf surface field $B_{1.*} \leq 2.4\times10^6(\mu_{32}/3)(R/R_{1,*})^{-3}\,\mathrm{G}$ (Meintjes 2002), which is perfectly consistent with the inferred field strengths suggested by the circular polarization data, as well as the magnetic fields of the white dwarfs in the DQ Her systems and intermediate polars.

A recent study of the spin down (Mauche 2006) of the white dwarf in AE Aquarii, using *ASCA, XMM-Newton* and *Chandra* X-ray observations spanning 10 years, combined with the accurate optical ephemerides derived using earlier data sets (de Jager et al. 1994), showed that in recent years the white dwarf in AE Aquarii is in fact braking harder (Mauche 2006), at a rate and sign which is inconsistent with pulsar-like dipole radiation. These latest findings virtually eliminate the pulsar-like spin-down model associated with AE Aquarii (Ikhsanov 1998; 2001), which has been proposed as being the driving mechanism behind the steady unpulsed X-ray emission in AE Aquarii (Ikhsanov 2006).

In this paper it is proposed that the closed coronal field lines of the secondary star in AE Aquarii may play an important role in the production of the unpulsed X-ray emission. The model proposed here depends on the interaction between the propeller ejected mass flow from the fast rotating white dwarf with the equatorial magnetic field of the secondary star, which envelopes a significant fraction of the system, including the white dwarf. It has been shown (Meintjes & Jurua 2006) that the surface polar magnetic field of the secondary star in the intermediate polars ($B_{\circ,2}$), as well as the ratio of the radial extent of the so-called dead zone (r_{d}) to the binary separation (a), i.e. (r_{d}/a), within the realm of a standard Mestel & Spruit stellar wind (Mestel & Spruit 1987; Mestel 1999, pp. 240-314 and Campbell 1997, pp. 268-278 for extensive reviews) scales

$$B_{\circ,2} \approx \left[112\left(\frac{P_{\mathrm{orb}}}{\mathrm{hr}}\right)+2530\right]\,\mathrm{G} \tag{3.148}$$

$$\frac{r_{\mathrm{d}}}{a} \approx \left[0.065\left(\frac{P_{\mathrm{orb}}}{\mathrm{hr}}\right)+1\right]. \tag{3.149}$$

For the AE Aquarii system, with $P_{\mathrm{orb}} \sim 10\,\mathrm{hrs}$, this results in $B_{\circ,2} \approx 3650$ G and $(r_{\mathrm{d}}/a) \approx 1.65$ (i.e. $r_{\mathrm{d}}/R_2 \rightarrow 4$), applicable for fast rotators in general ($\Omega_* \geq 50\Omega_\odot$) (Campbell 1997, p. 265-267; Meintjes & Jurua 2006). Here a and R_2 represent the binary separation and the radius of the secondary star respectively

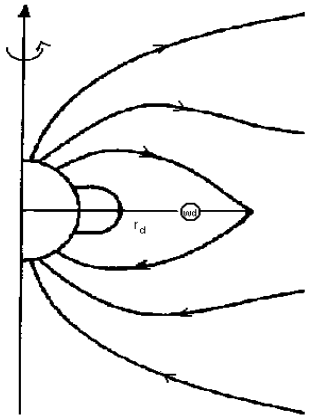

Figure 1: The coronal dead zone field of the secondary star.

(e.g. Figure 1). It has to be emphasized that the surface polar field of the secondary star, i.e. $B_{\circ,2} \approx 3600$ G, is not representing the average photospheric field, which may be substantially lower, except for isolated magnetically active regions, e.g. the star-spots, where the field intensity may be higher. The extent of the closed coronal field lines in AE Aquarii, i.e. prominences are in general agreement with recent findings (Collier Cameron 1996; Byrne et al. 1996; e.g. Priest & Forbes 2000, p. 438) which revealed the existence of unusually large prominences on some rapidly rotating flare stars. The geometry of these prominences were inferred from Hα observations of the fast rotating K-dwarf AB Doradus ($\Omega \sim 50\Omega_{\odot}$), suggesting that these large prominences extent between 3 - 9 stellar radii from the rotation axis of the star (Collier Cameron 1996; e.g. Priest & Forbes 2000, p. 438 for a discussion), similar to the inferred value for fast rotators in general, and hence for AE Aquarii.

Recent Roche tomography (Dunford & Smith 2005; Watson, Dhillon & Shahbaz 2006) showed evidence of star spot coverage ($\sim$ 20%) on the visible hemisphere of the secondary star in AE Aquarii, which may indicate magnetic activity. Although this finding supports the notion that the secondary star may have a substantial magnetic field, direct measurement of the magnetic field strengths are required to establish the magnetic nature of the secondary beyond doubt. The proximity of AE Aquarii ($D \sim 100\,\mathrm{pc}$) and the fact that the secondary star contributes > 90 % of the visible light of the system in quiescence, provide an interesting possibility of employing for example the Zeeman-Doppler Imaging (ZDI) technique or Zeeman broadening measurements to constrain the fields in the magnetically active regions. For example, Zeeman broadening of the lines is proportional to the field strength, the effective quantum Landé factor and the square of the wave-length, i.e. $\Delta\lambda \propto \lambda^2 g_{\mathrm{eff}} B$. Therefore, successful measurements of magnetic fields can be carried out using the red or IR lines with large effective g_{eff}. However, this technique is most successful for stars with strong surface fields (B $\geq$ 1000 G) and high surface field coverage. Therefore, it is questionable whether the 20 % field coverage and possibly lower average surface field strength on the secondary star in AE Aqr is sufficient for a positive detection.

The fact that $(r_{\mathrm{d}}/a) \approx 1.65$, implies that the closed field lines, i.e. the so-called dead zone (Mestel & Spruit 1987; Campbell 1997, pp. 251-279), will engulf a significant fraction of the binary system, including the white dwarf (e.g. Figure 1). Since the binary separation in AE Aquarii is $a \sim 1.8 \times 10^{11} (P_{\mathrm{orb}}/10\mathrm{hr})^{2/3}\,\mathrm{cm}$

(Frank, King & Raine 2002, p. 49), the ratio ($(r_{\rm d}/a) \approx 1.65$) implies that the extent of the dead zone in the equatorial plane is approximately $r_{\rm d} \sim 3 \times 10^{11}$ cm. It has been shown (Wynn, King & Horne 1997; Meintjes & de Jager 2000, Meintjes & Venter 2005) that the propeller ejection of material most probably occurs at the distance of closest approach of the stream from the white dwarf, i.e. $R_{\rm prop} \sim 10^{10}\,{\rm cm}$, which is incidentally of the same order as the circularization radius of the stream in the vicinity of the white dwarf (e.g. Meintjes & Venter 2005). This implies that the global mass flow dynamics in the vicinity of the white dwarf will most probably be unaffected by the enveloping magnetosphere of the secondary (e.g. Meintjes & Jurua 2006). The magnetic field profile of the lobe-filling secondary star in the equatorial plane, assuming a dipolar-like field configuration, at radial distances from the secondary star's surface [$R_{2,*} \sim 8 \times 10^{10}(P_{\rm orb}/10\,{\rm hr})\,{\rm cm}$] (e.g. Frank, King & Raine 2002, p. 55), corresponding to the distance of the white dwarf ($r_{\rm wd}$) and as the furthest point of the dead zone ($r_{\rm d}$) respectively , is of the order of

$$\begin{aligned} B_2(r_{\rm wd}) &\approx 320 \left(\frac{B_{\circ,2}}{3650\,{\rm G}}\right)\left(\frac{R_*}{R_2}\right)^3\left(\frac{r}{r_{\rm wd}}\right)^{-3}\,{\rm G} \\ B_2(r_{\rm d}) &\approx 70 \left(\frac{B_{\circ,2}}{3650\,{\rm G}}\right)\left(\frac{R_*}{R_2}\right)^3\left(\frac{r}{r_{\rm d}}\right)^{-3}\,{\rm G}, \end{aligned}$$

where $r_{\rm wd} = a \approx 1.8 \times 10^{11}\,{\rm cm}$ and $r_{\rm d} \sim 3 \times 10^{11}\,{\rm cm}$.

It is proposed that this so-called dead zone of the secondary star consists of closed magnetospheric flux tubes which are centrifugally extended, filled with a tenuous plasma. This conjecture is supported by spectroscopic observations of IP Peg and SS Cyg (Steeghs, Horne, Marsh & Donati 1996), which shows stationary emission sites between the two stars, which has been interpreted as gas-filled magnetospheric flux tubes ($n_{\rm e} \leq 10^{12}\,{\rm cm}^{-3}$) that is centrifugally extended, i.e. so-called sling-shot prominences.

The huge differential velocity between the magnetosphere of the secondary, which corotates with the binary period, and the propeller outflow from the magnetosphere of the white dwarf crossing the dead zone field in the equatorial plane, will induce huge field aligned potentials along the closed magnetospheric flux tubes, which will drive a substantial current (e.g. Haerendel 1994) in a large magnetospheric circuit, resulting in Ohmic heating of the gas trapped in the closed magnetic field lines of the so-called dead zone. The gas temperature in the flux tubes will be determined by energy losses due to heat conduction, expansion and radiation. A more quantitative discussion of this process will be presented in the following sections.

2. PROPELLER OUTFLOW

The mass transfer in AE Aquarii most probably consists of a stream of large diamagnetic blobs (e.g. Wynn, King & Horne 1997). Emission line studies (Eracleous & Horne 1996) infer a mass transfer rate from the secondary to the primary of the order of $\dot{M} = 4 \times 10^{17}$ g s^{-1}. The interaction between this stream and the fast rotating magnetosphere results in a very effective propeller process (Meintjes & de Jager 2000; Meintjes & Venter 2005; Venter & Meintjes 2006). It has been shown (Meintjes & de Jager 2000; Meintjes & Venter 2005) that the magnetohydrodynamic power dissipated on the mass flow from the secondary star is of the order

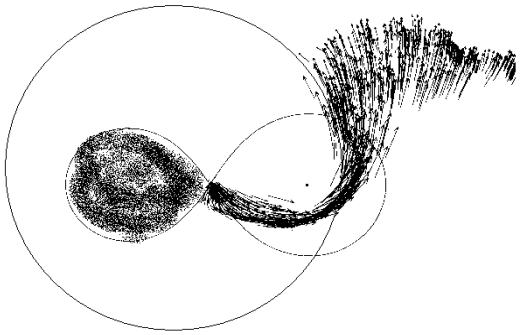

Figure 2: The outflow of the propeller according to Wynn, King & Horne (1997).

$$\begin{aligned} P_{\rm mhd} &= \frac{v_{\rm rel,\perp} B_1^2 A_{\rm stream}}{4\pi} \\ &\sim 10^{34} \left(\frac{v_{\rm rel,\perp}}{2\times10^9\,{\rm cm\ s^{-1}}}\right)\left(\frac{B_1(r_{\rm circ})}{300\,{\rm G}}\right)^2\left(\frac{A_{\rm stream}}{5\times10^{20}\,{\rm cm^2}}\right)\ {\rm erg\ s^{-1}}, \end{aligned} \tag{3.150}$$

where $v_{\rm rel,\perp}$ and $B_1(r_{\rm circ})$ represent the relative velocity between the fast rotating white dwarf magnetosphere and the flow and the white dwarf field in the propeller zone ($r_{\rm circ}$). Here $A_{\rm stream} \sim (2\pi R_{\rm stream})(2\pi R_{\rm circ})$ (Meintjes & Venter 2005) represents the inferred surface area of the outflow in the orbital plane, where $R_{\rm stream}$ and $2\pi R_{\rm circ}$ represent the inferred cross sectional radius and the circumference of the stream passing the white dwarf at the radius of closest approach which is of the order of the circularization radius (Meintjes & Venter 2005). It has been shown (Venter & Meintjes 2006) that the bulk of the material is propelled from the system (see Figure 2) with an azimuthal velocity $\rm v_\phi = v_{esc} \sim 1500$ km s^{-1} (Venter & Meintjes 2006) at the radius of closest approach of the stream. Doppler tomography shows that, further away, the ejected gas leaves the system with velocities of the order of $\rm v_r = 300$ km s^{-1} (Wynn, King & Horne 1997). The dissipated magnetohydrodynamic power is similar to the spin-down power of the white dwarf $P_{\rm sd} \sim 10^{34}$ erg s^{-1} and the reservoir driving the total transient thermal and non-thermal emission in the system with the exception of the contribution from the secondary star which dominates the emission in quiescence.

Confirming the stream parameters for the propeller outflow simulated by Wynn King & Horne (1997), it has been shown (Meintjes & Venter 2005) that the average ram pressure of the propeller outflow at the radius of closest approach of the stream to the white dwarf ($\langle\rho_{\rm flow}\rangle \sim 4\times10^{-10}$ g cm^{-3} ; $v_{\rm flow} = v_{\rm esc} \sim 1.5\times10^8$ cm s^{-1}) is $U_{\rm flow} \approx \langle\rho_{\rm flow}\rangle v_{\rm esc}^2 \sim 5\times10^6$ erg cm^{-3}, which exceeds by an order of magnitude the strongest magnetospheric pressure in the dead zone of the secondary star field that can be encountered by the flow while escaping from the system (e.g. Figure 1), which is approximately $U_{\rm mag} \sim 4\times10^3\,(B/B_2(r_{\rm wd}))^2$ erg cm^{-3}. This implies that the generator, i.e. where the flow crosses the magnetospheric field of the secondary, is a high β-plasma, i.e. $\beta_{\rm gen} = (8\pi\rho v_\phi^2/B_2^2(r_{\rm wd})) >> 1$, resulting in the generation of a significant azimuthal component of the secondary dead-zone field as a result of flux freezing. This scenario is conducive to the generation of a huge field aligned potential difference along the flux tubes connecting the generator to the secondary star, which acts as transmission lines (e.g. Haerendel 1994). For the purpose of the calculations we choose $\langle B_{\rm cor}\rangle \sim 2000$ G to represent the average field strength of the coronal flux tubes connecting the

photosphere and the generator. A necessary condition is that the coronal circuit, constitutes a low-β plasma. It can be shown that these plasma-filled tubes, i.e. the coronal circuit ($n_{\rm p} \leq 10^{12}\,{\rm cm}^{-3}$; $T_{\rm cor} \sim 10^7\,{\rm K}$; $\langle B_{\rm cor}\rangle \sim 2000\,{\rm G}$) constitute a low-$\beta$ plasma, i.e. $\beta_{\rm cir} = (8\pi nkT/\langle B_{\rm cor}\rangle^2) \sim 0.01$.

3. FIELD ALIGNED POTENTIALS

It has been shown (Haerendel 1994) that the differential motion between magnetospheric regions where $\beta_{\rm gen} >> 1$ (generator plasma) and the coronal flux tubes connecting these regions to the secondary star $\beta_{\rm cir} << 1$ (circuit) results in field aligned potentials being induced, which may result in particle acceleration and Ohmic heating of the gas trapped in the magnetospheric circuit. The underlying driver of the potential difference is the breakdown of the force-free condition of coronal field lines of the secondary corotating with the star (e.g Priest & Forbes 2000, pp. 482-486), which is most probably driven by the huge differential motion between the coronal field trapped in the propeller outflow and the footpoints anchored to the secondary star.

The potential difference may be estimated by noting that the differential motion between the magnetic flux tubes and the propeller outflow will result in the induction of a perpendicular field component ($B_\perp = B_\phi$) in the orbital plane, perpendicular to the unperturbed field. The maximum associated induced Poynting flux that will be transmitted along the field towards the secondary star is

$$\epsilon_{||} \quad = \quad J_{||}\Phi_{||} = \frac{(\Delta B_\perp)^2}{64\pi} c_A \tag{3.151}$$

where $J_{||}$ represents the current density along the flux tube and $c_{\rm A} = (\Delta B_\perp/\sqrt{4\pi\rho})$ represents the Alfvén velocity which is determined by $\Delta B_\perp$, i.e. the variation of the induced component of $B_\perp = B_\phi$ along the flux tube, i.e. the transmission line. This is determined by the maximum induced magnetic pitch in the outflow $\phi_{\rm m,max} \sim (B_\phi/B_2(r_{\rm wd}) \sim 10$ (Ghosh & Lamb 1991; Aly & Kuijpers 1991) before the fields reconnect, implying $B_\phi \sim B_{2,{\rm o}} \sim 3600\,{\rm G}$ can be achieved before the fields reconnect. It can be shown that even in the limit where $\phi_{\rm m,max} \rightarrow 10$ and the velocity of the propeller outflow $v_{\rm out} \rightarrow v_{\rm r} = 300$ km s^{-1} (probably outside the Roche lobe of the white dwarf), equipartition $\beta_{\rm gen} \rightarrow 1$ (i.e. $\rho_{\rm flow} v_{\rm out}^2 = B_\phi^2/8\pi$) implies $\rho_{\rm flow} \sim 6 \times 10^{-10}\,{\rm g\ cm}^{-3}$ (i.e. $n_{\rm flow} \sim 10^{14}\,{\rm cm}^{-3}$), which is in perfect agreement with the inferred particle density in the densest parts of the outflow in terms of the propeller model (Eracleous & Horne 1996: Wynn, King & Horne 1997; Meintjes & Venter 2005). This shows that for all $\phi_{\rm m} < \phi_{\rm m,max}$ and $v_{\rm out} \rightarrow v_{\rm r}$ = 300 km s^{-1}, $\beta_{\rm gen} > 1$ is still satisfied, which is required for the production of field aligned currents. It is encouraging that this scenario is in general agreement with the propeller mass flow dynamics inferred from an analysis of the UV emission line data associated with flaring (Eracleous & Horne 1996) as well as Doppler tomography (e.g. Wynn, King & Horne 1997). The factor ($\frac{1}{16}$) represents a conversion efficiency of liberated magnetic energy in the current sheet (e.g. Haerendel 1994). In general the current density is $J_{||} = nev_{\rm d}$ where $v_{\rm d}$ is the drift velocity, but may reach critical values for n $\rightarrow n_{\rm c}$ and $v_{\rm d} \rightarrow c_{\rm crit} = \alpha c_{\rm s}$, with $\alpha \geq 10$ and $c_{\rm s} = \sqrt{kT_{\rm e}/m_{\rm i}}$ representing the ion acoustic velocity (e.g. Haerendel 1994). It can be seen that $c_{\rm crit} \rightarrow \sqrt{(kT/m_{\rm e})}$, i.e. the electron thermal velocity. The current approaching critical values in the current sheet, i.e. $v_{\rm d} \rightarrow c_{\rm crit}$, will result in the triggering of MHD and micro-instabilities, resulting in enhanced resistivity in the gas, which may lead to events of particle acceleration and non-thermal emission (e.g. Hamilton, Lamb & Miller 1993). This provides an interesting alternative mechanism to explain the

continuous non-thermal radio outbursts in AE Aquarii, supplementing models associating the continuous non-thermal flaring with the propeller interaction between the fast rotating white dwarf magnetosphere and the mass transfer flow (Meintjes & de Jager 2000; Meintjes & Venter 2003, 2005; Venter & Meintjes 2006).

From the expression above, the potential difference is

$$\begin{aligned}\Phi_{||} &= \frac{300(\Delta B_{\perp})^3}{64\pi e\alpha n^{3/2}\sqrt{4\pi kT}}\ \text{Volt} \\ &\approx 10^6\left(\frac{\Delta B_{\perp}}{\langle B_{\rm cor}\rangle}\right)^3\left(\frac{\alpha}{1}\right)^{-1}\left(\frac{\langle n\rangle}{5\times10^{11}\,{\rm cm}^{-3}}\right)^{-3/2}\left(\frac{\langle T\rangle}{2\times10^7\,{\rm K}}\right)^{-1/2}\ \text{Volt}\end{aligned} \tag{3.152}$$

where we considered $\Delta B_{\perp} \sim \langle B_{\rm cor}\rangle \sim 2000\,{\rm G}$, which is still within the limit $\phi_{\rm m,max} \leq 10$. For $\alpha < 10$ the potential difference along the flux tubes may result in huge currents and resultant Ohmic heating of the trapped gas in the flux tubes. These potentials may result in an average electric field along the tube, which is of the order of

$$\langle E_{||}\rangle = \frac{\Phi_{||}}{L} \sim 5\times10^{-6}\left(\frac{\Phi_{||}}{10^6\,\text{Volt}}\right)\left(\frac{L}{r_{\rm d}}\right)^{-1}\ \text{Volt cm}^{-1}. \tag{3.153}$$

However, from the expression above it can be seen that for $\langle n\rangle \rightarrow 10^{11}\,{\rm cm}^{-3}$ and $\langle T\rangle \rightarrow 10^7\,{\rm K}$, the field aligned potential $\Phi_{||} \rightarrow 10^6$ Volt as $\alpha \rightarrow 10$, which is still sufficient to accelerate electrons to energies $\gamma \geq 2$ in magnetic fields $B = \langle B_{\rm cor}\rangle \sim 2000\,{\rm G}$. Electrons with these energies can radiate the maximum synchrotron emission at frequencies $\nu_{\rm max} \geq 2\times10^{13}(\gamma/2)^2(B/\langle B_{\rm cor}\rangle)$ Hz. This is perfectly consistent with the observed non-thermal radio-IR spectrum of AE Aquarii (e.g. Abada-Simon et al. 2002; Dubus et al. 2005; Meintjes & Venter 2003; Venter & Meintjes 2006).

The differential motion between the propeller outflow and the frozen-in secondary star dead zone field in the equatorial plane may result in magnetospheric potentials (e.g. Cheng & Ruderman 1989; Ghosh & Lamb 1991) $\Phi_{||} > 10^{12}\,{\rm V}$ as a result of the huge differential motion between propeller ejected gas and the frozen-in coronal dead zone field in the equatorial plane. This may pose an interesting alternative to existing models (de Jager 1994; Meintjes et al. 1994; Meintjes & de Jager 2000) to explain the reported TeV γ-ray emission (Bowden et al. 1992; Meintjes et al. 1992, 1994). A brief discussion is presented below:

It has been shown (Meintjes & de Jager 2000) that the TeV gamma-ray emission that has been reported occasionally (Bowden et al. 1992; Meintjes et al. 1992; 1994), presumably of hadronic origin, i.e. $p + p \rightarrow \pi^{\circ} \rightarrow 2\gamma$, implies a significant reservoir of target material $n_{\rm p} > 10^{13}\,{\rm cm}^{-3}$ (Meintjes & de Jager 2000). Previous studies (e.g. Meintjes et al. 1994; Meintjes & de Jager 2000) showed that the interaction between the fast rotating magnetosphere of the white dwarf and the propeller outflow may result in episodes of particle acceleration, presumably through magnetic reconnection and double layer formation (e.g. Meintjes & de Jager 2000). However, an interesting possibility exists in that the differential motion between the foot points of the coronal field of the secondary, anchored respectively on the secondary star and connected via turbulent diffusion to a large reservoir of orbiting propeller ejected gas in the equatorial plane (e.g. Wynn King & Horne 1997), may also result in episodes of particle acceleration to high energies. This may possibly be the scenario during periods of higher-than-average mass transfer from the secondary star, and hence, propeller action by the white dwarf, which may be the origin of the increased white dwarf spin down reported by Mauche (2006). For example, it has been shown (e.g. Cheng & Ruderman 1989: Ghosh & Lamb 1991) that the differential motion between magnetic flux tubes anchored on a fast rotating neutron star and

a Keplerian disc can result in the generation of huge field aligned potentials which can accelerate particles in the magnetospheres of accreting pulsars (e.g. Cheng & Ruderman 1989). In analogy to the scenario applicable to accreting neutron stars, it is anticipated that the magnetic coupling between the secondary star and a huge reservoir of gas in the vicinity of $r_{\rm d}$ may produce similar potentials. The magnetic field of the secondary corotates with it out to $\rm r_d$ with angular velocity $\Omega_* = 2\pi/\rm P_{orb}(s)$. If part of the ring of gas (reservoir) is magnetically coupled to the secondary inside the dead zone, a circuit may be completed between the star surface and the ring itself. In the ideal MHD limit the electric field $\mathbf{E} = \text{-}\mathbf{v} \times \mathbf{B}/\rm c$. Around a loop(1-8), indicated in Figure 3, the potential difference $\rm V = \int \mathbf{E}.\mathbf{dl} = 0$; i.e. integrating the electric field along the closed loop. The differential motion between the surface of the star and the ring will induce potential drops across the 'gap', which is

$$V = \frac{\rm v_\phi B_{\circ,2} R_2^3}{4c}(r_\circ^{-2} - r^{-2}) + \frac{\Omega_* B_{\circ,2} R_2^2}{2c}\left(\frac{R_2}{r_\circ} - \frac{R_2}{r}\right), \tag{3.154}$$

where $v_\phi \sim v_{\rm esc}$, $r_\circ$ is the inner radius of the gas ring, $\rm B_{\circ,2}$ is the polar strength of the magnetic field and Ω is the angular velocity of the secondary star. Due to the fast fall-off of the $1/\rm r^2$ terms, a ring of small radial dimension may be sufficient to carry a substantial current. The potential difference is of order of magnitude

$$\begin{aligned} V_{\rm max} &= \frac{v_\phi B_{\circ,2} R_2^3}{4c r_\circ^2} \\ &\sim 10^{13}\left(\frac{v_\phi}{v_{\rm esc}}\right)\left(\frac{R}{R_2}\right)^3\left(\frac{B}{B_{\circ,2}}\right)\left(\frac{r_\circ}{r_{\rm d}}\right)^{-2} \text{ Volt} \end{aligned} \tag{3.155}$$

where $B_{\circ,2} \sim 3650\,\rm G$, $R_2 \sim 8 \times 10^{10}\,\rm cm$ and $\rm r_\circ \sim r_d \sim 3 \times 10^{11}\,cm$. It must be stressed that this potential difference will only be generated as long as the footpoints of the flux tubes are frozen into a gas which has a significant differential velocity. It has been shown that anomalous resistivity due to microscopic or MHD instabilities in the current sheet may result in double layer formation and resultant particle acceleration (Hamilton, Lamb & Miller 1993), which may explain the reported transient burst-like VHE gamma ray emission from AE Aquarii (e.g. Bowden C.C.G. et al. 1992; Meintjes et al. 1992, 1994). It must be emphasized that the process described above will probably only occur when there is an abundance of propeller driven outflow in the orbital plane which can distort the slower magnetosphere of the secondary star as it attempt to drag the ejected gas, acting as a circumstellar disc, into corotation. This is also consistent with the observed TeV gamma-ray emission which requires an integrated surface density of at least $\Sigma \sim 50\rm g\ cm^{-2}$ (e.g. Meintjes et al. 1994; Meintjes & de Jager 2000). These results are encouraging, since it shows that the interaction of a dead zone field with the propeller ejected gas in the orbital plane can at least generate field aligned potentials $\Phi_{||} \geq 1$ Mega Volt, which, for $\alpha < 10$ and $\alpha > 10$ will drive both Joule heating and particle acceleration respectively. However, under certain conditions, possibly related to the amount of gas in the orbital plane, potentials of the order of $\Phi_{||} \sim 10$ Tera Volt can be generated, which provides an interesting vehicle to explain the reported TeV γ-ray emission in AE Aquarii.

In the following section a qualitative investigation will be presented of the effect of Ohmic heating of gas trapped in this large magnetospheric circuit.

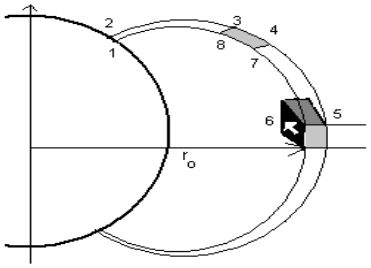

Figure 3: An illustration of a possible circuit connecting a star and a ring of material at radial distance $\mathrm{r_o}$.

4. JOULE HEATING

The effectiveness of current dissipation in the coronal loops heating the gas to X-ray temperatures will depend on the characteristic time scales upon which the MHD generator induce field aligned currents, and then, the time-scale for the conversion of electric energy to thermal energy when a current flows through the magnetically confined plasma.

It can be shown that the upper limit of the characteristic time-scale of the $\beta_{\rm gen} > 1$ generator, i.e. the time-scale upon which the fields get disturbed or dragged for an appreciable length scale (e.g. $\Delta L_{\rm drag} \sim 10^9\,{\rm cm}$) by the outflowing plasma crossing it with a velocity $v_{\rm out} \rightarrow v_{\rm r}$ (e.g. $v_{\rm r} << v_{\rm esc}$), is

$$\begin{aligned} \tau_{\rm gen} &= \frac{\Delta L_{\rm drag}}{v_{\rm out}} \\ &\leq 30 \left(\frac{\Delta L}{\Delta L_{\rm drag}}\right) \left(\frac{v_{\rm out}}{v_{\rm r}}\right)^{-1} {\rm s}. \end{aligned} \tag{3.156}$$

The time-scale of conversion of electric energy to thermal energy in the flux tubes, i.e. the Joule heating time-scale (Holman 1985) is of the order

$$\tau_{\rm j} = \left(\frac{nkT}{\mathbf{J}.\mathbf{E}}\right), \tag{3.157}$$

where n, T, $\mathbf{J}$ and $\mathbf{E}$ represent respectively the particle density, temperature, current density and electric field in the current carrying flux tube. The maximum electric field strength in a plasma for which current dissipation is converted into Joule heating is the so-called Dreicer field (e.g. Benz 1994, p. 217), which is

$$\begin{aligned} E_D &= 6 \times 10^{-8} \left(\frac{n}{T}\right) {\rm Volt\ cm^{-1}} \\ &\sim 10^{-3} \left(\frac{\langle n \rangle}{5 \times 10^{11}\,{\rm cm^{-3}}}\right) \\ &\quad \left(\frac{\langle T \rangle}{2 \times 10^7\,{\rm K}}\right)^{-1} {\rm Volt\ cm^{-1}}. \end{aligned} \tag{3.158}$$

For $E_{||} \geq E_{\rm D}$, impulsive run-away electron acceleration occurs in the plasma (e.g. Benz 1994, p. 216-220), which may manifest in non-thermal emission.

The current density is determined by the ion-acoustic velocity, resulting in a current density

$$J_{||} \sim 7 \times 10^9 (\langle n \rangle / 5 \times 10^{11}\,{\rm cm^{-3}}) (\langle T \rangle / 2 \times 10^7\,{\rm K})^{1/2}\,{\rm statampere\ cm^{-2}}. \tag{3.159}$$

The average Ohmic heating time scale for the trapped magnetospheric gas is then

$$\tau_{\rm J} \sim 10 \left(\frac{\langle n \rangle}{5 \times 10^{11}\,{\rm cm}^{-3}} \right) \left(\frac{T}{2 \times 10^{7}\,{\rm K}} \right) \times \left(\frac{\langle J \rangle}{J_{\rm i}} \right)^{-1} \left(\frac{E}{\langle E_{||} \rangle} \right)^{-1} {\rm s}, \tag{3.160}$$

while $\tau_{\rm J} \rightarrow 0.06$ s for $E \rightarrow E_{\rm D}$. However, the temperature of the diffuse plasma in the loops will eventually be determined by the relative effectiveness of the Joule heating with respect to the respective cooling mechanisms, i.e. bremsstrahlung, cyclotron and synchrotron emission. A qualitative discussion of these processes will be presented in Section 5.

The power dissipated in Ohmic heating in the magnetospheric circuit is therefore $\rm P = J_{||}\ A_J\ \Phi$, where $A_{\rm J}$ and Φ represent the combined surface area of the magnetospheric current sheet and the *Emf* respectively. If the X-ray emission is the result of current dissipation in magnetic flux tubes associated with the dead zone of the secondary star, it can be shown that the dissipated power for $\Phi \rightarrow 0.001\Phi_{||}$ in the coronal circuit with area $A_{\rm J} \sim 10^{20}\,{\rm cm}^2$, particle density $\langle n \rangle \sim 5 \times 10^{11}\,{\rm cm}^{-3}$ and temperature $T \sim 2 \times 10^{7}\,{\rm K}$ (Itoh et al. 2006) is

$$\langle P \rangle \sim 10^{31} \left(\frac{\langle n \rangle}{5 \times 10^{11}\,{\rm cm}^{-3}} \right) \left(\frac{\langle T \rangle}{2 \times 10^{7}\,{\rm K}} \right)^{1/2} \left(\frac{A_{\rm J}}{10^{20}\,{\rm cm}^{-2}} \right) \left(\frac{\Phi}{0.001\Phi_{||}} \right) {\rm erg\ s}^{-1}. \tag{3.161}$$

If Joule dissipation (or Ohmic heating) is to match this power, then $\langle \eta_{\rm eff} \rangle = (\langle J \rangle)^2 V = \langle P \rangle$, where $\langle \eta_{\rm eff} \rangle$, $\langle J \rangle$ and V represents respectively the average effective resistivity in the circuit, the average current density and volume of the X-ray emitting source. If the total X-ray source consists of the hot tenuous gas trapped in the dead zone flux tubes of the secondary star, assuming a total source volume of $V_{\rm source} = V_{\rm x} = A_{\rm J} l \sim 10^{30}\,{\rm cm}^3$ ($V_{\rm x} \sim l_{\rm x}^3$), the effective resistivity of the circuit is

$$\begin{aligned} \langle \eta_{\rm eff} \rangle &= \frac{\langle P \rangle}{\langle J \rangle^2 V} \\ &\sim 10^{-19} \left(\frac{\langle P \rangle}{10^{31}\,{\rm erg\ s}^{-1}} \right) \left(\frac{\langle J \rangle}{J_{||}} \right)^{-2} \left(\frac{V}{V_{\rm x}} \right)^{-1} {\rm e.s.u.} \end{aligned} \tag{3.162}$$

It can be shown that the resistivity of a plasma with similar properties as the X-ray emitting coronal plasma of AE Aquarii, i.e. a plasma of density $n \sim 10^{11}\,{\rm cm}^{-3}$ and temperature $T \leq 5 \times 10^{7}\,{\rm K}$ (Spitzer & Harm 1953; e.g. Lang 1980, p. 228), is

$$\begin{aligned} \eta &= 1.2 \times 10^{-8} \left(\frac{\ln \Lambda}{T^{3/2}} \right) \\ &\sim 10^{-19} \left(\frac{\ln \Lambda}{20} \right) \left(\frac{T}{5 \times 10^{7}\,{\rm K}} \right)^{-3/2} {\rm e.s.u}, \end{aligned} \tag{3.163}$$

where $\ln \Lambda \approx \ln(1.3 \times 10^4 (T^{3/2}/n_{\rm e}^{1/2})) \sim 20$ (e.g. Lang 1980, p. 224). It has been shown earlier that under circumstances where $\alpha \geq 10$, e.g. $v_{\rm d} \rightarrow c_{\rm crit}$, microinstabilities may be generated locally in the circuit, significantly enhancing the local effective resistivity. This will result in double layer formation where $E_{||} \geq E_{\rm D}$, resulting in a sudden impulsive run-away acceleration (e.g. Benz 1994, pp. 216-220) of the thermal electron population in that region to energies $\epsilon_e \sim 2$MeV. The total non-thermal radio-IR synchrotron emission from AE Aquarii, with $L \leq 10^{31}\,{\rm erg\ s}^{-1}$ (e.g. Meintjes & Venter 2003), can then be explained in terms of the superposition of non-thermal flashes occuring in the total magnetospheric circuit.

This will be consistent with the nature of the non-thermal radio-IR emission in AE Aquarii, which can readily be explained as a superposition of synchrotron emitting flares (e.g. Bastian, Dulk & Chanmugam 1988).

5. THE X-RAY EMISSION

From a global energy perspective in the magnetospheric circuits it has been shown that current dissipation in closed coronal flux tubes associated with the dead zone of the secondary star can comfortably power the observed unpulsed X-ray emission in AE Aquarii. It has also been shown that currents can be induced over sufficiently short time-scales, and dissipation in the coronal flux tubes can heat a thermal plasma with density $n \sim 10^{11}\,\mathrm{cm}^{-3}$ to temperatures $T \rightarrow 10^7\,\mathrm{K}$ with time scales between $\tau_\mathrm{J} = 0.05$-5 s. However, the temperature of the plasma will be determined by the effectiveness of the various cooling mechanisms in the plasma, i.e. thermal bremsstrahlung, cyclotron radiation, synchrotron radiation and possibly also thermal conduction. The global thermal balance in a flux tube will be determined by the following conservation law

$$\dot{\epsilon}_\mathrm{J} - \frac{F}{l_\mathrm{x}} - \dot{\epsilon}_\mathrm{rad} = 0, \tag{3.164}$$

where $\dot{\epsilon}_\mathrm{J} = \mathbf{J}.\mathbf{E}$ represents the Joule heating rate, $\frac{F}{l_\mathrm{x}}$ the order of magnitude of the heat loss rate per unit volume of gas due to thermal conduction and $\dot{\epsilon}_\mathrm{rad}$ the radiative losses. The energy dissipated in the current sheet, or dissipative region (DR) results in plasma heating, the effectiveness of which is determined by the thermal conduction (F = -$\kappa\frac{dT}{dx}$) and the respective radiative loss mechanisms. It has been shown that the coefficient of thermal conductivity for a fully ionized hydrogen plasma (Z=1) (Cuperman & Metzler 1973, Spitzer 1962), is

$$\kappa = 2 \times 10^{-4} \frac{T^{5/2}}{Z^4 \ln\Lambda}\,\mathrm{erg\ s^{-1}cm^{-1}K^{-1}} \tag{3.165}$$

where we assume $Z \approx 1$ and $\ln\Lambda \sim 20$ (e.g. Lang 1980, p 224). However, Spitzer (1962) also showed that the coefficient for thermal conductivity perpendicular to a magnetic field line is

$$\kappa_\perp \;=\; 1.5 \times 10^{-17} \frac{A_\mathrm{i}^{1/2} Z^2 n_i^2 \ln\Lambda}{T^{1/2} B^2}\,\mathrm{erg\ s^{-1}cm^{-1}K^{-1}}. \tag{3.166}$$

with A_i representing the mean molecular weight of the ions. It can be shown that

$$\begin{aligned} \frac{\kappa}{\kappa_\perp} &\approx 10^{13} \frac{T^3 B^2}{(n_\mathrm{i} \ln\Lambda)^2} \\ &\sim 10^{15} \left(\frac{T_\mathrm{e}}{2\times10^7\,\mathrm{K}}\right)^3 \left(\frac{\langle B\rangle}{1000\,\mathrm{G}}\right)^2 \times \\ &\quad \left(\frac{n_i}{5\times10^{11}\,\mathrm{cm^{-3}}}\right)^{-2} \left(\frac{\ln\Lambda}{20}\right)^{-2} \end{aligned} \tag{3.167}$$

for the relevant parameters. This implies that heat conduction will most likely occur parallel to the field, unless an extremely (probably unrealistic) steep temperature gradient exists perpendicular to the current sheet in the flux tube. The maximum heat flux will occur in the limit where $\nabla.\mathbf{F} \rightarrow 0$ at which point effective heat conduction is limited by generated ion-acoustic turbulence in the sheet (e.g. Galeev, Rosner

& Vaiana 1979). This will most probably result in anomalous resistivity in the plasma, resulting in particle acceleration instead of Ohmic heating of the plasma.

It has been shown (Galeev, Rosner & Vaiana 1979) that the respective radiative cooling rates due to the processes mentioned above are

$$\dot{\epsilon}_{\rm br} \approx 1.3 \times 10^5 P^2 T_{\rm e}^{-3/2} \,{\rm erg\ cm^{-3} s^{-1}} \tag{3.168}$$

$$\dot{\epsilon}_{\rm cyc} \approx 3.9 \times 10^{-9} P B^2 \,{\rm erg\ cm^{-3} s^{-1}} \tag{3.169}$$

$$\dot{\epsilon}_{\rm syn} \approx 2.7 \times 10^{-18} P T_{\rm e} B^2 \,{\rm erg\ cm^{-3} s^{-1}}, \tag{3.170}$$

where $P = nkT_{\rm e}$. From the equations above it can be seen that for a thermal plasma with $T_{\rm e} < 10^9\,{\rm K}$ cyclotron radiation will dominate synchrotron radiation. It has been shown that a tenuous magnetospheric plasma ($n \sim 5 \times 10^{11}\,{\rm cm^{-3}}$) with electron temperature $T_{\rm e} \sim 2 \times 10^7\,{\rm K}$ trapped in magnetospheric fields $\langle B_{\rm cor} \rangle \sim 2000$ G, constitutes a very low beta plasma, i.e. $\beta \sim 0.01$. For such a low β plasma it can be shown that

$$\begin{aligned} \frac{\dot{\epsilon}_{\rm br}}{\dot{\epsilon}_{\rm cyc}} &= 2 \times 10^{-4} \beta n_{\rm e} T^{-1/2} \\ &\sim 200 \left(\frac{\beta}{0.01} \right) \left(\frac{n_{\rm e}}{5 \times 10^{11}\,{\rm cm^{-3}}} \right) \left(\frac{T_{\rm e}}{2 \times 10^7\,{\rm K}} \right)^{-1/2}, \end{aligned} \tag{3.171}$$

which implies that bremsstrahlung radiation is by far the dominant radiation loss mechanism for the parameters presented. This also explains the dominant $T_{\rm e} \sim 1$ keV thermal bremsstrahlung component of the X-ray spectrum in AE Aquarii (e.g. Itoh et al. 2006). The relative effectiveness of bremsstrahlung radiation with respect to thermal heat conduction results in

$$\frac{F/l_{\rm x}}{\dot{\epsilon}_{\rm br}} \sim 1 \left(\frac{T_{\rm e}}{2 \times 10^7\,{\rm K}} \right)^3 \left(\frac{l_{\rm x}}{10^{10}\,{\rm cm}} \right)^{-2} \left(\frac{n_{\rm e}}{5 \times 10^{11}\,{\rm cm^3}} \right)^{-2}. \tag{3.172}$$

This shows that thermal bremsstrahlung and thermal conduction along a flux tube may contribute equally to dissipate electric energy. It can be shown that thermal bremsstrahlung can dissipate electric energy in a total volume $V = V_{\rm x} \sim l_{\rm x}^3$ (e.g. $l_{\rm x} = (2-3) \times 10^{10}\,{\rm cm}$) at a rate

$$\begin{aligned} L_{\rm br} &= \dot{\epsilon}_{\rm br} V \\ &\sim 10^{31} \left(\frac{n_{\rm e}}{5 \times 10^{11}\,{\rm cm^{-3}}} \right)^2 \left(\frac{T_{\rm e}}{2 \times 10^7\,{\rm K}} \right)^{1/2} \left(\frac{V}{V_{\rm x}} \right) \,{\rm erg\ s^{-1}}, \end{aligned} \tag{3.173}$$

which is consistent with the observed unpulsed X-ray luminosity of AE Aquarii. These results are promising since it shows that current dissipation in coronal flux tubes can, with a rather modest choice of parameters, drive a total thermal bremsstrahlung dominated unpulsed X-ray luminosity $L_{\rm x} \sim 10^{31}\,{\rm erg\ s^{-1}}$.

These results also explain the resemblance of the x-ray spectrum of AE Aquarii with stars exhibiting coronal activity, e.g. the RS CVn stars, where Joule dissipation of current possibly also contributes significantly to the heating of the plasma trapped in the coronal flux tubes. It has to be emphasized that the coronal activity driving the quiescent unpulsed X-ray emission in AE Aquarii is pumped by the propeller outflow of material from the fast rotating white dwarf, with approximately ~ 0.1 % of the spin-down power dissipated in the coronal circuit.

6. DISCUSSION

It has been shown that the coronal loops of the secondary star may provide a magnetic corona that will be pumped magnetohydrodynamically by the propeller outflow crossing the dead zone field in the equatorial plane. The dissipation of MHD power at a rate of $P_{\rm mhd} \sim 10^{34}\,{\rm erg\ s^{-1}}$ provides a generator for the induction of field aligned currents flowing in the magnetospheric flux tubes connecting the generator with the star. These flux tubes may serve as transmission lines for a magnetospheric circuit. The dissipative region, i.e. the part of the circuit between the generator and the photosphere of the secondary star, is a low β-plasma (i.e. $\beta \sim 0.01$). It has been shown that Ohmic dissipation of current in a tenuous plasma with density $n \sim 10^{11}\,{\rm cm^{-3}}$ can result in an Ohmic heating time scale $\tau_{\rm J} \rightarrow$ 0.05-10 s, with a resultant integrated luminosity $\langle P \rangle \sim 10^{31}\,{\rm erg\ s^{-1}}$ for a very moderate selection of parameters. This power also infers an effective magnetospheric resistivity $\eta_{\rm eff} \sim 10^{-19}$ e.s.u., which corresponds to the so-called *Spitzer* resistivity of a fully ionized plasma. It has been shown that the dominant cooling mechanism, e.g. thermal bremsstrahlung, combined with thermal conduction, will probably be the dominant mechanisms dissipating electric energy in the circuit. This will result in the tenuous plasma ($n_{\rm e} \sim {\rm few} \times 10^{11}\,{\rm cm^{-3}}$; $T_{\rm e} \sim {\rm few} \times 10^{7}\,{\rm K}$) trapped in this coronal circuit driving the bremsstrahlung dominated X-ray luminosity being of the order of $L_{\rm x} \sim 10^{31}\,{\rm erg\ s^{-1}}$.

Another positive aspect of the magnetospheric X-ray source in AE Aquarii is that local instabilities in the current can result in anomalous resistivity which increases $\langle E_{||} \rangle > E_{\rm D}$, i.e the so-called Dreicer field, resulting in a fast impulsive acceleration of the whole thermal electron population in the plasma. This is an attractive alternative mechanism to explain the continuous non-thermal outbursts in AE Aquarii, which exhibits the properties of a superposition of synchrotron emitting flares. It has also been shown that the differential rotation between the secondary star field and the propeller outflow during periods of enhanced mass outflow may result in the generation of field aligned potentials which can reach $\Phi_{||} \sim 10^{13}\,{\rm Volt}$. Potentials of this magnitude will probably be associated with double layer formation and flashes of particle acceleration and associated TeV γ-ray emission. This provides an interesting mechanism to explain the burst-like VHE γ-ray emission reported contemporaneously by two independent groups (Bowden et al. 1992; Meintjes et al. 1992;1994).

ACKNOWLEDGMENTS

The authors whish to thank an anonymous referee for his critical assessment of the paper, and his valuable suggestions leading to a much improved paper.

Chapter 4

Conclusion

AE Aquarii is a binary star consisting of two dwarf stars with an orbit that could fit into the Sun, but it displays emission from radio to TeV γ-rays, including pulsed and highly variable unpulsed emission at different frequencies. The red dwarf secondary star contributes to the system's luminosity in the infra-red to visible frequency range. The contribution from the surface of the white dwarf is dominated by the 33 s pulsations observed in the optical, UV and X-ray light and is attributed to a small amount of accretion onto the magnetic poles of the star. The observed spin-down of the white dwarf and the low luminosity of the pulsed emission, suggests that the mass transfer flow from the secondary star is ejected from the system, carrying with it the angular momentum lost by the spinning white dwarf. The spin-down power mainly drives the mechanical escape of the mass flow that is propelled outward by its interaction with the white dwarf's corotating magnetosphere. But in this study we have shown that this large energy reservoir may also be responsible for emission in the system other than that directly connected to either of the two stars in the system. The emission is related to the mass outflow and the consequences of this flow interacting with the magnetic field of the secondary star.

Radio emission from AE Aqr has been detected from the low GHz upto the mid-IR frequencies and is attributed to mildly relativistic electrons spiraling around magnetic field lines and emitting synchrotron emission. A non-thermal particle acceleration mechanism is assumed to be responsible for energizing the synchrotron electrons. The radio data show no periodicity, but is highly variable and continuous in nature. This observation makes the continuous KH driven propeller action a prime candidate to drive the non-thermal radio-to-mid-IR emission. The KH mixing of the magnetospheric field and the stream provide a natural mechanism of creating magnetized bubbles of accelerated electrons due to magnetic reconnection, which releases both magnetic energy and the bubbles from the stream. The bubbles can then leave the Roche lobe of the white dwarf and, as they expand, emit synchrotron emission.

Large optical flares are a further peculiar signature of AE Aqr. These flares are also aperiodic, but observations indicate that they originate in a region of velocity space compatible with a propeller outflow. The driving mechanism for the flares may be connected to the KH driven propeller, which pumps turbulent energy into the outflow. The turbulent energy cascades to dissipative scales over time scales that allow the outflow to leave the Roche lobe before being heated and producing the optical flares.

Observations suggest that the unpulsed X-ray component is not dependent on orbital phase and that

The multiple facets of AE Aqr.

Variable radio emission

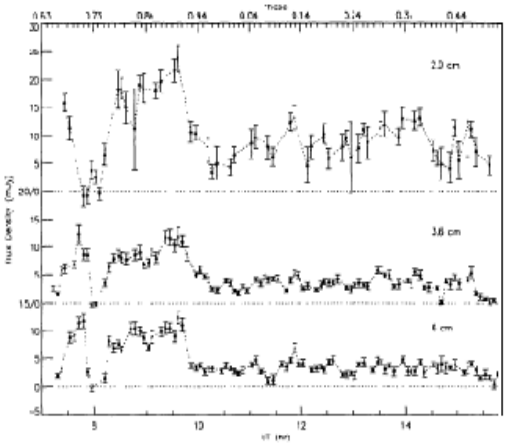

Optical flares

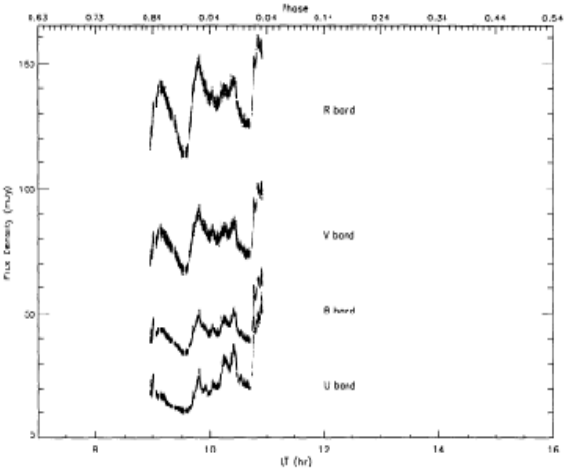

KH instability

Manetospheric propeller

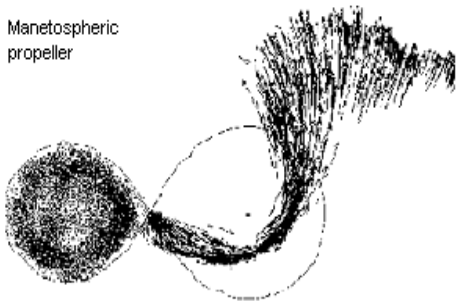

Outflow: radio-IR and optical flares

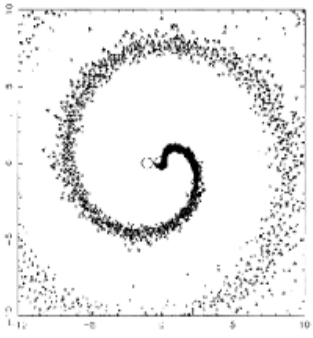

Red dwarf field: X-ray emission

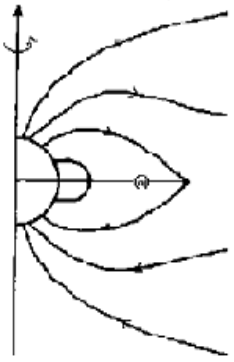

the source is comparable in size to the binary. The creation of such a large source at X-ray temperatures T $>$ 10^7 K, can also be the result of the propeller action in the system. However, here the magnetosphere or dead zone field of the red dwarf secondary interacts with the propeller mass outflow. The outflow disturbs the dead zone field, which envelopes the white dwarf. The disruption of the field induces potential differences and current dissipation heats plasma to X-ray emitting temperatures. The density and size of the volume of plasma heated in this manner, is compatible with the parameters inferred from the observations.

AE Aqr is currently a totally unique, multi-wavelength astronomical object. The highly efficient propeller, which may drive the highly variable and continuous radio emission, optical flares, X-ray and γ-ray emission, is a fascinating astrophysical process that begs investigation using a multi-faceted, multi-wavelength approach.

Future study

Future study of AE Aqr should investigate the dependence of the spin-down rate $\dot{P}_{spin}$, on the mass transfer rate $\dot{M}_2$. This would need to include a more detailed description of the interaction between the mass flow and the magnetospheric propeller and its influence on the efficiency of the angular momentum transfer that drives the outflow. At the current mass transfer rate, the propeller is highly efficient and virtually all mass transfer is ejected, carrying away the angular momentum of the white dwarf and characterizing the current spin-down phase. As reported by Mauche (2006), the spin-down rate of the primary star does appear to change over observable time scales and monitoring of the spin period is therefore a crucial endeavor. Future observations at MHz frequencies may also provide evidence for the proposed radio remnant surrounding AE Aqr.

Appendix A

The VDL model

The Van der Laan(1963) model parameterizes a single synchrotron flare from an ensemble of electrons and gives the flux density as

$$S(\nu) = k_1 B^{-1/2} \theta^2 \nu^{5/2} \ , [\nu \ll \nu_m] \tag{A.1}$$

and

$$S(\nu) = k_2 C B^{(\delta+1)/2} \theta^3 \nu^{-(\delta-1)/2} \ , [\nu \ll \nu_m] \tag{A.2}$$

where k_1 and k_2 are constants and C is the coefficient in the energy distribution

$$N(E)dE = CE^{-\delta}dE.$$

Here it can be seen that a synchrotron spectrum has distinctive power law indexes associated with the two frequency ranges and a turning point where the flux is a maximum.
The following is assumed :

$$\begin{aligned} \mathrm{B} &= \mathrm{B}_\circ (r/r_\circ)^{-2} && \text{(A.3)} \\ \mathrm{E} &= \mathrm{E}_\circ (r/r_\circ)^{-1} \ , [\text{for a single particle}] && \text{(A.4)} \\ \text{and} & && \text{(A.5)} \\ \theta &= \theta_\circ (r/r_\circ) && \text{(A.6)} \end{aligned}$$

indicating that the magnetic flux is conserved, the gas cools adiabatically and the angular diameter of the source varies with r. The ratio $r/r_\circ$ is also written as ρ. The source function of synchrotron emission is

$$B_\nu \propto \nu^{5/2}$$

and then the intensity of the source is

$$S_\nu = B_\nu (1 - \exp^{-\tau_\nu}) \tag{A.7}$$

The amount of $B_\nu \exp^{-\tau_\nu}$ is absorbed along the line of sight in the source.
Thus

$$S_\nu \propto \nu^{5/2} (1 - \exp^{-\tau_\nu}) \tag{A.8}$$

and then we have

$$S(\nu_m, \rho) \propto \nu_m^{5/2}(1 - \exp^{-\tau_{\nu_m}}) \tag{A.9}$$

This then gives

$$\frac{S(\nu,\rho)}{S(\nu_m,\rho)} = \left(\frac{\nu}{\nu_m}\right)^{5/2}\left[\frac{1-\exp^{-\tau_\nu}}{1-\exp^{-\tau_{\nu_m}}}\right]$$

$$S(\nu,\rho) = S_{m\circ}\rho^{\frac{-(7\delta+3)}{(\delta+4)}}\left[\frac{\nu}{\nu_{m\circ}\rho^{-(4\delta+6)/(\delta+4)}}\right]^{5/2}\left[\frac{1-\exp^{-\tau_\nu}}{1-\exp^{-\tau_{\nu_m}}}\right]$$

and this reduces to

$$S(\nu,\rho) = S_{m\circ}\left(\frac{\nu}{\nu_{m\circ}}\right)^{5/2}\rho^3\left[\frac{1-\exp^{-\tau_\nu}}{1-\exp^{-\tau_{\nu_m}}}\right] \tag{A.10}$$

Now the optical depth τ_ν depends on the absorption coefficient k_ν as follows(Pacholczyk 1970)

$$\begin{aligned}\tau_\nu &= \int_0^s k_\nu dl \\ &= \frac{c_s(\delta)sC\mathrm{B}^{(\delta+2)/2}}{(2c_1)^{-(\delta+4)/2}}\nu^{-(\delta+4)/2}\end{aligned}$$

and therefore

$$\frac{\tau_\nu}{\tau_{\nu_m}} = \frac{\nu^{-(\delta+4)/2}}{\nu_m^{-(\delta+4)/2}} \tag{A.11}$$

and then also

$$\begin{aligned}\tau_\nu &= \tau_{\nu_m}\left(\frac{\nu}{\nu_m}\right)^{-(\delta+4)/2} \\ &= \tau_{\nu_m}\left(\frac{\nu}{\nu_{m\circ}}\right)^{-(\delta+4)/2}\rho^{-(2\delta+3)}\end{aligned} \tag{A.12}$$

Therefore the flux density is given by(VDL 1963, BDC 1988)

$$S(\nu,\rho) = S_{m\circ}\left(\frac{\nu}{\nu_{m\circ}}\right)^{5/2}\rho^3\frac{1-\exp^{-\tau_{\nu_m}\left(\frac{\nu}{\nu_{m\circ}}\right)^{-(\delta+4)/2}\rho^{-(2\delta+3)}}}{1-\exp^{-\tau_{\nu_m}}} \tag{A.13}$$

where $S_{m\circ}$ is the maximum flux density at initial time $\mathrm{t}_\circ$, $\nu_{m\circ}$ id the frequency at this maximum and τ_m is the optical depth at this frequency. The optical depth τ_ν, is frequency dependent but most of the emission is emitted for $\tau_\nu \approx \tau_m \approx 1$.

Now if $\nu \ll \nu_m$: $\frac{\nu}{\nu_m} \to 0$ and the exponential term in the numerator of the above equation vanishes. Thus

$$S(\nu,\rho) = S(\nu)\rho^3 \ \ [\nu \ll \nu_m] \tag{A.14}$$

Then if $\nu \gg \nu_m$ or $\nu \gg \nu_{m\circ}$:

$$\tau_m(\nu/\nu_{m\circ})^{-(\delta+4)/2}\rho^{-2\delta+3)}$$

becomes small and thus we can use $\exp^x = 1 + x$ for small x.
Therfore

$$\begin{aligned} S(\nu,\rho) &= S_{m\circ}\rho^3 \frac{\tau_m(\nu/\nu_{m\circ})^{-(\delta+4)/2}\rho^{-2\delta+3)}}{1-\exp(-\tau_m)} \\ &= S(\nu)\rho^{-2\delta} \quad , \quad [\nu \gg \nu_m] \end{aligned} \tag{A.15}$$

VDL(1963) gives the relation of the radius to the expansion time as

$$\rho = \left(1 + \frac{tv_\circ}{\beta r_\circ}\right)^\beta \tag{A.16}$$

with $v_\circ$ the initial velocity of expansion and β a constant dependent on the medium the cloud is expanding into($\beta = 1$ for constant expansion velocity, $\beta = 2/5$, asymptotically in a uniform medium and $\beta = 2/3$, asymptotically, into a stellar wind(Woodsworth & Hughes 1976)).

Now initially(for small t) we have that

$$\rho \approx \left(1 + \frac{(t=0)v_\circ}{\beta r_\circ}\right)^\beta + \beta\left(1 + \frac{(t=0)v_\circ}{\beta r_\circ}\right)^{\beta-1} \frac{v_\circ}{\beta r_\circ} t$$

and thus

$$\rho \propto t \Rightarrow \rho^3 \propto t^3$$

Also at later times(large t) :

$$\rho \approx \left(\frac{\mathrm{t}v_\circ}{\beta r_\circ}\right)^\beta \Rightarrow \rho \propto \mathrm{t}^\beta$$

and thus $\rho^{-2\delta} \propto \mathrm{t}^{-2\beta\delta}$.

Therefore we see that the flux density for a frequency $\nu < \nu_{m\circ}$, initially increases approximately like $\rho^3 \propto t^3$ to reach a maximum when $\tau_\nu = \tau_m \approx 1$.
After this the flux diminishes like $\rho^{-2\delta} \propto \mathrm{t}^{-2\beta\delta}$ in an optically thin medium.

The evolution of such a synchrotron source is important when modelling the evolution of the emission from a blob-like source with time.

The frequency ν_m depends on radius as

$$\nu_m(\rho) = \nu_{m\circ}\rho^{-(4\delta+6)/(\delta+4)} \tag{A.17}$$

This means that $\nu_m \leq \nu_{m\circ}$.

Eq. A.15 and Eq. A.17 also give :

$$\begin{aligned} S(\nu=\nu_m,\rho) &= S_\circ(\nu=\nu_m)\rho^{-2\delta} \\ &= k_1 C \mathrm{B}_\circ^{(\delta+1)/2}\theta_\circ^3 \nu_m^{-(\delta-1)/2}\rho^{-2\delta} \\ &= k_1 C \mathrm{B}_\circ^{(\delta+1)/2}\theta_\circ^3 [\nu_{m\circ}\rho^{-(4\delta+6)/(\delta+4)}]^{-(\delta-1)/2}\rho^{-2\delta} \\ &= S_\circ(\nu=\nu_{m\circ})\rho^{\frac{-(7\delta+3)}{(\delta+4)}} \end{aligned} \tag{A.18}$$

The frequency of maximum flux is given by Dulk (1985) as

$$\nu_{m\circ} \approx 2.8\times 10^7 \left(\frac{\mathrm{E}_c}{1MeV}\right)^{(2\delta-2)/(\delta+4)} \left(\frac{\delta-1}{\delta+2} N_\circ r_{11}\right)^{2/(\delta+4)} \mathrm{B}_\circ^{(\delta+2)/(\delta+4)} \tag{A.19}$$

An average value of $< \theta > = 60^\circ$ is assumed for the angle between the magnetic field and the line of sight. Define the source radius as r_{ν_m}. Then from Eq. A.17 we have

$$r_{\nu_m} = r_\circ \left(\frac{\nu_m}{\nu_{m\circ}} \right)^{-(\delta+4)/(4\delta+6)} \tag{A.20}$$

The initial parameters of a synchrotron blob is taken as $\mathrm{r}_\circ$, $\mathrm{B}_\circ$ and $\mathrm{N}_\circ$.
$\nu_{m\circ}$ can therefore be calculated from Eq. A.19 for assumed values of E_c, δ and $\mathrm{N}_\circ$.

The brightness temperature of the source is expressed as

$$\mathrm{T}_B = \frac{\mathrm{S}_\nu \mathrm{c}^2 D^2}{2\mathrm{k}\nu^2 \pi r_s^2} \tag{A.21}$$

πr_s^2 is the projected source area, D is the distance to the source and k is Boltzmann's constant.

Now we get

$$S_{\nu_m} = 2\mathrm{k}\mathrm{T}_B \frac{\nu_m^2}{\mathrm{c}^2} \frac{\pi r_{\nu_m}^2}{D^2} \tag{A.22}$$

We consider the case $\tau_\nu \approx 1$ and then $\mathrm{T}_B \approx \mathrm{T}_{eff}$.
Then this gives(Dulk 1985)

$$\mathrm{T}_{eff} \approx 2.8 \times 10^9 \times 2^{-\delta/2} \left(\frac{\nu}{\nu_B} \right)^{1/2}. \tag{A.23}$$

$\nu_B = \mathrm{eB}/2\pi \mathrm{m}_e \mathrm{c}$ is the gyrofrequency.

The maximum flux density (zero expansion, $\rho = 1$) can be estimated from Dulk (1985), which is summarized in Bastian, Dulk & Chanmugam (1988).

For single flare events we have

$$S_{m,\circ} = A_1 \left[A_2 \frac{\delta - 1}{\delta + 2} \left(\frac{\mathrm{E}_c}{1MeV} \right)^{\delta-1} \mathrm{N}_\circ \right]^{3/(2\delta+3)} [r_\circ^{(4\delta+9)/3} \mathrm{B}_\circ^{(\delta+3)/6}]^{3/(2\delta+3)} \nu_m^{(7\delta+3)/(4\delta+6)} \tag{A.24}$$

with $A_1 = 3.3 \times 10^6 \times 2^{-\delta/2} \pi k / c^2 D^2$, $A_2 = (2.8 \times 10^7)^{(\delta+4)/2} / 10^{11}$ and

$$\mathrm{N}_\circ = A_3 \left[\frac{\delta + 2}{\delta - 1} \left(\frac{\mathrm{E}_c}{1MeV} \right)^{-(\delta-1)} \frac{\mathrm{B}_\circ^{2\delta+9}}{r_\circ} \right]^{1/(\delta+5)} \tag{A.25}$$

where $\mathrm{N}_\circ$ represents the electron number density assuming equipartition between the magnetic and relativistic electron energy densities or

$$\frac{\mathrm{B}_\circ^2}{8\pi} = \mathrm{N}_\circ \mathrm{k} \mathrm{T}_{eff}.$$

The constant $A_3 = [3.2 \times 10^4 \times 10^{\delta/2} (10^{11})^{1/(\delta+4)}]^{(\delta+4)/(\delta+5)}$.

By substituting Eq. A19 , Eq. A24 and Eq. A25 into Eq. A13, the expected flux densities of individual flares can be calculated.

Bibliography

[1] Abada-Simon M., Lecacheux A., Bookbinder J., Dulk G.A., 1993, ApJ, 406, 692

[2] Abada-Simon M., Bastian T.S., Horne K., Bookbinder J.A., 1995a, in Buckley D.A.H., Warner B., eds, ASP conf. Ser. Vol 85, Proc. Cape Workshop on Magnetic Cataclysmic Variables. Astron Soc. Pac., San Francisco, p. 355

[3] Abada-Simon M., Bastian T.S., Bookbinder A.J., 1995b, in Lecture Notes in Physics, 454, 268

[4] Abada-Simon M., Mouchet M., Aubier M., Barrett P., de Jager O.C., de Martino D., Ramsay G., 1999, in ESA SP-427, Proc. The Universe as seen by *ISO*. ESA, Paris, p.257

[5] Abada-Simon, M. et al. 2002, SF2A Semaine de lAstrophysique Francaise, Paris, June 24-29, 2002, Eds.:F. Combes and D. Barret, EdP-Sciences Conference Series, p. 497

[6] Aly J.J., Kuijpers J., 1990, A&A, 227, 473

[7] Arons J., Lea S.M., 1976, ApJ, 207, 914

[8] Arons J., Lea S.M., 1980, ApJ, 235, 1016

[9] Bastian T.S., Beasley A.J., Bookbinder J.A., 1996, ApJ, 461, 1016

[10] Bastian T.S., Dulk G.A., Chanmugam G., 1988, ApJ, 324, 431

[11] Beardmore A.P., Osborne J.P., 1997, MNRAS, 290, 145

[12] Beasley A.J., Bastian T.S., Ball L., Wu K., 1994, ApJ, 108, 2207

[13] Beskrovnaya N.G., Ikhsanov N.R., Bruch A., Shakhovskoy N.M., 1995, in Buckley D.A.H.Warner B., eds, ASP Conf. Ser. Vol. 85, Proc. Cape Workshop on Magnetic Cataclysmic Variables. Astron. Soc. Pac. San Fransisco, p. 364

[14] Beuermann K., 1988, in Polarized radiation of circumstellar origin, eds G.V. Coyne, S.J. Magathaës, A.F.J. Moffat, R.E. Schulle-Ladbeck, S. Topia, D.T. Wickramasinghe, Vatican Observatory, Vatican City, p. 125

[15] Biskamp, D., 2003, Magnetohydrodynamic Turbulence, Cambridge University Press, Cambridge, pp.33-65, 47, 57-64

[16] Blandford R.D., Payne D.G., 1982, MNRAS, 199, 883

[17] Bookbinder J.A., Lamb D.Q., 1987, ApJ, 323, L131

[18] Bowden et al. 1992, Astropart. Phys, 1, 47

[19] Bruch A., 1991, A&A, 251, 59

[20] Burnard D.J., Lea S.M., Arons J., 1983, ApJ, 266, 175

[21] Campbell C.G., 1997, Magnetohydrodynamics in binary stars, Kluwer Academic Publishers, Chpt. 12

[22] Chandrasekhar, S. 1961, Hydrodynamic & Hydromagnetic Stability, (Oxford University Press:New York), pp. 481-514

[23] Chanmugam G., Frank J., 1987, ApJ, 320, 746

[24] Chanmugam G., Ray A., 1984, ApJ, 285, 252

[25] Chapman, S., Ferraro, V. C. A., 1931, MNRAS, 89, 470

[26] Choi, C-S., Dotani, T., Agrawal, P.C., 1999, ApJ, 525, 399

[27] Choi C-S., Dotani T., 2006, ApJ, 646, 1149

[28] Choudhuri A.R., 1998, The physics of fluids and plasmas, Cambridge Univ Press, Cambridge, pp. 141-148, 158-175, 165-169

[29] Clayton K.L., Osborne J.P., 1995, in Buckley D.A.H., Warner B., eds, ASP conf. Ser. Vol 85, Proc. Cape Workshop on Magnetic Cataclysmic Variables. Astron Soc. Pac., San Francisco, p. 379

[30] Cropper M., 1986, MNRAS, 222, 225

[31] Cuperman S., Metzler N., 1973, ApJ, 182, 961

[32] Cromwell D., McQuillan P., Brown J.C., 1988, SoPh, 115, 289

[33] Davidson K., Ostriker J.P., 1973, ApJ, 179, 585

[34] de Jager O.C., 1994, ApJS, 90, 775

[35] de Jager O.C., 1995, ASPC, 85, 373

[36] de Jager O.C., Meintjes P.J., O' Donoghue D., Robinson A.L., 1994, MNRAS, 267, 577

[37] Dubus G., Campbell R., Kern B., Taam R.E., Spruit H.C., 2004, MNRAS, 349, 869

[38] Dulk G.A., 1985, ARA&A, 23, 169

[39] Drell S.D., Foley H.M., Ruderman M.A., 1965, J. Geophys. Res., 70, 3131

[40] Elsner, R. F., Lamb, F. K., 1976, Natur., 262, 356E

[41] Elsner, R. F., Lamb, F. K., 1977, ApJ, 215, 897

[42] Eracleous M., Patterson J., Halpern J.P., 1991, ApJ, 370, 330

[43] Eracleous M., Halpern J., Patterson J., 1991, ApJ, 382, 290

[44] Eracleous M., Horne K., Robinson E.L., Zhang Z., Marsh T.R., Wood J.H., 1994, ApJ, 433, 313

[45] Eracleous M., Horne K.D., 1996, ApJ, 471, 427

[46] Eracleous, M. 1999, ASP Conf. Ser. 157: Annapolis Workshop on Magnetic Cataclysmic Variables, 343

[47] Frank J., King A.R., Raine D., 2002 (3 rd ed), Accretion Power in Astrophysics, Cambridge Univ. Press, Cambridge, p. 60

[48] Fried B.D., Gould R.W., 1961, Phys. Fluids, 4, 139

[49] Friedjung M., 1997, New Astron., 2, 319

[50] Galeev, A. A.; Rosner, R.; Vaiana, G. S., 1979, ApJ, 229, 318

[51] Goldreich P., Julian W.H., 1969, ApJ, 157, 869

[52] Ghosh P., Lamb F., 1979a, ApJ, 232, 259

[53] Ghosh P., Lamb F., 1979b, ApJ, 234, 296

[54] Hamada T., Salpeter E.E., 1961, ApJ, 134, 683

[55] Hameury J.M., King A.R., Lasota J.P., 1986, MNRAS, 218, 695

[56] Hameury J.M., King A.R., Lasota J.P., 1986, MNRAS, 237, 845

[57] Hamilton R.J., Lamb F.K., Miller M.C., 1994, ApJS, 90, 837

[58] Hellier C., 2001, Cataclysmic variable stars, Springer

[59] Horne K.D., 1999, in Hellier K., Mukai K., eds, ASP Conf. Ser. Vol. 157, Annapolis Workshop on Magnetic Cataclysmic Variables., ASP Conf. Ser., San Francisco, p. 357

[60] Illarionov A.F., Sunyaev R.A., 1975, A&A, 39, 185

[61] Ikhsanov N.R. , 1998, A&A, 338, 521

[62] Ikhsanov N.R., Neustroev V.V., Beskrovnaya N.G., 2004, A&A, 421, 1131

[63] Ikhsanov N.R., 2006, ApJ, 640, L59

[64] Itoh K., Okada S., Ishida M., Kunieda H., 2006, ApJ, 639, 397

[65] Jackson J.D., 1975, Classical Electrodynamics 2 nd ed., Wiley, New York,

[66] Jameson R.F., King A.R., Sherrington M.R., 1980, MNRAS, 191, 559

[67] Joy A.H., 1954, ApJ, 120, 377

[68] King A.R., 1993, MNRAS, 261, 144

[69] King A.R., Lasota J.-P., 1991, ApJ, 378, 674

[70] King A.R, Regev O., 1994, MNRAS, 268, L69

[71] Kuijpers, J., Fletcher, L., Abada-Simon, M., Horne, K. D., Raadu, M. A., Ramsay, G., Steeghs, D., 1997, A&A, 322, 242

[72] Kuijpers J., Pringle J.E., 1982, A&A, 114, L4

[73] Lamb D. Q., 1988, in Coyne G. V., Magalhaes A. M., Moffat A. F., Schulte-Ladbeck R. E., Tapia S., eds, Polarized Radiation of Circumstellar Origin. Vatican Observatory, Vatican City State, p. 151

[74] Lamb D.Q., 1995, ASPC, 85, 519

[75] Lamb, F. K., Pethick, C. J., Pines, D., 1973, ApJ, 184, 271

[76] Landau L.D., Lifshitz E.M., 1960, The electrodynamic of continuous media, Pergamon Press, Oxford, p. 228

[77] Landau L.D., Lifshitz E.M., 1987, Fluid Mechanics, 2 nd ed., Pergamon Press, Oxford, pp. 132-133

[78] Lang K.R., 1998, Astrophysical Formulae, Third Edition, Springer Verlag, p. 209

[79] Lang K.R., 1980, Astrophysical Formulae, Springer-Verlag, Berlin, p. 31

[80] Litwin C., Rosner R., and Lamb D.Q., 1999, MNRAS, 310, 324

[81] Livio M., Pringle J.E., 1994, MNRAS, 259, short comm., 23p

[82] Lubow S.H. & Shu F.H., 1975, ApJ, 198, 383

[83] Matsumoto R., Kodoh T., Shibata K., Hayashi M.R., 1998, ASPC, 137, 286

[84] Mauche, C.W., 2006, MNRAS, 369, 1983

[85] Meintjes P.J., Raubenheimer B.C., de Jager O.C., Brink C., Nel H.I., North A.R., van Urk G., Visser B.,1992, APJ, 401, 325

[86] Meintjes P.J., de Jager O.C., Raubenheimer B.C., Nel H.I., North A.R., Buckley D.A.H., Koen C., 1994, ApJ, 434, 292

[87] Meintjes P.J., de Jager O.C., 1995, ASPC, 85, 396

[88] Meintjes P.J., de Jager O.C., 2000, MNRAS, 311, 611

[89] Meintjes P.J. 2002, MNRAS, 336, 265

[90] Meintjes P.J., 2004, MNRAS, 352, 416

[91] Meintjes, P. J., Jurua, E., 2006, MNRAS, 372, 1279

[92] Meintjes P.J., Venter, L.A., 2003, MNRAS, 341, 891

[93] Meintjes P.J., Venter, L.A., 2005, MNRAS, 360, 573

[94] Melrose D.B., 1994, ApJS, 90, 623

[95] Mestel L., Spruit H.C., 1987, MNRAS, 226, 57

[96] O' Donoghue D., et al. 1995, in Buckley D.A.H., Warner B., eds., ASP Conf Ser., 85, Proc. Cape Workshop on Magnetic Cataclysmic Variables, Astron. Soc. Pacific, San Francisco, p. 348

[97] Osaki Y., 1974, Publ. Astron. Soc. Japan, 26, 429

[98] Osterbrock D.E., 1989, Astrophysics of Gaseous Nebulae and Active Galactic Nuclei, Mill Valley: University Science Books

[99] Pacholczyk A.G., 1970, Radio Astrophysics, W.H. Freeman & Co, p. 170-171

[100] Parker E.G., 1976, in Seti G., ed. , The Physics of Non-Thermal Radio Sources, Reidel, Dordrecht, p. 137

[101] Patterson J., 1979, ApJ, 234, 978

[102] Patterson J., Branch D., Chincarini G. & Robinson E.L., 1980, ApJ, 240, L133

[103] Patterson J., 1994, PASP, 897, 209

[104] Pearson K.J., Horne K.D., Skidmore W., 2003, MNRAS, 338, 1067

[105] Pearson K.J., Horne K.D., Skidmore W., 2004, in Vrielman S., Cropper M., eds, ASP conf. Ser. Vol 190, Proc. Cape Workshop on Magnetic Cataclysmic Variables. Astron Soc. Pac., San Francisco, p. 279

[106] Priest E.R., Forbes T., 2000, Magnetic Reconnection: MHD theory and applications, Cambridge University Press, Cambridge, p. 120, 240, 177-228

[107] Priest E.R., 1981, in Priest ed., Solar Flare Magnetohydrodynamics. Gordon & Breach, New York,

[108] Reinsch K., Beuermann K., 1994, A&A, 282, 493

[109] Reinsch, K.; Beuermann, K.; Hanusch, H.; Thomas, H.-C., 1995, ASPC, 85, 115

[110] Schenker K., King A.R., Kolb U., Wynn G.A., Zhang Z., 2002, MNRAS, 337, 1105

[111] Schmidt G.D., 1999, ASP Conf. Ser. Vol 157, 207

[112] Shore S.N, 1992, *An introduction to astrophysical Hydrodynamics*, Academic Press Inc., San Diego, p. 292

[113] Spitzer L., 1962, Physics of Fully ionized gases (2d ed.; New York: Interscience)

[114] Steeghs, D., Horne, K., Marsh, T. R., Donati, J. F., 1996, MNRAS, 281, 626

[115] Tanzi E.G., Chincarini G., Tarenghi M., 1981, PASP, 93, 68

[116] Tritton D.J., 1977, Physical Fluid Dynamics, Van Nostrand Reinhold, pp. 233-237

[117] van der Laan H., 1963, MNRAS, 126, 535

[118] van der Laan H., 1966, Nature, 211, 1131

[119] van Paradijs J., Kraakman H., van Amerongen S., 1989, A&A Suppl. Ser.,79, 205

[120] Venter L.A., Meintjes P.J., 2004, in Vrielman S., Cropper M., eds, ASP conf. Ser. Vol 190, Proc. Cape Workshop on Magnetic Cataclysmic Variables. Astron Soc. Pac., San Francisco, p. 307

[121] Venter L.A., Meintjes P.J., 2006, MNRAS, 366, 557

[122] Watson C.A., Dhillon V.S., Shahbaz T., 2006, MNRAS, 368, 637

[123] Wang Y-M, 1987, A&A, 183, 257

[124] Wang Y-M., Robertson J.A., 1984, A&A, 139, 93

[125] Wang Y-M., Robertson J.A., 1985, A&A, 151, 361

[126] Warner B, 1995, Cataclysmic Variable Stars, Cambridge University Press, p. 376

[127] Warner B., Wickramasinghe D.T., 1991, MNRAS, 248, 370

[128] Watson, M.G., 1986, in Physics of Accretion onto Compact Objects, eds. K.O. Mason, M.G. Watson & N.E. White, Springer-Verlag, Berlin, p. 97

[129] Welsh W.F., Horne K.D., Oke J.B., 1993, ApJ, 401, 229

[130] Welsh W.F., Horne K.D., Gomer R., 1995, MNRAS, 275, 649

[131] Welsh W.F., Horne K.D., Gomer R., 1998, MNRAS, 298, 285

[132] Welsh G.A., 1999, in Hellier C., Mukai K., eds, ASP Conf. Ser., Annapolis Workshop on Magnetic Cataclysmic Variables, ASP Conf. Ser., San Francisco, 57, 357

[133] Wickramasinghe D.T., Wu K., Ferrario L., 1991, MNRAS, 249, 460

[134] Woodsworth A.W., Hughes V.A., 1976, ApJ, 208, 863

[135] Wynn G.A., King A.R., 1995, MNRAS, 275,9

[136] Wynn G.A., King A.R., Horne, K., 1997, MNRAS, 286, 436

[137] Zinner, E., 1938, Astron. Nach., 265, 345